

**ELECTRONIC, MAGNETIC
STRUCTURE AND PHASE
STABILITY IN SUBSTITUTIONAL
BINARY ALLOYS
A THEORETICAL STUDY**

**THESIS SUBMITTED FOR THE DEGREE OF
DOCTOR OF PHILOSOPHY (SCIENCE)
OF THE
UNIVERSITY OF JADAVPUR
2004**

Durga Paudyal
SATYENDRANATH BOSE NATIONAL CENTRE
FOR BASIC SCIENCES
JD BLOCK, SECTOR 3, SALT LAKE CITY
KOLKATA 700 098, INDIA

**ELECTRONIC, MAGNETIC
STRUCTURE AND PHASE
STABILITY IN SUBSTITUTIONAL
BINARY ALLOYS :
A THEORETICAL STUDY**

**THESIS SUBMITTED FOR THE DEGREE OF
DOCTOR OF PHILOSOPHY (SCIENCE)
OF THE
UNIVERSITY OF JADAVPUR
2004**

Durga Paudyal
SATYENDRANATH BOSE NATIONAL CENTRE
FOR BASIC SCIENCES
JD BLOCK, SECTOR 3, SALT LAKE CITY
KOLKATA 700 098, INDIA

CERTIFICATE FROM THE SUPERVISORS

This is to certify that the thesis entitled "Electronic, Magnetic Structure and Phase Stability in Substitutional Binary Alloys : a Theoretical Study" submitted by Sri Durga Paudyal, who got his name registered on January 29, 2003 for the award of Ph.D. (Science) degree of Jadavpur University, is absolutely based upon his own work under the supervision of Dr. Tanusri Saha-Dasgupta and Prof. Abhijit Mookerjee at S. N. Bose National Centre For Basic Sciences, Kolkata, India and that neither this thesis nor any part of it has been submitted for any degree/diploma or any other academic award anywhere before.

Tanusri Saha-Dasgupta 30/11/04
1. TANUSRI SAHA-DASGUPTA

FACULTY FELLOW
S.N. BOSE NATIONAL CENTRE
FOR BASIC SCIENCES
JD- Block, Sec-III, Salt Lake
Kolkata-700 098

Abhijit Mookerjee
2. ABHIJIT MOOKERJEE
30/11/04

अभिजित मुखर्जी / ABHIJIT MOOKERJEE
वरिष्ठ अध्यापक एवं अध्यक्ष (शि.का.) / Sr. Professor & Dean (A.P.)
एस.एन. बसु राष्ट्रीय मौलिक विज्ञान केन्द्र
S. N. Bose National Centre for Basic Sciences
साल्ट लेक, कोलकाता-700 098
Salt Lake, Kolkata-700 098

Acknowledgments

First of all, I express my gratitude to Prof. Abhijit Mookerjee and Dr. Tanusri Saha-Dasgupta for introducing and inspiring me in the fascinating field of electronic structure and alloy phase stability. Their kind help, constant guidance and encouragement made this work possible.

I would like to acknowledge the use of the Stuttgart TB-LMTO package in this work and would like to thank Prof. O.K. Andersen (Max Planck Institute, Stuttgart, Germany) for allowing me to do so. I am also grateful to him for useful discussions on electronic structure theory.

I would like to thank the Department of Science and Technology, Government of India for the research fellowship thus enabling me to pursue my Ph.D. work in India. I would also like to thank Prof. S. Dattagupta, Director, S.N. Bose National Centre for Basic Sciences, Kolkata, India for providing me with an opportunity to work at the centre. I also express my gratitude to Dr. Ranjan Chaudhury of the centre for useful discussions regarding magnetism. I am grateful to Prof. G.P. Das (Indian Association for Cultivation of Sciences, Kolkata) for useful discussions related to alloy phase stability. I wish to thank staff members of this centre for their cooperation and help. My sincere thank goes to IIT, Kanpur, India, International Centre for Theoretical Physics, Italy and the Department of Physics, Dhaka University, Bangladesh for inviting me to attend summer schools and conferences hosted by them.

I am thankful to my friends at the S.N. Bose National Centre for Basic Sciences for making my stay in Kolkata enjoyable.

This acknowledgment cannot end without mentioning the constant support from my father and my wife Seema. Final thanks goes to my daughter Dakshina who has made my stay in India enormously enjoyable and entertaining.

List of Publications

1. **Study of phase stability in NiPt systems**
Durga Paudyal, Tanusri Saha-Dasgupta and Abhijit Mookerjee
J. Phys.: Condens. Matter **15** 1029 (2003)
2. ***Electronic structure and ground state properties of non-magnetic NiPt systems**
Durga Paudyal, Abhijit Mookerjee
Int. J. Mod. Phys. B **17** 4447(2003).
3. **Magnetic properties of X-Pt (X = Fe, Co, Ni) alloy systems**
Durga Paudyal, Tanusri Saha-Dasgupta and Abhijit Mookerjee
J. Phys.: Condens. Matter **16** 2317 (2004)
4. ***Phase stability and magnetism in NiPt and NiPd alloys**
Durga Paudyal and Abhijit Mookerjee
J. Phys.: Condens. Matter **16**, 5791 (2004)
5. ***Spin-orbit coupling; a recursion method approach**
Ain-ul Huda, *Durga Paudyal*, Abhijit Mookerjee and Meshbahuddin Ahmed
Physica B Condensed Matter **351**, 63 (2004)
6. **Phase stability analysis in Fe-Pt and Co-Pt alloy systems: An augmented space study**
Durga Paudyal, Tanusri Saha-Dasgupta and Abhijit Mookerjee
J. Phys.: Condens. Matter **16**, 7247 (2004)
7. ***Magnetic transition in Ni-Pt alloy Systems : Experiment and Theory**
(theory : *Durga Paudyal* and Abhijit Mookerjee, experiment : Uday Kumar. K. G. Padmalekha, and P. K. Mukhopadhyay)
accepted for publication in Journal of Magnetism and Magnetic Materials (cond-mat/0407661)
8. **Ordering in 3d-5d (CuAu) and segregation in 3d-4d (CuAg) Systems**
Durga Paudyal and Abhijit Mookerjee
submitted to Physica B Condensed Matter (2004)

*The papers marked * have not been included in the main body of the thesis, but represent closely related work.*

Contents

1	Introduction	1
2	Theoretical and computational methods	9
2.1	Theoretical methods	11
2.1.1	Density functional theory	11
2.1.2	Linear muffin tin orbital method	12
2.1.3	Configuration averaging in disordered systems	17
2.1.4	The augmented space theorem	20
2.2	Recursion method	27
2.3	Augmented space recursion	30
2.3.1	The Hamiltonian in augmented space	30
2.3.2	Generalized augmented space recursion	37
2.3.3	The effective pair interactions	42
2.4	Computational details	47
2.4.1	Ordered alloys	47
2.4.2	Disordered alloys	49
2.4.3	Phase stability analysis	63
2.5	Summary	66
3	Electronic and magnetic properties of X-Pt (X=Fe,Co,Ni) alloy systems	67
3.1	Results and discussions	68
3.1.1	Lattice parameters	68
3.1.2	Magnetism of Fe-Pt alloys	70
3.1.3	Magnetism in Co-Pt alloys	76
3.1.4	Magnetism in Ni-Pt alloys	81
3.2	Summary	84
4	Study of phase stability in NiPt systems	86
4.1	Results and discussions	87
4.2	Summary	97

5	Phase stability analysis in Fe-Pt and Co-Pt alloy systems	99
5.1	Results and discussions	101
5.1.1	Pair interaction energies	101
5.1.2	Effective pair potential surfaces	104
5.1.3	Instability temperatures	106
5.1.4	Short range order	108
5.2	Summary	110
6	Ordering in 3d-5d (CuAu) and segregation in 3d-4d (CuAg) Systems	112
6.1	Results and discussions	113
6.1.1	Calculations on ordered alloys	113
6.1.2	Calculations on disordered alloys	116
6.1.3	Short-ranged order	117
6.2	Summary	117
7	Concluding remarks	118

List of Figures

2.1	Variation of total energy and magnetic moments as a function number of k points in the Brillouin Zone (BZ) for Ni ₃ Pt alloy system.	48
2.2	Variation of total energy and magnetic moments as a function of tetragonal distortion in NiPt alloy system.	49
2.3	Nearest neighbour distance vs concentration of Pt with the choice of neutral charge spheres. For comparison the average bond length given by Vegard's law is shown in solid line.	51
2.4	Variation of magnetic moments as a function of short range order parameter in Ni ₄₅ Pt ₅₅ alloy system.	56
2.5	Log-log plot of the number of sites as we increase the number of shells in augmented space.	57
2.6	Fermi energy, band energy and magnetic moments as a function of recursion steps in Ni ₃ Pt.	62
2.7	Fermi energy, band energy and magnetic moments as a function of seed energy points in Ni ₃ Pt.	63
2.8	First nearest neighbour pair interaction energy as a function of recursion steps in NiPt ₃ alloy system.	64
3.1	Magnetic moments in disordered Fe-Pt alloy systems using two different configuration averaging methods namely augmented space recursion (ASR) and coherent potential approximation (CPA) as compared to available experimental values given in Landoldt series [Wijn (1986)].	73
3.2	Magnetic moments as a function of lattice parameters for 25% concentration of Pt in disordered Fe-Pt alloy. Circles and squares denote local magnetic moment on Fe site and Pt site respectively. Diamonds represent average magnetic moment.	74

3.3	Variation of magnetic moments as a function of short range order parameter (α) for 75% in Fe-Pt system. Circles, squares and diamonds denote the local magnetic moments on Fe sites, on Pt sites and average magnetic moments respectively.	76
3.4	Magnetic moments in disordered Co-Pt alloy systems using two different linearized muffin-tin orbital (LMTO) based configuration averaging methods namely augmented space recursion (ASR) and coherent potential approximation (CPA) as compared to available experimental values given in Landoldt series [Wijn (1986)]. CPA-LCAO and KKR-CPA denote coherent potential approximation based linear combination of atomic orbitals method of Koepernik <i>et al</i> (1997) and Korringa Kohn Rostoker coherent potential approximation method of Ebert <i>et al</i> (1992) respectively.	79
3.5	Variation of magnetic moments as a function of short range order parameter (α) in Co-Pt systems. Circles, squares and diamonds denote the local magnetic moments on Co sites, on Pt sites and average magnetic moments respectively.	80
3.6	Magnetic moments in disordered Ni-Pt alloy systems using two different configuration averaging methods namely augmented space recursion (ASR) and coherent potential approximation (CPA) as compared to experimental values given by Parra and Cable (1980). ASR (SRO) denotes the results taking short range ordering effect into account.	83
4.1	Formation energy vs concentration of Pt with the choice of neutral charge spheres.	88
4.2	(i) The effective pair potentials calculated with the choice of charged spheres including scalar relativistic corrections.	93
4.3	(i) The effective pair potentials as a function of energy, calculated with charge neutral potential parameters including scalar relativistic corrections. (ii) Comparison between the first nearest neighbour effective pair potentials with scalar relativistic corrections and without scalar relativistic corrections by taking charge neutral potential parameters. (iii) The effective pair potentials as a function of shell numbers with charge neutral potential parameters including scalar relativistic corrections.	94

4.4	The $V(\vec{k})$ surface for NiPt alloy system with potential parameters calculated with the choice of (i) charged spheres (ii) charge neutral spheres, on $k_z = 0$ plane. The figures in inset show the enlarged view of the corresponding $V(\vec{k})$ surfaces on $k_z = 0$ plane in the vicinity of the (100) to (110) direction.	95
4.5	The effective pair potentials vs concentration of Pt with the choice of potential parameters with (i) charged spheres including scalar relativistic corrections and (ii) charge neutral spheres including scalar relativistic corrections.	96
4.6	Ordering energy, anti-phase boundary energy and instability temperatures vs concentration of Pt with the choice of charge neutral potential parameters including scalar relativistic correction.	97
5.1	Plot of first nearest neighbour pair interaction energies (V_1) in Fe-Pt and Co-Pt alloys showing the concentration dependence.	102
5.2	Density of states and first nearest neighbour pair interaction energy as a function of energy in Co_3Pt alloy system.	103
5.3	The calculated pair interaction energies as a function of shell numbers in Co_3Pt as compared to experimental estimates of Capitan <i>et al</i> (1999). . . .	104
5.4	Effective pair potential $V(\mathbf{k})$ surfaces for Co_3Pt alloy system in the (hk0) plane using our theoretically calculated pair interaction energies (i) without magnetic contribution and (ii) with magnetic contribution and (iii) using extracted pair interaction energies by Capitan <i>et al</i> (1999) from their experiment.	106
5.5	Effective pair potential $V(\mathbf{k})$ surfaces for CoPt_3 alloy system in the (hk0) plane using (i) our theoretically calculated pair interaction energies and (ii) extracted pair interaction energies by Kentzinger <i>et al</i> (2000) from their experiment.	106
5.6	Theoretically calculated instability temperatures as compared to experimentally measured order disorder transition temperatures.	107
5.7	Plot of SRO, $\alpha(100)$ values in Fe-Pt and Co-Pt alloys which shows the concentration dependence in the short range order.	109

- 5.8 SRO ($\alpha(\mathbf{k})$) patterns for Co_3Pt alloy system in the $(\mathbf{hk0})$ plane using our theoretically calculated pair interaction energies (i) without magnetic contribution and (ii) with magnetic contribution and (iii) using real space SRO parameters from the ferromagnetic experimental measurement of Capitan *et al* (1999). The peaks in the contour plots locate the peaks in the short range order patterns. The plots were drawn at 10 K above the calculated instability temperature. 110
- 5.9 SRO ($\alpha(\mathbf{k})$) patterns for CoPt_3 alloy system in the $(\mathbf{hk0})$ plane using (i) our theoretically calculated pair interaction energies and (ii) experimentally measured real space SRO values by Kentzinger *et al* (2000). The peaks in the contour plots locate the peaks in the short range order patterns. The plots were drawn at 10 K above the calculated instability temperature. . . 110
- 6.1 The short range order map $\alpha(\mathbf{k})$ for (left) CuAu and (right) CuAg. . . . 117

List of Tables

2.1	The special points and stars of the <i>FCC</i> structure.	66
3.1	The equilibrium lattice parameters in a.u. of FePt, CoPt and NiPt systems in ordered structures with various choices of exchange correlation functionals. See text for various abbreviations.	69
3.2	The local and average magnetic moments of Fe-Pt system in ordered structures with various choices of exchange correlation functionals.	71
3.3	Various estimates of the local and averaged magnetic moments in Bohr-magnetons for disordered Fe ₇₅ Pt ₂₅ alloy.	75
3.4	The local and average magnetic moments of Co-Pt system in ordered structures with various choices of exchange correlation functionals.	77
3.5	The local and average magnetic moments of Ni-Pt system in ordered structures with various choices of exchange correlation functionals.	81
4.1	Formation energies for Ni _x Pt _y with the choice of neutral charge spheres including scalar relativistic corrections. The values in brackets are without relativistic corrections. The corresponding estimate for charged sphere calculations are shown with *'s. ** refers to calculations without combined correction. *** refers to disordered formation energy.	89
4.2	The effective pair potentials for NiPt alloy system calculated with potential parameters taken from calculations with the choice of charged spheres and including scalar relativistic corrections. (O-L) refers to calculations without multipole corrections, M refers to calculations with multipole corrections and SCI to calculations with screened Coulomb interactions. US-PP refers to ultrasoft pseudo-potentials. * refers to non-relativistic calculations. . . .	91

4.3	The effective pair potentials for NiPt alloys with potential parameters taken from calculations with the choice of charge neutral spheres including scalar relativistic corrections. The corresponding estimate for non relativistic calculations are shown with *'s.	92
4.4	The anti-phase boundary energies for Ni_xPt_y alloys from charged and neutral sphere calculations. The values in brackets are without relativistic corrections.	96
5.1	Pair interaction energies upto fourth nearest neighbour in mRyd/atom. The values inside bracket in the case of 25% concentration of Pt in Co-Pt are with the magnetic contribution.	101
5.2	Effective potentials $V < \mathbf{hkl} >$. The values inside bracket in the case of 25% concentration of Pt in Co-Pt are with the magnetic contribution. . . .	105
5.3	Short range order $\alpha < \mathbf{hkl} >$. The values inside bracket in the case of 25% concentration of Pt in Co-Pt are with the magnetic contribution.	109
6.1	Formation energies in mRyd/atom. The values shown in the brackets are without relativistic corrections.	113
6.2	Potential parameters (Δ_d) in mRyd/atom. The values shown in the brackets are without relativistic corrections.	114
6.3	Integrated number of electrons (n) of each angular momentum type within the atomic spheres of Cu, Ag and Au in CuAg and CuAu alloys. The values shown in the brackets are without relativistic corrections. The table also shows the difference $\Delta n = n_{rel} - n_{nonrel}$	115
6.4	Pair energies in mRyd/atom. The values shown in the brackets are without relativistic corrections. $V_n = E_{RR'}^{(2)}$ where R' is a n-th nearest neighbour of R	116

Chapter 1

Introduction

Metals and alloys are materials of a continuing scientific and technological importance. These include steels, permanent magnets, high-temperature refractory compounds, catalytic nano-assemblies just to mention a few. Design of new materials with desired or new properties is a frontier area of research in condensed matter physics and materials science. Valuable knowledge of phase stability in metallic alloys comes from both theory and experiment. Developing theoretical methods lead to microscopic understanding of the observed phenomena which in turn provides the clue for designing of materials with desired or improved properties. The purpose of the present work is to develop a general and reliable theoretical method to predict alloy phase stability from first principles, and to apply it to alloys that have important properties. First we shall define some terms and concepts.

An alloy is a mixture or solid solution of two or more elements. In a substitutional alloy the atoms of one element replace the atoms of the other . An interstitial alloy with atoms of one element occupying interstitial positions between the atoms of the other can be viewed as a substitutional alloy with substituted interatomic vacancies treated as a type of atoms. Properties of materials are related to their microstructure, which is determined by the number of phases present, their proportion, and their composition. The key issues in alloys are the identification of stable phases and the instability of these stable phases on raising temperature as one varies the composition. A phase diagram, which helps to predict or explain the microstructure, is a graphical plot showing the relationships between

the various phases that appear in a particular system under equilibrium conditions. A major component of such understanding is the understanding of electronic structure of alloys.

Most of the the properties of solids can be traced to the behaviour of electrons, the “glue” that holds atoms together to form a solid. An important aim of the condensed matter theory is therefore calculating the electronic structure of solids. The theory of electronic structure is not only helpful in understanding and interpreting experiments, but it also becomes a predictive tool of the Physics and Chemistry of condensed matter and material science.

Electrons have an effective interaction that is different depending on whether they have the same spin or not. Since electrons with opposite spin can occupy the same space, they have a higher potential energy of interaction on average. Thus all else being equal, electrons would want to have the same spin in order to lower the system’s potential energy. A system with electrons that have the same spin direction is a ferromagnet. In general the magnetic structures are described in terms of exchange coupling between the nearest neighbours. There is competition between electronic potential energy which favors magnetism, and the electronic kinetic energy, which favors a non-magnetic electronic structure. As pressure is increased, electrons are pushed close together, and the relative potential energy changes between paired and unpaired electrons become less important; bands become wider, making the kinetic energy cost smaller, so that in general materials become non-magnetic with increasing pressure.

As temperature is raised the magnetic-moment directions on each atom fluctuates more and more rapidly, and at some critical temperature, called the Curie temperature, or T_C in ferromagnets, the moments will disorder. In general, there are still magnetic moments on the ions above T_C , but they are just disordered in direction.

Antiferromagnets have moments of opposite direction on alternating sites. It is the different hybridization of electronic states that leads to antiferromagnetic rather than ferromagnetic order, so that the kinetic energy is lowered. This is sensitive to pressure, so some ferromagnets become antiferromagnetic with increasing pressure, as in FCC iron.

In a simple ferrimagnet the exchange coupling between the nearest neighbours may favour antiparallel alignment, but because neighbouring magnetic sites are not identical and their moments will not cancel, leaving the net moment for the solid as a whole. In some cases the lowest free energy state has non-collinear spins.

To gain some basic understanding about the electronic structure and properties of materials even very simple models based on empirical tight binding approach which describe bonding in terms of the local environment of atoms may be used. These models involve a number of uncontrolled approximations, and while they give valuable insight and can even predict trends in properties, they contain parameters which must be fitted either to experimental data or to the results of some more sophisticated calculations. A lot of structural and dynamical properties of solids can be predicted from first principles (*ab initio*) calculations, where the atomic numbers of the constituent atoms and, usually some structural informations are the only pieces of empirical input data. Such calculations are routinely performed within the framework of density functional theory [Hohenberg and Kohn (1964)] in which the complicated many body motion of all electrons is replaced by an equivalent but simpler problem of a single electron moving in effective potential. The calculated total energies are used to obtain various electronic properties of atoms or alloys.

The band structure methods are based on density functional theory. Methods having plane waves as well as tight binding basis are capable to describe most of the ordered metallic alloys. The tight binding linear muffin tin orbital method (TB-LMTO) [Andersen and Jepsen (1984)] is one of the widely used method in which the potential in the solid is divided into atomic centred close to spherically symmetric part and a flat interstitial part and the energy dependent basis set are linearized to derive the energy independent basis set in the form of muffin tin orbitals. This method is mostly used within the atomic sphere approximation which substitutes the muffin tin spheres with slightly overlapping (space-filling) atomic spheres.

Most of the solids around us are disordered. Deviation from crystallinity seems to be the rule rather than exception. Any deviation from a perfectly periodic lattice arrange-

ments of atoms leads to disorder. Broadly speaking there are three kinds of disordered materials. (a) Compositionally disordered solids like random alloys both in substitutional and interstitial. (b) Structurally disordered solids where the underlying lattice has random structural distortions. (c) Magnetic alloys with compositional as well as structural disorder like metallic glasses. For study of disordered alloys the above mentioned band structure methods based on lattice periodicity are therefore not suitable. Historically the single site coherent potential approximation (CPA) [Soven (1967)] was the only method to study the physical properties of disordered alloys. In 1973 Mookerjee [Mookerjee (1973)] introduced the augmented space (direct product of real and configurational space) theorem which enables us to obtain configuration averaged quantities related to electronic structure of disordered alloys. After the introduction of first principles method like tight binding linear muffin tin orbital (TB-LMTO) [Andersen and Jepsen (1984)], there have been attempts at calculating the electronic structure of disordered alloys from first principles and most of the works are based on the mean field, single site coherent potential approximation (CPA) in the conjunction with the first principles methods [Kudrnovský and Drchal (1990)]. Though these CPA based first principles methods give reasonable descriptions of many disordered alloy systems, in equally many cases it is expected to fail in describing effects involving correlated multisite scattering like clustering, local lattice distortions, short range ordering etc. The augmented space recursion (ASR) [Saha *et al* (1994)] method which is based on the augmented space theorem for general configuration averaging and recursion done on this extends the theory beyond CPA and is capable of handling effects arising from multi-site correlations. Randomness destroys the periodicity and for a disordered system the Bloch wave vector no longer remains a good quantum number. This is reflected in the smearing out of the van Hove singularities in the densities of states. As a result k-space technique demands the introduction of some artificial periodicity via the mean field theories like CPA. On the other hand the ASR method based on real space technique has the power of exploiting the environmental effects. The recursion processes define the hierarchy of environments with the relative influence of environments explicitly displayed in the local properties one is interested in. Since the successively more distant environments have lesser effects on local properties, the recursion process

is dominated by environments close to local site and finite size cluster calculations with terminators appended give reasonably accurate results.

The knowledge of electronic structure also provides the information of phase stability of substitutional alloy systems. It requires accurate approximations of the configurational energy on one hand and use of statistical model in the other. Different models have been proposed in which the configurational energies are expressed in terms of effective multi-site interactions, in particular the effective pair interactions, which amounts to mapping the binary alloy problem to an effective Ising model problem. The problem of stability analysis thus reduces to obtaining ground states of the three dimensional Ising model whose interaction parameters are obtained by first principles electronic structure calculations. There are two different approaches of obtaining the effective pair interactions. One approach starts with electronic structure calculations of the ordered super-structures of the alloy and to invert the total energies to obtain the effective pair interactions. This is the Connolly-Williams [Connolly and Williams (1983)] method. An alternative approach [Gonis *et al* (1987)], which we follow, is to start from the disordered alloy and study the instability of the disordered solid solution phase with respect to the statistic concentration wave perturbations corresponding to the particular superstructure formation. This is indicated by the minima in the Fourier transform of the effective pair interaction.

Most of the work on the phase stability and ordering or segregation in alloys have been based on the CPA. The CPA being a single-site approximation as pointed out above cannot take into account the effect at a site of its immediate environment which is important in the analysis of ordering or segregation in alloys. In an attempt to go beyond the single site approximation, de Fontaine and his group followed a different approach of direct configurational averaging (DCA) [de Fontaine (1994)] without resorting to any kind of single-site approximation. The effective pair and multi-site interactions were calculated directly in real space for given configurations and the averaging was done in a brute force way by summing over different configurations. Invariably, the number of configurations was finite and convergence of the results with increasing number of configurations is yet to be available. As an alternative approach the ASR based method is capable of providing the

effective pair interaction energies accurately enough. The effective pair interactions within this scheme are calculated by coupling the ASR with orbital peeling technique of Burke [Burke (1976)] which peels the orbitals (deletes rows and columns of the Hamiltonian) of the embedded atoms on the averaged medium to determine the small energy differences without involving errors due to subtraction of large numbers.

The subject of this thesis is the theoretical study of electronic, magnetic structure phase stability in substitutional binary alloys. The thesis has been broadly divided into two parts. First part deals with the first principles electronic structure methods which, over the years, have proved to be reliable and accurate tools in modeling the materials of many kinds. In this part, we have discussed the formalisms used along with their various merits, in particular to study alloys which are substitutionally disordered. In the other part we have demonstrated the applications to transition metal based alloys, which has been the subject of extensive investigations particularly in relation to their fascinating electronic, magnetic, ordering and phase stability properties. The reason for choosing these kind of alloys is two fold : First, to establish that our formalisms are capable of producing the electronic and magnetic properties and phase stability of random alloys in an accurate manner both quantitatively and qualitatively, in cases where earlier theories based on mean-field techniques had been proved to be inadequate. The second reason for the choice of these alloy systems is to study the effect of magnetism on chemical ordering of these systems.

This thesis is organized as follows. In Chapter 2, we first overview the methods for addressing ordered as well as disordered alloys. We start with the motivation of doing electronic structure calculations from first principles. We briefly state the density functional theory and make a brief overview of TB-LMTO band structure method. We state the augmented space theorem and describe briefly CPA along with its relation with augmented space. We describe the limitations of CPA and necessity of doing augmented space recursion along with its generalized formulation to take into account the effects which can not be tackled by single site mean field methods. In next step, we introduce and discuss the orbital peeling technique in conjunction with the augmented space re-

cursion in TB-LMTO basis to calculate the chemical pair interactions in substitutional binary alloys. We also extend this technique to take into account of magnetic effect in the chemical pair interaction energies. In this chapter we also present the computational details examining some of the effects in electronic structure calculations. This includes the effect of magnetic moments as we vary the irreducible k points in Brillouin Zone mesh in using TB-LMTO method. The lattice relaxation effect is checked in the ordered alloys using TB-LMTO method and in the disordered counterpart it is checked using augmented space recursion taking the relaxed and unrelaxed potential parameters from corresponding TB-LMTO calculations as inputs. We also point out the simple procedure for the approximate treatment of Madelung potential in the disordered alloys. The convergence on the magnetic moments in disordered alloys is also checked with the variation of recursion steps and number of seed recursion. The convergence of Fermi energy and pair interaction energy as a function of recursion steps are also checked. The discussion of these computational details shows the reliability of our calculations in subsequent chapters. The computational aspects of relative stability and ordering are explained at the end of this chapter.

In Chapter 3, we study the magnetic properties of ordered as well as disordered Fe-Pt, Co-Pt and Ni-Pt alloys. For ordered alloys we have used the TB-LMTO method and studied the effect of different exchange correlation functionals on lattice parameters and the magnetic moments of these alloys. In disordered case we have used the augmented space recursion and make comparative study with the results obtained using CPA in these alloys. The subject of short range ordering and its interrelation with magnetism is one of the interesting area of research. In this chapter we study the effect of short range ordering and its interrelation with magnetism in these alloys within the first principles generalized augmented space recursion method.

In Chapter 4, we study the phase stability in Ni-Pt alloys. We examine the necessary effects like relativity (scalar : mass velocity and Darwin corrections), charge transfer and lattice distortion which play important role in the phase stability in the alloys which has large size mismatch and contains heavy element as one of the constituents of the

alloy. In this study we also focused on the instability temperatures computed using pair interaction energies within the mean field statistical model and made comparison of instability temperatures obtained using CPA based methods.

In Chapter 5, we apply the extension of orbital peeling technique in conjunction with the augmented space recursion in a TB-LMTO basis to Co_3Pt alloy system where we encounter the situation that the Curie temperature is higher than the order disorder transition temperature. In such cases there should be the effect of magnetism in the ordering and phase stability of the alloy and therefore one needs to incorporate the magnetic effect on the calculation of pair interaction energies. We also make a systematic study of phase stability in Fe-Pt and Co-Pt alloys.

In Chapter 6, we study alloy ordering and segregation taking the example of CuAu (3d-5d) and CuAg (3d-4d) alloys. We attempt to understand the contrasting properties between CuAu and CuAg : CuAu stable and has ordering tendency while that of CuAg unstable and has segregation tendency.

Chapter 7 includes the concluding remarks of our work.

Chapter 2

Theoretical and computational methods

First principles description of the electronic structure, for the study of physical properties of disordered alloys, is a challenging problem. The absence of translational symmetry is the main difficulty in construction of a quantitative theory comparable in accuracy and efficiency with those for crystalline solids, based on the Bloch theorem and standard band structure methods. For the description of physical properties of disordered systems one needs to carry out configuration averaging in the first principles basis. One of the widely used configuration averaging methods is the mean-field based single-site coherent potential approximation (CPA) which overcomes these difficulties by introducing a translationally symmetric effective Hamiltonian. However, whenever local environment effects become important : like short-ranged ordering, chemical affinity driven local clustering or local lattice distortions due to size mismatch between the constituent atoms, we need a more general configuration averaging method. The augmented space recursion (ASR) is one such general method for configuration averaging developed in our group [Saha *et al* (1994)]. In this chapter we shall illustrate the application of this method and its suitability in tackling different effects like lattice relaxation, charge transfer along with the short-range ordering. Since remarks have often been made about the numerical accuracy of the recursion method, we shall examine the convergence properties of various physical quantities calculated with the ASR.

In its early days, most of the work on disordered systems used semi-empirical tight-binding Hamiltonians to describe electronic properties. A major step towards constructing

first principles tight-binding Hamiltonians began with the tight-binding linear muffin-tin orbitals method (TB-LMTO) within the framework of density functional theory proposed by Andersen and Jepsen (1984). In the TB-LMTO, the Hamiltonian is characterized by a set of potential parameters which are derived self-consistently from a first principles theory and are not empirical. For the ASR calculation, potential parameters are initially generated for the constituent atoms from a most-localized, TB-LMTO calculation. The augmented space Hamiltonian is then generated from it [Mookerjee (1973)] and the recursion method in the augmented space is employed to calculate the partial density of states and charge densities [Haydock *et al* (1972)]. The charge densities are then used to generate the new potential parameters within the local density approximation of the density functional theory (LDA). This is then iterated to self-consistency. The flexibility in the choice of atomic sphere radii keeping constant average volume in random binary alloys makes approximate, yet accurate and consistent treatment of charge transfer effect [Kudrnovský and Drchal (1990)].

Since the ASR allows us to go beyond a single site mean field approximation, it is suitable for the consideration of randomness in the structure matrices in terms of occupation probabilities of those sites as well as their local environment. The terminal point approximation [Kudrnovský and Drchal (1990)] assumes that the disorder is dominated by the occupation of the two sites at the extremities of the structure matrix. In this chapter we briefly revisit the procedure and apply it to the case where there is substantial size mismatch between the alloy constituents.

Short-range ordering plays an important role in the actual determination of either ordering or segregation tendency in alloys. It also helps us to understand the interplay between magnetism and chemical order. The ASR allows us to introduce short-range ordering in a simple manner [Mookerjee and Prasad (1993)].

In this chapter we shall also demonstrate the convergence of various physical quantities calculated within the ASR. The emphasis on these convergences properties with probable errors will illustrate the reliability and suitability of the computational aspects of our method.

2.1 Theoretical methods

Within first principles methods the electronic structure is described by a Hamiltonian

$$H = \sum_{i=1}^{N_e} \frac{p_i^2}{2m_e} - \sum_{\mathbf{R}_I} \sum_{i=1}^{N_e} \frac{Z_I e^2}{|\mathbf{r}_i - \mathbf{R}_I|} + \frac{1}{2} \sum_{i,j}^{N_e} \frac{e^2}{|\mathbf{r}_i - \mathbf{r}_j|} + \sum_{\mathbf{R}_I, \mathbf{R}_J} \frac{Z_I Z_J}{|\mathbf{R}_I - \mathbf{R}_J|} \quad (2.1)$$

The four terms are recognized as the kinetic energy of electrons, the ion-electron interaction, and the electron-electron repulsion and ion-ion interaction. Within this Hamiltonian the ionic motion is ignored using the essence of *Born Oppenheimer approximation* which allows us to separate ionic motion and electronic motion since ionic mass \gg electronic mass (m_e). The nuclei, therefore, considered as classical particles and their positions (\mathbf{R}_I) can be taken as parameters that appear in the potential of the electronic part of the Schrödinger equation.

2.1.1 Density functional theory

Within density functional theory (DFT), the ground state energy of an interacting system of electrons in an external potential is written as a functional of the ground state electronic density [Hohenberg and Kohn (1964)]. DFT is particularly appealing since it does not rely on the knowledge of the complete N -electron wave function but only of the electronic density. Although the theory is in principle exact, the energy functional contains an unknown quantity, called the exchange-correlation energy, that must be approximated in any practical implementation of the method. The most commonly used are the local density approximation (LDA) and the generalized gradient approximation (GGA). Below we briefly describe the essence of this theory.

In the Kohn-Sham formulation of density functional theory [Kohn and Sham (1976)], the ground state density is written in terms of single-particle orbitals obeying the equations in atomic units ($\hbar = e = m = 1$):

$$\left\{ -\frac{1}{2} \nabla^2 + v_{\text{ext}}(\mathbf{r}) + \int \frac{\rho(\mathbf{r}')}{|\mathbf{r} - \mathbf{r}'|} d\mathbf{r}' + v_{\text{xc}}([\rho]; \mathbf{r}) \right\} \psi_i = \epsilon_i \psi_i, \quad (2.2)$$

where

$$\rho(\mathbf{r}) = \sum_{i=1}^N |\psi_i(\mathbf{r})|^2. \quad (2.3)$$

The electronic density is constructed by summing over the N lowest energy orbitals where N is the number of electrons. $v_{\text{ext}}(\mathbf{r})$ is the external potential. The exchange-correlation

potential $v_{xc}([\rho]; \mathbf{r})$ is the functional derivative of the exchange-correlation energy $E_{xc}[\rho]$ that enters in the expression for the total energy of the system:

$$E = -\frac{1}{2} \sum_{i=1}^N \int \psi_i \nabla^2 \psi_i \, d\mathbf{r} + \int \rho(\mathbf{r}) v_{\text{ext}}(\mathbf{r}) \, d\mathbf{r} + \frac{1}{2} \iint \frac{\rho(\mathbf{r})\rho(\mathbf{r}')}{|\mathbf{r} - \mathbf{r}'|} \, d\mathbf{r} \, d\mathbf{r}' + E_{xc}[\rho]. \quad (2.4)$$

The exact functional form of $E_{xc}[\rho]$ is not known therefore it is necessary to make approximations for this term. The local density approximation [Kohn and Sham (1976)] is the simplest and most widely used exchange-correlation functional:

$$E_{xc}^{\text{LDA}}[\rho] = \int \rho(\mathbf{r}) \epsilon_{xc}^{\text{LDA}}(\rho(\mathbf{r})) \, d\mathbf{r}, \quad (2.5)$$

where $\epsilon_{xc}^{\text{LDA}}(\rho)$ is the exchange-correlation energy per particle of a homogeneous electron gas of density ρ . In order to handle magnetic systems, one needs spin-polarized calculations, for which the local spin density approximation (LSDA) has to be invoked instead of LDA (von Barth and Hedin 1971). The fundamental quantity $\rho(\mathbf{r})$ is then replaced by two quantities: *spin-up density* $\rho_{\uparrow}(\mathbf{r})$ and *spin-down density* $\rho_{\downarrow}(\mathbf{r})$, which in turn define the *total charge density* $\rho(\mathbf{r})$ and the *spin density* $\sigma(\mathbf{r})$ as

$$\rho(\mathbf{r}) = \rho_{\uparrow}(\mathbf{r}) + \rho_{\downarrow}(\mathbf{r}) \quad \sigma(\mathbf{r}) = \rho_{\uparrow}(\mathbf{r}) - \rho_{\downarrow}(\mathbf{r})$$

Accordingly one has to calculate two sets of single-particle wave functions for up-spin and down-spin electrons, with the corresponding one-electron eigenvalues from the spin-polarized KS equation. L(S)DA in general overestimates the binding energy and underestimates the bond length of weakly bound molecules and solids. In an attempt to improve upon L(S)DA, the *generalized gradient approximation* is used replacing $\epsilon_{xc}[\rho(\mathbf{r})]$ by a local function of the density and the magnitude of its gradient $\epsilon_{xc}[\rho(\mathbf{r}), |\nabla\rho(\mathbf{r})|]$.

$$E_{xc}^{\text{GGA}}[\rho] = \int \rho(\mathbf{r}) \epsilon_{xc}^{\text{GGA}}(\rho(\mathbf{r}), |\nabla\rho(\mathbf{r})|) \, d\mathbf{r} \quad (2.6)$$

It can be expected that GGA will give better ground-state properties than LDA, since GGA was constructed to be a more precise approximation to the true density functional.

2.1.2 Linear muffin tin orbital method

In LMTO method, an energy independent basis set is derived from the energy dependent basis set in the form of muffin tin orbitals (MTO) [Andersen (1975)]. The set is constructed in such a way it has following characteristics: (a) it is appropriate to the one

electron effective potential of the solid. (b) it is a minimal basis set and (c) it is continuous and singly differentiable in all space. A muffin tin -potential is spherically symmetric inside non-overlapping spheres surrounding the atoms and constant in between. The inside solutions for a MT can be obtained from the numerical solutions of the radial Schrödinger equation

$$[r\phi_{Rl}(\varepsilon, r)]'' = \left[V_R(r) + \frac{l(l+1)}{r^2} - \varepsilon \right] r\phi_{Rl}(\varepsilon, r) \quad (2.7)$$

The outside solutions for constant potential can be represented as linear combination of the spherical Bessel $j_l(\kappa^2, r)$ (regular at origin) and Neumann functions $n_l(\kappa^2, r)$ (regular at infinity, divergent at the origin). The muffin tin orbitals are written as

$$\chi_{RL}(\varepsilon, \kappa^2, r_R) = Y_L(\hat{r}_R) \times \begin{cases} \phi_{Rl}(\varepsilon, r_R) + P_{Rl}(\varepsilon, \kappa^2) j_l(\kappa^2, r_R), & r_R \leq s_R \\ n_l(\kappa^2, r_R), & r_R > s_R \end{cases} \quad (2.8)$$

Here L is used as a combined index for $\{lm\}$ and r_R refers to $|\mathbf{r} - \mathbf{R}|$. $\kappa^2 = \varepsilon - V_0$ can be interpreted as the “kinetic energy in the interstitial region”. In this relation we have added $P_{Rl}(\varepsilon, \kappa^2) j_l(\kappa^2, r_R)$ to the partial wave. This makes the tail (in the interstitial) independent of the muffin-tin potential within the muffin-tin sphere.

The tail $n_L(\kappa^2, r_R)$ can be expanded about other site as :

$$n_L(\kappa^2, \mathbf{r}_{R'}) = \sum_{L'} j_{L'}(\kappa^2, \mathbf{r}_{R'}) S_{R'L', RL}(\kappa^2) \quad (2.9)$$

Here the expansion coefficients $S(\kappa^2)$ is the Hermitian KKR structure matrix. The MTO-tails from neighboring sites (R') cancel the “unphysical” term $P_{Rl}(\varepsilon, \kappa^2) j_L(\kappa^2, r_R)$ of the MTO at the site R which directly leads to the KKR set of homogeneous linear equations

$$\sum_{RL} \left[P_{R'l'}(\varepsilon, \kappa^2) \delta_{R'R} \delta_{L'L} - S_{R'L', RL}(\kappa^2) \right] c_{RL}(\varepsilon) = 0, \quad \text{for each } R', L'. \quad (2.10)$$

These have solutions c_{RL} for those energies where

$$\det | P(\varepsilon, \kappa^2) - S(\kappa^2) | = 0 \quad (2.11)$$

This is the KKR secular equation with separate potential and structure dependent parts. However, the structure constants $S(\kappa^2)$ are strongly energy dependent and are

long ranged in real space. For close-packed solids and low energies, one often uses the atomic-spheres approximation (ASA), which substitutes the MT-spheres with slightly overlapping (space-filling) atomic spheres and sets $\kappa^2 = 0$, so that the envelope functions become simple multipole potentials $r^{-l-1}Y_{lm}(\hat{r})$. In the ASA, the ingredients to the band structure are potential parameters, obtained from the radial functions at the sphere radii, s_R and a structure matrix \mathbf{S} . In open structures, also the potentials in the voids are taken to be spherically symmetric. It has been argued that if the overlap between the Wigner-Seitz spheres is less than 20% then ASA is good approximation and gives reliable results.

Invoking ASA means that instead of integrating the atomic potential out as far as the *MT* sphere, we integrate out a bit more up to the *WS* sphere. In this process we (apparently) include the region of flat potential. Nevertheless, it is possible to calculate the exact difference between the integrals of the interstitial functions over the WS polyhedron and the sphere. This is called the combined correction (CC) term.

The long range of the envelopes with $\kappa^2 = 0$ can be got rid of by screening with multipoles on the neighboring sites. This has made it possible to generate the structure matrix in real space. The screened structure matrix \mathbf{S}^α can be obtained from the canonical structure matrix \mathbf{S}^0 by the unitarity transformation :

$$\mathbf{S}^\alpha = \mathbf{S}^0 \left(\mathbf{1} - \mathbf{Q}^\alpha \mathbf{S}^0 \right)^{-1}$$

The diagonal screening matrix \mathbf{Q}^α which defines the above transformation is unique for all closely packed structures, and yields the most localized structure constant with exponential decay rather than the usual power law behaviour.

In the most tight-binding representation, a LMTO basis orbital of collective angular momenta index $L = (lm)$ centred at site R, is given in the ASA, by the expression :

$$\chi_{RL}^\alpha(r_R) = \phi_{RL}(r_R) + \sum_{R'L'} \dot{\phi}_{R'L'}^\alpha(r_{R'}) h_{R'L',RL}^\alpha \quad (2.12)$$

The function ϕ_{RL} is the solution of the wave-equation inside the spheres of radius S_R at R for some reference energy $E_{\nu RL}$ and is normalized within the sphere. The potential inside the sphere is calculated using the local density functional approximation (LDA). The radial part of the $\dot{\phi}_{RL}^\alpha$ is related to the energy derivative of $\phi_{RL}^\alpha(r_R)$ at the reference energy :

$$\dot{\phi}_{RL}^\alpha(r_R) = \dot{\phi}_{RL}(r_R) + \phi_{RL}(r_R) o_{RL}^\alpha$$

The quantity $o^\alpha = \langle \phi_{Rl} | \dot{\phi}_{Rl}^\alpha \rangle$ is the overlap. The expansion coefficients h_α are given

by

$$h_{RL,R'L'}^\alpha = (C_{RL}^\alpha - E_{\nu RL}) \delta_{RR'} \delta_{LL'} + \sqrt{\Delta_{RL}^\alpha} S_{RL,R'L'}^\alpha \sqrt{\Delta_{RL}^\alpha} \quad (2.13)$$

Where C_{RL}^α and Δ_{RL}^α are the potential parameters to be obtained from the potential function at the reference energy $E_{\nu RL}$. $S_{RL,R'L'}^\alpha$ is the screened structure matrix whose elements in the most tight-binding representation are essentially zero beyond the second shell of neighbours in all closed packed structures.

The summation over the composite angular momentum index suggest that the TB-LMTO orbital do not preserve pure L character. Further $\dot{\phi}_{RL}^\alpha(r_R)$ and $\phi_{RL}^\alpha(r_R)$ are truncated outside the Wigner-Seitz spheres and the expansion coefficients vanish beyond the second shell of neighbours in all closed packed structures, so that all TB-LMTO orbitals are short ranged, resulting in a sparse Hamiltonian in this representation. This is ideal for real space calculations based on the recursion method. The Hamiltonian and overlap matrices for this basis are given by (with neglect of small terms) :

$$H = h + hoh + (I + ho)E_\nu(I + ho) \quad (2.14)$$

$$o = \langle \chi | \chi \rangle = (I + ho)(I + ho) \quad (2.15)$$

In these equations the summation indices RL, are suppressed for convenience. The matrix o is diagonal in RL representation and its value is determined by the logarithmic derivative of the function $\dot{\phi}$ at the sphere boundary. The Löwdin orthonormalized Hamiltonian in the ASA is given by :

$$H^{(2)} = E_\nu + h - hoh + hohoh - \dots \quad (2.16)$$

and the first order Hamiltonian is given by

$$H^{(1)} = E_\nu + h \quad (2.17)$$

The parameter o determines the degree of non-orthogonality of the basis. Again o^{-1} has the dimension of energy and provides a measure of the energy window about the reference energy E_ν for which the density of states obtained with $H^{(1)}$ are reliable.

In order to perform self-consistent calculation in ASA, one needs the electron density $\rho_R(r)$

$$\rho_R(r) = \frac{1}{4\pi} \sum_l \left[m_{Rl}^{(0)} \phi_{Rl}(r)^2 + 2m_{Rl}^{(1)} \phi_{Rl}(r) \dot{\phi}_{Rl}(r) + m_{Rl}^{(2)} \{ \dot{\phi}_{Rl}(r)^2 + \phi_{Rl}(r) \ddot{\phi}_{Rl}(r) \} \right] \quad (2.18)$$

where $m_{Rl}^{(q)}$ represents energy moments

$$m_{Rl}^{(q)} = \int^{E_F} dE N_{Rl}(\varepsilon) (\varepsilon - E_{\nu, Rl})^q \quad (2.19)$$

and density matrix $N_{Rl}(\varepsilon)$ represents projected density of states

$$\begin{aligned} N_{Rl}(\varepsilon) &= \sum_j \delta(\varepsilon - \varepsilon_j) \sum |c_{Rl,j}|^2 \\ &= \Omega/(2\pi)^3 \int d\mathbf{k} \delta[\varepsilon - \varepsilon_j(\mathbf{k})] \sum |c_{Rl,j}(\mathbf{k})|^2 \end{aligned}$$

The zeroth moment $m^{(0)}$ determines the number of l -electrons, and $m^{(1)}$ and $m^{(2)}$ determine the radial redistribution of the l -charge. Here $\rho_R(r)$ is only the valence electron charge density, to which one has to add the spherically symmetric core electron (atomic) contribution, in order to obtain the total spheridized electron density.

In each iteration, after obtaining the charge density and the potential, one has to solve the radial Schrödinger (or Dirac-Pauli) equation again to obtain the basic quantities $\phi_{Rl}, \dot{\phi}_{Rl}, \ddot{\phi}_{Rl}$ and the potential parameters $C_{Rl}, \Delta_{Rl}, \gamma_{Rl}$ and p_{Rl} ; and this cycle is to be repeated.

It is essential to mix input and output densities in an appropriate proportion to obtain a new input density. The simplest procedure is linear mixing [Dederichs and Zeller (1983)]

$$\rho_{M+1}^{in} = \zeta \rho_M^{out} + (1 - \zeta) \rho_M^{in} = \rho_M^{in} + \zeta \{F[\rho_M^{in}] - \rho_M^{in}\}$$

where ζ is the mixing parameter ($0 < \zeta \leq 1$) that moderates the large charge oscillations and $F[\rho]$ is the Kohn-Sham functional. Several other iteration schemes like 'Anderson mixing' [Anderson (1964), Hamann (1979)], 'Broyden mixing' [Broyden (1965), Johnson (1988)] have been developed.

In standard LMTO calculation, one solves either the non-relativistic Schrödinger equation or the scalar-relativistic (Dirac-Pauli) equation; in the latter, one omits the spin-orbit coupling term (thus keeping spin as a good quantum number), but retaining all other relativistic kinematic effects [Koelling and Harmon (1977)].

While performing density functional calculations one needs to solve not only Schrödinger equation but also Poisson equation, and with the ASA method this involves approximating not only the potential but also the charge density. Thus the ASA total energy per unit cell can be written as

$$E = T + \sum_R U_R + U_M \quad (2.20)$$

First term in right hand side denotes kinetic energy of valance electrons. The second term is intra-sphere interaction energy between electrons and ion in that sphere and the third term is inter-sphere electrostatic energy (Madelung) term.

2.1.3 Configuration averaging in disordered systems

The concept of configuration averaging is central to the study of the disordered systems. The potentials which describe the disordered solids are characterized by random parameters. A particular realization of these parameters in a given sample is the configuration of the system. One needs to take the average over all possible configuration to study the physical properties of solids. The averaging over configurations is carried out with the idea of spatial ergodicity. Since the system is microscopically large one can partition it into subsystems each of which resembles a configuration of the system. The average over the subsystem is the same as the average over all configurations. There are several approaches for configuration averaging in disordered systems.

Rigid band approximation (RBA)

In the rigid band approximation, the shape of the density of states is taken to be same throughout the concentration range with only shift in the position of the Fermi energy due to change in the filling. This gives crude picture of the effect of change in electron to atom ratio on alloying.

The virtual crystal approximation (VCA)

In the virtual crystal approximation, the actual random alloy potential is replaced by an average periodic potential which is taken as the concentration weighted arithmetic mean of the constituent's potential. The effective Hamiltonian has no randomness and this approximation clearly misses out any scattering caused by random potential fluctuations about the average. The approximation is reasonable only if the random variation of the diagonal terms is very small. This serves as the starting point of more sophisticated iterative self consistent methods which are capable of capturing features characteristics of the disorder.

The Coherent Potential Approximation

The idea of a single site mean field approximation in a disordered system goes back as early as Raleigh. Landau and Lifshitz (1975) discussed about a mean field approximation in a problem of dielectric behaviour of spherical globules of one dielectric randomly dispersed in another. Soven (1967) applied almost similar ideas to the problem of motion of electrons in a random potential. He called this approximation the single-site coherent potential approximation or the CPA. The basic underlying idea is to obtain an effective Hamiltonian H^{eff} which is lattice translationally symmetric and the representations of its Green function or resolvent $G^{\text{eff}}(z) = (zI - H^{\text{eff}})^{-1}$ are good approximations of the averaged Green function or resolvent of the random Hamiltonian. In general, such an effective ‘‘Hamiltonian’’ is both complex and energy dependent and hence not hermitian.

Within a coherent potential approximation, for a tight binding random Hamiltonian of the form

$$H = \sum_R \varepsilon_R p_R + \sum_R \sum_{R'} V_{RR'} t_{RR'} \quad (2.21)$$

popularly known as Anderson model is given by

$$H^{\text{eff}} = \sum_R E(z) p_R + \sum_R \sum_{R'} V_{RR'} t_{RR'}$$

Here $p_R = |R\rangle\langle R|$ and $t_{RR'} = |R\rangle\langle R'|$ are projection and transfer operators on the space spanned by the tight-binding basis $\{|R\rangle\}$ and ε_R are random alloy potential.

By definition,

$$\ll G(z) \gg = G^{\text{eff}}(z)$$

The effective diagonal term $E(z)$ may be complex but lattice translationally symmetric, i.e. independent of the label i . We have assumed that the off-diagonal terms $V_{RR'}$ are unchanged. If we write $E(z) = \ll \varepsilon \gg + \Sigma(z)$, the correction to the VCA, $\Sigma(z)$, is called the *self-energy*. Within the CPA the self-energies are totally diagonal.

The effective coherent potential $E(z)$ is unknown. To estimate it, let us consider the effective Hamiltonian and replace the effective potential $E(z)$ at any one site, say R , by the exact random potential ε_R . The Hamiltonian of this system is like that of a single random impurity

$$H^{(R)} = H^{\text{eff}} + (\varepsilon_R - E(z)) p_R = H^{\text{eff}} + h$$

Simple algebra gives,

$$G_{RR}^{(R)}(z) = \frac{G_{RR}^{\text{eff}}}{1 - (\varepsilon_R - E(z)) G_{RR}^{\text{eff}}}$$

The coherent potential approximation chooses that $E(z)$ which satisfies :

$$\ll G^{(R)}(z) \gg_R = G^{\text{eff}}(z) = \ll G(z) \gg$$

That is,

$$\left\langle \frac{\varepsilon_R - E(z)}{1 - ((\varepsilon_R - E(z)) \ll G_{RR}(z) \gg)} \right\rangle = 0$$

Let us consider the case where the ε_R has a binary distribution, taking the values ε_A and ε_B with probabilities x and y respectively. The above equation then reduces to

$$\Sigma(z) = \frac{xy(\varepsilon_A - \varepsilon_B)^2 \ll G_{RR}(z) \gg}{1 - (\tilde{\varepsilon} - \Sigma(z)) \ll G_{RR}(z) \gg} \quad (2.22)$$

where $\tilde{\varepsilon} = y\varepsilon_A + x\varepsilon_B$.

This is a self-consistent equation for the CPA self-energy. Müller-Hartmann (1973) has shown that the above implicit equation always has a solution with the following properties :

- (i) $\Sigma(z)$ has singularities only on the real z axis.
- (ii) It is analytic everywhere outside the real z axis. The imaginary part of $\Sigma(z)$ is always negative or zero in the upper half z -plane and always positive or zero in the lower half.
- (iii) In case the spectrum of $\ll G(z) \gg$ is bounded, $\Sigma(z) \rightarrow 0$ as $z \rightarrow \pm\infty$ along the real z axis.

The averaged Green function is said to be *herglotz* if the self-energy satisfies these properties. This ensures that the density of states is always positive or zero and the spectrum is always real. Green functions of hermitian Hamiltonians are always herglotz. However, effective Hamiltonians are not necessarily hermitian and we must ensure that they yield herglotz Green functions to be physically relevant approximations. The CPA is a good approximation in this sense. Moreover, the self-energy has the correct form in the two solvable limits : the impurity limit $x \rightarrow 0$ and the weak scattering limit $\varepsilon_A \rightarrow \varepsilon_B$. We note that the self-energy is indeed diagonal. This yields the result $\ll G(z) \gg = G^{VCA}(z - \Sigma)$, which indicates that the CPA Green function is a mapping of the VCA one via the energy dependent mapping $z \rightarrow z - \Sigma(z)$.

2.1.4 The augmented space theorem

Mathematical description of the configuration space

One of the main conceptual hurdles in understanding the augmented space theorem has been the visualization of the configuration space of a set of random variables. Yet the idea is quite common in other fields. A very simple, yet essentially non trivial example is that of the Ising model. Since most readers seem comfortable enough with this model, we shall illustrate some of the basic ideas behind our description with it.

The model consists of a set of *spins* $\{\sigma_R\}$ arranged on a discrete lattice labeled by R . Each spin σ_R can have two possible *states* or *configurations* which we can denote as $|\uparrow_R\rangle$ and $|\downarrow_R\rangle$. The collection of all linear combinations of these two states : $\{a|\uparrow_R\rangle + b|\downarrow_R\rangle\}$ is called the *configuration space* of σ_R . It is of rank two and is *spanned* by the states $|\uparrow_R\rangle$ and $|\downarrow_R\rangle$. Let us call this space ϕ_R .

The set of, say, N spins then have 2^N possible *configurations* each of which can be written as a *sequence* of m up-states and $(N-m)$ down-states. The ordering of this sequence is crucial, since different orderings correspond to different configurations. The number $(N-m)$ is defined as the *cardinality* of the configuration and the sequence $\{C\}$ of sites $\{R_{i_1}, R_{i_2}, \dots, R_{i_k} \dots R_{i_{N-m}}\}$ where the down-states are called the *cardinality sequence* of the configuration. For example, take a particular configuration of 5 spins : $|\uparrow_1\downarrow_2\downarrow_3\uparrow_4\downarrow_5\rangle$. It has cardinality 3 and a cardinality sequence $\{2, 3, 5\}$. Another configuration $|\downarrow_1\uparrow_2\downarrow_3\downarrow_4\uparrow_5\rangle$ also has a cardinality 3, but its cardinality sequence is $\{1, 3, 4\}$. These two configurations are distinct from each other.

Note that the cardinality sequence uniquely describes the configuration and is a very convenient way of labeling the different configurations $\{|C_k\rangle\}$ (where $k=1, 2, \dots, 2^N$) of the set of N spins. The configuration space Φ is of rank 2^N and can be written as a direct product of the configuration spaces of the individual spins.

$$\Phi = \prod_R \phi_R$$

The generalization of these ideas when the *spins* can have $n > 2$ states is quite straightforward. The configurations of an individual spin can be labeled as $|k_R\rangle$, where $k_R=1, 2, \dots, n$. The rank of ϕ_R is now n . The set of N spins has n^N configurations. The cardinality of the configuration of an individual spin is defined as the particular k_R and the cardinality sequence uniquely describes a configuration of the set of N spins is the sequence $\{k_1, k_2, \dots, k_N\}$.

If we now translate our ideas from spins σ_R to the random variables ε_R of the Anderson model, we can immediately visualize the configuration space of the Hamiltonian variables

$\{\varepsilon_R\}$. When these terms have a binary distribution, their configuration space is isomorphic to the one for a collection of Ising spins.

Let us now assume that the variables $\{\varepsilon_R\}$ are independently distributed and the probability densities are given by $p(\varepsilon_R)$. We shall take into account only those probability densities which have finite moments to all orders. Physically relevant densities almost all fall in this category. Since the probability densities are positive definite functions, we can always write them as spectral densities of a positive definite operator as follows :

$$\begin{aligned} p(\varepsilon_R) &= (-1/\pi) \Im m \langle \emptyset | ((\varepsilon_R + i0)I - M_R)^{-1} | \emptyset \rangle \\ &= (-1/\pi) \Im m g(\varepsilon_R + i0) \end{aligned} \quad (2.23)$$

If ε_R has a binary distribution, taking the values 0 and 1 with probabilities x and $y=1-x$, then a representation of M is

$$\begin{pmatrix} x & \sqrt{xy} \\ \sqrt{xy} & y \end{pmatrix}$$

We may interpret this in terms of the configuration space ϕ_R introduced earlier. The configuration space is spanned by the states $|0\rangle$ and $|1\rangle$, which are eigenstates of M_R with eigenvalues 0 and 1. This is rather similar to the description in quantum mechanics, where an observable taking a random set of values is associated with an operator whose eigenvalues are the possible values observed and the states of the system in which the observable takes a particular value corresponds to the related eigenstate. The operator M_R in the configuration space ϕ_R will be associated with the random variable ε_R . The representation of M_R shown above is in a different basis :

$$\begin{aligned} |\emptyset\rangle &= (\sqrt{x} |0\rangle + \sqrt{y} |1\rangle) \\ |\{R\}\rangle &= (\sqrt{y} |0\rangle - \sqrt{x} |1\rangle) \end{aligned}$$

The reason for choosing this particular basis will become clear later. The state $|\emptyset\rangle$ will be called the *average state* of the system.

For a general probability distribution, we may always find the representation of the operator M_R in a similar basis by first expanding the probability density as a continued fraction.

$$g(\varepsilon_R) = -(1/\pi) \frac{1}{\varepsilon_R - a_0 - \frac{b_1^2}{\varepsilon_R - a_1 - \frac{b_2^2}{\ddots}}} \quad (2.24)$$

Here $p(\varepsilon_R) = \Im m g(\varepsilon_R)$. Since it is a positive definite function with finite moments to all orders, $p(\varepsilon_R)$ can be expanded as a convergent continued fraction. The required representation of the matrix M_i is given by

$$\begin{pmatrix} a_0 & b_1 & 0 & 0 & \dots \\ b_1 & a_1 & b_2 & 0 & \dots \\ 0 & b_2 & a_2 & b_3 & \dots \\ \dots & \dots & \dots & \dots & \dots \end{pmatrix}$$

The average state is defined by $|\emptyset\rangle = \sum_k \sqrt{x_k} |k\rangle$ where k are the random values taken by ε_R with probabilities x_k . The other members of the countable basis $|n\rangle$, in which the above representation of M_R is given, may be obtained recursively from the average state through :

$$\begin{aligned} |0\rangle &= |\emptyset\rangle \\ b_1|1\rangle &= M_R|0\rangle - a_0|0\rangle \\ b_n|n\rangle &= M_R|n-1\rangle - a_{n-1}|n-1\rangle - b_{n-1}|n-2\rangle \end{aligned}$$

The close relation of the above procedure to the recursion method described in the previous chapter should be noted. This is not surprising, since the projected density of states and the probability density are both positive definite and integrable functions. Convergence of the continued fraction further requires finite moments to all orders in both the cases.

The augmented space theorem

Let us now consider the average of a well-behaved function $f(\varepsilon_R)$ of ε_R . By definition :

$$\ll f(\varepsilon_R) \gg = \int f(\varepsilon_R) p(\varepsilon_R) d\varepsilon_R \quad (2.25)$$

Equation (2.25) may be rewritten as :

$$\ll f(\varepsilon_R) \gg = \oint f(z) g(z) dz$$

The integral is taken over a closed contour enclosing the singularities of $g(z)$ but not any of $f(z)$. We assume here that $f(z)$ is well behaved, in the sense that it has no singularities in the neighbourhood of a singularity of $g(z)$.

We now expand the function $g(z)$ in the basis of its eigenstates $\{|\mu\rangle\}$ of M_i . These may be either discrete or continuous. This expansion can be written as a Stielje's integral in terms of the spectral density function $\rho(\mu)$ of M_i

$$\begin{aligned} \ll f(\varepsilon_R) \gg &= \int d\rho(\mu) \langle \emptyset | \mu \rangle \left[\oint f(z) (z - \mu)^{-1} \right] \langle \mu | \emptyset \rangle \\ &= \langle \emptyset | \left[\int d\rho(\mu) |\mu\rangle f(\mu) \langle \mu| \right] | \emptyset \rangle \end{aligned}$$

The second line requires the function to be well behaved at infinity. The expression in brackets on the right side of the bottom equation is, by definition, the operator $f(M_R)$. It is the same functional of M_R as $f(\varepsilon_R)$ was of ε_R . For example, if $f(\varepsilon_R)$ is ε_R^2 then $f(M_R)$ is M_R^2 . This yields the central equation of the augmented space theorem :

$$\ll f(\varepsilon_R) \gg = \langle \emptyset | f(M_R) | \emptyset \rangle \quad (2.26)$$

The result is significant, since we have reduced the calculation of averages to a particular matrix element of an operator in the configuration space of the variable. Since we have applied the theorem to a single variable alone, the power of the above theorem is not apparent. Let us now go back to the Anderson model where we have a set of random variables $\{\varepsilon_i\}$ which we have assumed to be independently distributed. The joint probability distribution is given by :

$$P(\varepsilon_{R_1}, \varepsilon_{R_2}, \dots, \varepsilon_{R_i} \dots) = \prod_i p(\varepsilon_{R_i}) \quad (2.27)$$

The generalization of the above theorem to averages of functions of the set of random variables is straightforward.

$$\ll f(\{\varepsilon_R\}) \gg = \langle \emptyset | \tilde{f}(\{\widetilde{M}_R\}) | \emptyset \rangle \quad (2.28)$$

All operators in the full configuration space Φ will be denoted by tilde variables. The operators \widetilde{M}_R are built up from the operators M_R as :

$$\widetilde{M}_R = I \otimes I \otimes \dots \otimes M_R \otimes I \otimes \dots \quad (2.29)$$

This is the *augmented space theorem* (Mookerjee (1973)).

If we wish to carry out the configuration averaging of, say, the Green function element

$$G_{RR}(z) = \langle R | (zI - H(\{\varepsilon_{R'}\}))^{-1} | R \rangle$$

The theorem leads to :

$$\ll G_{RR}(z) \gg = \langle R \otimes \emptyset | (z\tilde{I} - \tilde{H}(\{\tilde{M}_{R'}\}))^{-1} | R \otimes \emptyset \rangle \quad (2.30)$$

where,

$$\tilde{H} = \sum_R p_R \otimes \tilde{M}_R + \sum_R \sum_{R'} V_{RR'} t_{RR'} \otimes \tilde{I}$$

The power of the theorem now becomes apparent. The average is seen to be a particular matrix element of the Green function of an augmented Hamiltonian. This is constructed out of the original random Hamiltonian by replacing the random variables by the corresponding configuration space operators built out of their probability distributions. This augmented Hamiltonian is an operator in the augmented space $\Psi = \mathcal{H} \otimes \Phi$ where \mathcal{H} is the space spanned by the tight binding basis and Φ the full configuration space. The result is *exact*. Approximations can now be introduced in the actual calculation of this matrix element in a controlled manner. The augmented Hamiltonian has no randomness in it and therefore various techniques available for the calculation of the Green functions for non-random systems may be resorted to. In particular we shall show that the recursion method is ideally suited for obtaining matrix elements in augmented space. Since configuration averaging is an intrinsically difficult problem, we must pay the price for the above simplification. This comes in the shape of the enormous rank of the augmented space. For some time it was thought that recursion on the full augmented space was not a feasible proposition. However, we shall describe later that, if randomness is homogeneous in the sense that $p(\varepsilon_R)$ is independent of the label R , then the augmented space has a large number of local point group and lattice translational symmetries. These can be utilized to reduce vastly the rank of the effective space on which the recursion can be carried out. Recursion on augmented space can be done with ease, even on desktop computers.

The coherent potential approximation within the augmented space formalism

The coherent potential approximation can be derived from the augmented space Hamiltonian using the mean field ideas of Soven. Let us partition the augmented space of an Anderson model into the subspace which includes a particular site, say R and its configurations ϕ . For a binary distribution of the diagonal elements this space is of rank two and is spanned by $|R \otimes \{\emptyset\}\rangle$ and $|R \otimes \{R\}\rangle$. We project the remainder part of Φ onto the subspace spanned by configurations of cardinality zero and replace the

Hamiltonian in the subspace by a lattice translationally symmetric effective Hamiltonian : $\sum_{R' \neq R} E(z) \mathcal{P}_{R'} + \sum_{R''} \sum_{R'} V_{R'R''} \mathcal{I}_{R'R''}$. This is equivalent to replacing the entire Hamiltonian except that of the site R by the effective Hamiltonian, as was done in the derivation of the usual CPA. The Hamiltonian becomes :

$$\left(\begin{array}{c|cccc} \bar{\varepsilon} & W & V & V & V & \dots \\ \hline W & \tilde{\varepsilon} & V & V & V & \dots \\ V & V & E(z) & V & V & \dots \\ V & V & V & E(z) & V & \dots \\ V & V & V & V & E(z) & \dots \\ \dots & \dots & \dots & \dots & \dots & \ddots \end{array} \right)$$

where $W = xy(\varepsilon_A - \varepsilon_B)^2$.

We shall now use the partition or downfolding theorem, which states that if we partition a space into two subspaces \mathcal{A} and \mathcal{B} and consequently the Hamiltonian as

$$\left(\begin{array}{c|c} H_A & H_{AB} \\ \hline H_{BA} & H_B \end{array} \right)$$

then the resolvent in the subspace \mathcal{A} is,

$$\mathcal{P}_A(zI - H)^{-1} \mathcal{P}_A = \mathcal{P}_A(zI - \hat{H})^{-1} \mathcal{P}_A$$

where

$$\hat{H} = H_A + H_{AB} \mathcal{P}_B(zI - H_B)^{-1} \mathcal{P}_B H_{BA}$$

If \mathcal{A} is the subspace spanned by $|i \otimes \{\emptyset\}\rangle$, then by the augmented space theorem the Green function projected on this subspace is the configuration averaged Green function. With this interpretation the above two equations become :

$$\ll G_{RR}(z) \gg = \langle R \otimes \{\emptyset\} | (zI - \hat{H})^{-1} | R \otimes \{\emptyset\} \rangle$$

and

$$\hat{H} = \bar{\varepsilon} + W G_{(R\{R\}), (R, \{R\})}^{(R\{\emptyset\})}(z) W = \bar{\varepsilon} + \Sigma(E)$$

We note that in order to calculate the Green function on the right hand side of the above equation, we have to consider the full effective CPA Hamiltonian and replace the diagonal matrix element $E(z)$ at the site labeled by R by $\tilde{\epsilon}$. This is the familiar single impurity problem and the relevant Green function can be written down immediately

$$G_{(R\{R\}), (R\{R\})}^{(R\{\emptyset\})}(z) = \frac{\ll G(z) \gg}{(1 - (\tilde{\epsilon} - \Sigma(z)) \ll G(z) \gg)}$$

Substituting this in the expression for \hat{H} we get

$$\Sigma(z) = \frac{xy(\epsilon_A - \epsilon_B)^2 \ll G_{RR}(z) \gg}{1 - (\tilde{\epsilon} - \Sigma(z)) \ll G_{RR}(z) \gg}$$

This is exactly the expression for the CPA self-energy derived earlier.

Properties and limitations of CPA

The CPA preserves the analytical properties of the Green function for any range of alloy parameters (i.e. for any compositional concentration and any scattering strength of constituents atoms). In particular, the CPA yields the coherent potential functions and Green functions, total as well as conditionally averaged, which are analytic everywhere in the complex energy plane except for poles and branch cuts along the real axis inside the host and impurity bands. This generally means that the CPA yields analytic, physically meaningful results, in particular non-negative densities of states or Bloch spectral functions.

The CPA becomes exact in three important limiting cases, namely in the low concentration limit, in the weak scattering limit, and in the so-called split-band limit (the separation of constituents bands is large as compared to their bandwidths). The last case corresponds to alloys of transition metals with simple metals or transition-metal alloys with vacancies. The CPA also provides a good interpolation procedure between these limits, and it is more accurate than any other single-site theory.

Despite the lack of including local environmental fluctuations and cluster effects, the CPA generally gives reliable concentration dependent trends for ground-state physical quantities like the local density of states, charge densities, magnetization densities, total energies, lattice constants, and related quantities. Generally, the accuracy of the CPA decreases with decreasing dimensionality of the translational invariance, or, more chemically speaking, with decreasing nearest-neighbor coordination. In particular, cluster effects influence physical quantities more in two-dimensional alloys than in their three-dimensional counterparts.

The essence of an application of the CPA in the framework of the LMTO formalism consists in two steps: first, the configurational average of the auxiliary Green function of the system in a non-random LMTO representation is performed and second, the transformation to the physical, orthogonal LMTO representation is performed in order to obtain the corresponding site-diagonal and site non-diagonal blocks of the configurationally averaged physical Green function matrix, from which all quantities of interest can be determined.

As it is well known, a single-site, mean-field theory fails to take into account statistical fluctuations with respect to the chemical composition of an alloy. Short-range order effects can significantly influence certain physical properties of alloys such as the formation of magnetic moments or the localization of states in disordered systems. Also charge transfer effects in alloys cannot be fully described within a single-site theory.

There have been many attempts to develop a cluster generalization of the CPA but most of them failed because of lacking analytical properties of the resulting configurationally averaged Green function. The traveling cluster approximation and the augmented-space recursion method seem to provide an improvement of the CPA while preserving its analytical properties.

2.2 Recursion method

The local environment approach in the electronic structure of solids require an alternative to band theory for solving the Schrödinger equation. When the electrons interact strongly within the atom the band theory picture breaks down and the properties essentially depend on only the first few shells of neighbour of each atom. The d- electrons of the transition metals are prime examples of this regime. While the band theory is still a valid formal solution to the Schrödinger equation, the physics is better understood by means of solution that explicitly accounts for the role of local environment. The recursion method introduced by Haydock *et al* (1972) is a lucid approach in this direction. It expresses the Hamiltonian in a form that couples an atom to its first neighbour, then through them to its distant neighbours and so on.

Mathematically, a new orthonormal basis set $\{|u_n\rangle\}$ in which the Hamiltonian is tridiagonal is constructed by a three term recurrence relation.

$$\tilde{H}|u_n\rangle = a_n|u_n\rangle + b_{n+1}|u_{n+1}\rangle + b_n|u_{n-1}\rangle$$

The recursion coefficients a_n and b_n are generated by

$$\begin{aligned} a_n &= \langle u_n | \tilde{H} | u_n \rangle \\ b_n &= \langle u_{n-1} | \tilde{H} | u_n \rangle \end{aligned}$$

The configuration averaged Green function then can be written as a continued fraction

$$\langle\langle G_{RL,RL}(z) \rangle\rangle = \frac{1}{z - a_0 - \frac{b_1^2}{z - a_1 - \frac{b_2^2}{\dots \frac{b_N^2}{z - a_N - b_{N+1}^2 T(z)}}}}$$

For an infinitely large system the continued fraction does not terminate at any finite step. The continued fraction approach is meaningful only if we can estimate what its asymptotic part would be from a set of initial coefficients. This asymptotic part is called the *terminator*. The theory of convergent continued fractions indicates that the asymptotic part determines the essential singularities of the Green function, *i.e.* the band edges and the band weights. The band edges can be determined, first crudely, from a few initial continued fraction coefficients and then refined by noting how they converge as we include a few more coefficients. Once the band edges e_{min} and e_{max} and the band weight w are estimated, the model herglotz function is generated as :

$$F(z) = 8 w \left[z - \frac{e_{max} + e_{min}}{2} - \sqrt{(z - e_{min})(z - e_{max})} \right] / (e_{max} - e_{min})^2$$

The continued fraction coefficients which yield $F(z)$ are

$$\begin{aligned} \hat{a}_n &= (e_{max} + e_{min})/2 && \text{for all } n \\ \hat{b}_n &= (e_{max} - e_{min})/4 && \text{for all } n \end{aligned}$$

Luchini and Nex (1987) suggested that rather than butt-joining of the terminator coefficients to the first n_1 exactly calculated coefficients, we splice them smoothly as follows :

$$\hat{a}_n = \begin{cases} a_n & n < n_1 \\ 1/2 \{ (1 - \sin\{\delta(n + \phi)\})a_n + (1 + \sin\{\delta(n + \phi)\})\hat{a}_n \} & n_1 < n < n_2 \\ \hat{a}_n & n_2 < n \end{cases}$$

$$\hat{b}_n = \begin{cases} b_n & n < n_1 \\ 1/2 \{ (1 - \sin\{\delta(n + \phi)\})b_n + (1 + \sin\{\delta(n + \phi)\})\hat{b}_n \} & n_1 < n < n_2 \\ \hat{b}_n & n_2 < n \end{cases}$$

where $\delta = \pi/(n_2 - n_1)$ and $\phi = -(n_1 + n_2)/2$.

We now proceed to obtain run two further recursions. The first one obtains two sets of orthogonal polynomials corresponding to the three term recursion :

$$\begin{aligned} P_{n+1}(z) &= (z - a_n)P_n(z) - b_n^2 P_{n-1}(z) \\ Q_{n+1}(z) &= (z - a_n)Q_n(z) - b_n^2 Q_{n-1}(z) \end{aligned}$$

where $P_1(z) = 0 = Q_0$ and $P_0 = 1 = Q_{-1}$.

The second one, starts with a state $|0\rangle = F(z)$ and obtains a set of coefficients $\{\gamma_n, \delta_n\}$ from :

$$|n+1\rangle = (z - \gamma_n)|n\rangle - \delta_n^2 |n-1\rangle$$

where the inner product is defined by a union of Gauss-Chebyshev quadrature :

$$\langle f|g\rangle = \sum_i \omega_i f(\alpha_i)g(\alpha_i)$$

with

$$\omega_i = \frac{\pi w}{n+1} \sin^2 \vartheta_i$$

$$\alpha_i = a_i + (1 - \cos \vartheta_i)(e_{max} - e_{min})/2$$

$$\vartheta_i = \frac{i\pi}{n+1}$$

From these continued fraction coefficients, exactly as above, we generate two sets of orthogonal polynomials

$$\begin{aligned} R_{n+1}(z) &= (z - \gamma_n)R_n(z) - \delta_n^2 R_{n-1}(z) \\ S_{n+1}(z) &= (z - \gamma_n)S_n(z) - \delta_n^2 S_{n-1}(z) \end{aligned}$$

The terminator is then

$$T(z) = \frac{S_{n_2-2}(z) - F(z)R_{n_2-1}(z)}{\delta_{n_2-1}^2 [S_{n_2-3}(z) - F(z)R_{n_2-2}(z)]} \quad (2.31)$$

Since $F(z)$ is a herglotz function and $R_n(z)$ and $S_n(z)$ are polynomials, the above equation shows that the terminator $T(z)$ is also herglotz. The Green function is then given by

$$G(z) = \frac{Q_{n_2-2}(z) - b_{n_2-1}^2 T(z)Q_{n_2-3}(z)}{P_{n_2-1}(z) - b_{n_2}^2 T(z)P_{n_2-2}(z)} \quad (2.32)$$

There is an extensive literature on the construction of terminators (Luchini and Nex (1987)). We refer the reader to these for further mathematical details. All terminators are herglotz and require no further input other than the first n_1 continued fraction coefficients.

2.3 Augmented space recursion

We shall propose a different path to implement the incorporation of the effects of environment fluctuation in disordered system. We wish to apply the recursion method, described by Haydock in the previous section directly on the augmented space without carrying out any mean-field like approximations. We shall describe the method in a realistic model for binary alloys.

2.3.1 The Hamiltonian in augmented space

The starting point for the augmented space recursion is the most localized, sparse, tight-binding Hamiltonian, derived systematically from the LMTO-ASA theory and generalized to substitutionally disordered random binary alloys :

$$\begin{aligned}
H_{RL,R'L'}^\alpha &= \hat{C}_{RL} \delta_{RR'} \delta_{LL'} + \hat{\Delta}_{RL}^{1/2} S_{RL,R'L'}^\alpha \hat{\Delta}_{R'L'}^{1/2} \\
\hat{C}_{RL} &= C_{RL}^A n_R + C_{RL}^B (1 - n_R) \\
\hat{\Delta}_{RL}^{1/2} &= (\Delta_{RL}^A)^{1/2} n_R + (\Delta_{RL}^B)^{1/2} (1 - n_R)
\end{aligned} \tag{2.33}$$

Here R labels the lattice sites and $L=(\ell m)$ are the orbital indices (for transition metals $\ell < 2$), C_{RL}^A , C_{RL}^B and Δ_{RL}^A , Δ_{RL}^B are the potential parameters of the constituents A and B of the alloy. n_R are the local site occupation variables which randomly take values 1 and 0 according to whether the site is occupied by an A atom or not. From the discussion in section 4, it is clear that the Hamiltonian in augmented space \tilde{H} consists of replacing the local site occupation variables $\{n_R\}$ by $\{M_R\}$, and is given by :

$$\begin{aligned}
\tilde{H} &= \sum_{RL} \left(C_{RL}^B \tilde{I} + \delta C_{RL} \tilde{M}_R \right) \otimes \mathcal{P}_R + \dots \\
&+ \sum_{RL} \sum_{R'L'} \left((\Delta_{RL}^B)^{1/2} \tilde{I} + \delta \Delta_{RL} \tilde{M}_R \right) S_{RL,R'L'}^\alpha \left((\Delta_{R'L'}^B)^{1/2} \tilde{I} + \delta \Delta_{R'L'} \tilde{M}_{R'} \right) \otimes \mathcal{T}_{RR'}
\end{aligned}$$

where,

$$\begin{aligned}
\delta C_{RL} &= (C_{RL}^A - C_{RL}^B) \\
\delta \Delta_{RL} &= \left((\Delta_{RL}^A)^{1/2} - (\Delta_{RL}^B)^{1/2} \right)
\end{aligned}$$

Other parameters have their usual meaning and \tilde{I} is the identity operator defined in the augmented space, \tilde{M}_R is given by:

$$\tilde{M}^R = x \mathcal{P}_R^0 + y \mathcal{P}_R^1 + \sqrt{xy} \left(\mathcal{T}_R^{01} + \mathcal{T}_R^{10} \right) \tag{2.34}$$

\mathcal{P}_R^0 and \mathcal{T}_R^{10} are projection and transfer operators in the augmented space, where each site R is characterized by two states labeled 0 and 1, which may be identified with the up and down states of an Ising system. The configuration states are stored extremely efficiently in bits of words and the algebra of the Hamiltonian in the configuration space mirrors the multi-spin coding techniques used in numerical works with the Ising model.

The augmented Hamiltonian is an operator in a much enlarged space $\Phi = \mathcal{H} \otimes \prod \phi^R$ (the augmented space), where \mathcal{H} is the Hilbert space spanned by the countable basis set $\{|R\rangle\}$ (the real space). The enlarged Hamiltonian does not involve any random variables

but incorporates within itself the full information about the random occupation variables. If we substitute for M_R , then with the aid of little algebra we can show that the augmented space Hamiltonian contains operators of the following types :

- (a) $\mathcal{P}_R \otimes \tilde{I}$ and $\mathcal{T}_{RR'} \otimes \tilde{I}$. These operators acting on a vector in the augmented space changes only the real space label, but keeps the configuration part unchanged.
- (b) $\mathcal{P}_R \otimes \mathcal{T}_R^{01}$, $\mathcal{P}_R \otimes \mathcal{T}_{R'}^{01}$, $\mathcal{T}_{RR'} \otimes \mathcal{T}_R^{01}$ and $\mathcal{T}_{RR'} \otimes \mathcal{T}_{R'}^{01}$. These operators acting on an augmented space vector may or may not change the real space label. In addition, they may also change the configuration at the site R or R' . This resembles a single spin-flip Ising operator in configuration space.
- (c) $\mathcal{P}_R \otimes \mathcal{T}_R^{01} \otimes \mathcal{T}_{R'}^{01}$ and $\mathcal{T}_{RR'} \otimes \mathcal{T}_R^{01} \otimes \mathcal{T}_{R'}^{01}$. These operators may change the real space label, as well as the configuration either at R or R' or both. This resembles a double spin flip Ising operator in the configuration space.

A basis $|m\rangle$ in the Hilbert space \mathcal{H} is represented by a column vector C_m with zeros everywhere except at the m -th position. The inner products are defined as

$$\langle m|n\rangle = C_m^T C_n$$

$$\mathcal{P}_m C_p = \delta_{mp} C_p$$

$$\mathcal{T}_{mn} C_p = \delta_{np} C_m$$

We may represent this basis by a collection of binary words (strings of 0's and 1's) . As described earlier, the number of 1's define the cardinality of the basis and the sequence of positions at which we have 1's $\{ C \}$ called the cardinality sequence labels the basis

Thus a binary sequence $B[\{ C \}]$ is a representation of the member of the basis in the configuration space. The inner product between the basis members is then

$$(B[\{ C \}], B[\{ C' \}]) = \delta(\{ C \}, \{ C' \})$$

A careful examination of the operations (a)-(c) defined on the configuration space, reveals that these operations change the cardinality and the cardinality sequence . Since the operations are defined on the bits of words, one can easily employ the logical functions in a computer, to define these operations.

Symmetry reduction of the augmented space rank

We note that the recursion basis $|u_n\rangle$ is generated from the starting state $|u_0\rangle$ by repeated application of the Hamiltonian. If the starting state belongs to an irreducible subspace of \mathcal{H} then all subsequent recursion generated states will belong to the same irreducible subspace. Physically we may understand this as follows : the recursion states $|u_n\rangle$ carry information of distant environment of the starting state. For example, $|u_1\rangle$, which, apart from the orthogonalization subtractions, is essentially $H|u_0\rangle$, is a combination of states in the nearest shell with which $|u_0\rangle$ couple via the Hamiltonian. Similarly, $|u_n\rangle$ is a combination of n-th neighbour shell with which $|u_0\rangle$ is coupled via the Hamiltonian. If \mathfrak{R} is a point group symmetry of the Hamiltonian, then all n-th neighbour shell states which are related to one another through the symmetry operator must have equal coupling to $|u_0\rangle$. Hence, it is useful to consider among the n-th neighbour shell states of which $|u_n\rangle$ is a linear combination, only those belonging to the irreducible subspace and redefine the Hamiltonian operation.

As an example, take a nearest neighbour s-state Anderson model on a square lattice. The starting state $|(00)\rangle$ belongs to the one dimensional representation of the square lattice point group. This state then couples with linear combinations of states on neighbour shells which are symmetric under square rotations :

$$\begin{aligned} |(0m)\rangle &= (|(0m)\rangle + |(m0)\rangle + |(\bar{m}0)\rangle + |(0\bar{m})\rangle) / 2 \\ |(11)\rangle &= (|(11)\rangle + |(1\bar{1})\rangle + |(\bar{1}1)\rangle + |(\bar{1}\bar{1})\rangle) / 2 \\ |(nm)\rangle &= (|(nm)\rangle + |(\bar{n}m)\rangle + |(n\bar{m})\rangle + |(\bar{n}\bar{m})\rangle + \dots \\ &\quad |(mn)\rangle + |(\bar{m}n)\rangle + |(m\bar{n})\rangle + |(\bar{m}\bar{n})\rangle) / (2\sqrt{2}) \end{aligned}$$

If we go up to N shells (if N is large) there are about $2N^2$ states in the diamond shaped nearest neighbour cluster. However there are only $(N^2/4 + N/2) \sim N^2/4$ states with square symmetry. We need only to work in 1/8 of the lattice but attach correct weights to the states to reproduce correct matrix elements. This reduction is standard in Brillouin zone integrations in reciprocal space, but not so prevalent in real space calculations.

If $|I\rangle$ and $|J\rangle$ are two states coupled to each other via the Hamiltonian, and both belong to the same irreducible subspace, and let $|I_1\rangle, |I_2\rangle \dots |I_{W_I}\rangle$ be states obtained by operating on $|I\rangle$ by the symmetry group operations of the real space lattice. W_I is called the *weight* associated with the state labeled by I . If we wish to retain only the states in the irreducible subspace and throw out the others and yet obtain the same results, we redefine the Hamiltonian matrix elements as follows :

$$\langle I|H|J\rangle \rightarrow \sqrt{\frac{W_J}{W_I}}\beta_J(LL')\langle I|H|J\rangle$$

The factor $\beta_J(LL')$ requires explanation. The new irreducible basis, which is a linear combination of the tight-binding basis, reflects not only the symmetries of the underlying lattice, but the symmetry of the starting orbital (spherical if it is a s-state, cylindrical if it a p-state and an e_g or t_{2g} symmetry if it is a d-state) also. This symmetry of the starting orbital prohibits overlap at particular sites. These positions we shall define to be the *symmetry positions* with respect to the overlapping orbitals. These position depends on the L and L' content of I and J. If the state J is a symmetry position with respect to LL' then $\beta_J(LL')$ is 0 otherwise it is 1.

If disorder is homogeneous, then the cardinality sequence in configuration space itself has the symmetry of the underlying lattice. For example, in square lattice, the four configurations are equivalent. It is obvious they are related to one another by the symmetries of the square lattice. Thus in augmented space equivalent states are $|R \otimes \{C\}\rangle$ and the set $|\mathfrak{R}R \otimes \{\mathfrak{R}\{C\}\}\rangle$ for all different symmetry operators \mathfrak{R} of the underlying lattice.

Diagonal formulation of ASR

In this formulation the Hamiltonian is put in the effective diagonal disorder form. To do this, we first suppress all the indices and express the Green function in the following form

$$\begin{aligned} \ll G(E) \gg &= \langle 1|(EI - H)^{-1}|1\rangle \\ &= \langle 1|(EI - C - \Delta^{1/2}S\Delta^{1/2})^{-1}|1\rangle \\ &= \langle 1|\Delta^{-1/2} \left[\frac{EI - C}{\Delta} - S \right]^{-1} \Delta^{-1/2}|1\rangle \end{aligned} \quad (2.35)$$

We now convert the above equation into augmented space. The augmented space theorem gives [Mookerjee (1973)]

$$\ll G_{RL,RL}(E) \gg = \langle R, L, \{\emptyset\} | (EI - H)^{-1} | R, L, \{\emptyset\} \rangle$$

First we note that :

$$\tilde{\Delta}_L^{-1/2}|R, L, \{\emptyset\}\rangle = \mathbf{A}(\Delta_L^{-1/2})|R, L, \{\emptyset\}\rangle + \mathbf{F}(\Delta_L^{1/2})|R, L, \{R\}\rangle = |1\rangle \quad (2.36)$$

and if we define $[\mathbf{A}(1/\Delta_L)]^{1/2} |1\rangle$ as $|1\rangle$, then this latter ket is normalized. We arrive at the convenient expression :

$$\ll G_{RL,RL}(E) \gg = \langle 1 | (E I - \hat{A} + \hat{B} + \hat{F} - \hat{S})^{-1} | 1 \rangle \quad (2.37)$$

where

$$\begin{aligned} \hat{A} &= \{\mathbf{A}(C_L/\Delta_L)/\mathbf{A}(1/\Delta_L)\} \mathcal{I} \otimes \mathcal{I} \otimes \mathcal{I} \\ \hat{B} &= \{\mathbf{B}((E - C_L)/\Delta_L)/\mathbf{A}(1/\Delta_L)\} \sum_{RL} \mathcal{P}_R \otimes \mathcal{P}_L \otimes \mathcal{P}_1^R \\ \hat{F} &= \{\mathbf{F}((E - C_L)/\Delta_L)/\mathbf{A}(1/\Delta_L)\} \sum_{RL} \mathcal{P}_R \otimes \mathcal{P}_L \otimes \{\mathcal{T}_{10}^R + \mathcal{T}_{01}^R\} \\ \hat{S} &= \sum_{RL} \sum_{R'L'} \left\{ \mathbf{A}(1/\Delta_L)^{-1/2} \right\} S_{RL,R'L'} \left\{ \mathbf{A}(1/\Delta_L)^{1/2} \right\} \mathcal{T}_{RR'} \otimes \mathcal{T}_{LL'} \otimes \mathcal{I} \end{aligned} \quad (2.38)$$

where

$$\begin{aligned} \mathbf{A}(P) &= x P_A + (1 - x) P_B \\ \mathbf{B}(P) &= (1 - 2x) (P_A - P_B) \\ \mathbf{F}(P) &= \sqrt{x(1 - x)} (P_A - P_B) \end{aligned}$$

This equation is now exactly in the form in which the recursion method may now be applied. The computational burden is considerably reduced due to this diagonal formulation, the recursion now becomes energy dependent as is clear from the form of the effective Hamiltonian and discussed in Biswas *et al* (1995), Ghosh *et al* (1999). This energy dependence makes the recursion technique computationally unsuitable because to obtain the Green functions we have to carry out recursion per energy point of interest. This problem has been tackled using *seed recursion technique* Ghosh *et al* (1999). The idea is to choose a few seed points across the energy spectrum uniformly, carry out recursion over those points and then interpolate the values of coefficients across the band. In this way one may reduce computation time. For example, if one is interested in an energy spectrum of 250 points, in the bare diagonal formulation recursion has to be carried out at all the 250 points but in the seed recursion technique one needs to perform recursions only at 30-40 points. The whole idea stems from the fact that in most of the cases of binary alloys, it is seen that the recursion coefficients a_n and b_n vary quite weakly across the energy spectrum. At this point we note that the above expression for the averaged $\ll G_{LL}(E) \gg$ is exact.

LSDA self-consistency within the ASR

The local potentials seen by constituent atoms in a disordered alloy are very different from their atomic values or from their values in the corresponding ordered alloys. This is basically due to the redistribution of the valence charge densities on alloying. These potentials have to be self-consistently obtained within the LSDA.

The initial TB-LMTO potential parameters are obtained from suitable guess potentials : either from their atomic values or from the nearest related ordered configuration. In subsequent iterations the potentials parameters are obtained from the solution of the Kohn-Sham equation

$$\left\{ -\frac{\hbar^2}{2m} \nabla^2 + V^{\nu\sigma} - E \right\} \phi_{\sigma,L}^{\nu}(r_R, E) = 0 \quad (2.39)$$

where,

$$V^{\nu\sigma}(r_R) = V_{core}^{\nu\sigma}(r_R) + V_{har}^{\nu\sigma}(r_R) + V_{xc}^{\nu\sigma}(r_R) + V_{mad} \quad (2.40)$$

Here ν refers to the species of atom sitting at R and σ the spin component. The electronic position within the atomic sphere centered at R is given by $r_R = r - R$. The core potentials are obtained from atomic calculations and are available for most atoms.

The core potential is chosen to be identical to the free atom. The Hartree and exchange-correlation potentials within the LSDA are assumed to be functionals of the charge densities $\rho_{\sigma}^{\nu}(r_R)$ within the atomic spheres labeled by R . These local charge densities are obtained from the partially averaged Green functions :

$$\rho_{\sigma}^{\nu}(r_R) = \sum_L \int_{-\infty}^{E_F} dE |\phi_{\sigma,L}^{\nu}(r_R, E)|^2 n_{R,L}^{\nu,\sigma}(E)$$

where

$$n_{R,L}^{\nu,\sigma}(E) = -(1/\pi) \Im m \ll G_{RL,RL}^{\nu,\sigma}(E) \gg$$

where $\ll G_{RL,RL}^{\nu,\sigma}(R) \gg$ is the partially averaged Green function, with the atomic sphere centered at R occupied by an atom of the type ν and spin σ and the rest configurationally averaged over. These partial averages are obtained through the ASR.

The Hartree potential needs discussion. We call the atomic sphere centered at R : S_R . If we wish to obtain the Hartree potential within the atomic sphere S_R when an atom of the type ν sits at R , the configuration space at the site R is projected onto the fixed

configuration ν , while the configurations at the remaining sites is, say, random binary. Let us denote the ‘‘average state’’ by $\{\nu \in R \otimes \emptyset\}$.

$$V_{\text{har}}^{\nu\uparrow}(r_R) = e^2 \left[\int_{S_R} d^3 r'_R \frac{\rho_{\uparrow}^{\nu}(r'_R)}{|r_R - r'_R|} + \sum_{R'' \neq R} \int_{S_{R''}} d^3 r'_{R''} \frac{\langle \rho(r'_{R''}) \rangle}{|r_R - r'_{R''}|} + \sum_{R'' \neq R} \int_{S_{R''}} d^3 r'_{R''} \frac{\delta \rho(r'_{R''})}{|r_R - r'_{R''}|} \right]$$

where

$$\begin{aligned} \delta \rho(r'_{R''}) = & \int_{-\infty}^{E_F} dE \left[\langle \{r'_{R''} \otimes A \in R'' \otimes \emptyset\} | \tilde{\Gamma}(E) \otimes \tilde{M}_{R''} | \{r'_{R''} \otimes A \in R'' \otimes \emptyset\} \rangle \dots \right. \\ & \left. \dots - \langle \{r'_{R''} \otimes B \in R'' \otimes \emptyset\} | \tilde{\Gamma}(E) \otimes \tilde{M}_{R''} | \{r'_{R''} \otimes B \in R'' \otimes \emptyset\} \rangle \right] \end{aligned}$$

$\tilde{\Gamma}(E) = (-1/\pi) \Im m \tilde{G}(E)$, where $\tilde{G}(E)$ is the augmented space resolvent $(z\tilde{I} - \tilde{H})^{-1}$ and $\tilde{M}_{R''}$ is the configuration operator, e.g. for the binary randomness $\tilde{M}_{R''} = I \otimes \dots M_{R''} \otimes I \otimes \dots$ and, if x is the concentration of the A component :

$$M_{R''} = \begin{pmatrix} 0 & \sqrt{x(1-x)} \\ \sqrt{x(1-x)} & 1-x \end{pmatrix}$$

The first two terms are identical to the usual expressions for the CPA [Ling *et al* (1995)]. Of course, the partially averaged and averaged charge densities in the ASR have the effects of configuration fluctuation of the immediate environment of the atomic site associated with the atomic sphere included in them. The last term represents configuration fluctuations in the charge densities associated with atomic spheres other than S_R . This correction is taken only up to the nearest neighbour environment of S_R .

The exchange-correlation potential is a functional of the charge and magnetic moment densities : $\rho^{\nu}(r_R) = \rho^{\nu\uparrow}(r_R) + \rho^{\nu\downarrow}(r_R)$, and $m^{\nu}(r_R) = \rho^{\nu\uparrow}(r_R) - \rho^{\nu\downarrow}(r_R)$. Various forms of the exchange-correlation function are available. For example, that proposed by von Barth and Hedin is the most commonly used.

2.3.2 Generalized augmented space recursion

Ordering or segregation phenomena in binary alloys and their electronic properties are closely related to each other. The electronic energy is order-dependent and, in turn, governs the formation and stability of ordered, disordered and segregated structures. We

shall address the important problem of developing a first principles theory for predicting the tendency of ordering or segregation from electronic structure calculations. The tendency of ordering or segregation is governed by correlations in concentration between the neighbouring sites expressed in terms of the Warren-Cowley short range order parameter. Such correlations between constituent species are directly related to the behaviour of diffuse scattering and can be obtained from the quantitative intensity measurements on a single crystal. One needs a self-consistent first principles theory of correlated disorder in order to analyze such ordering tendencies.

A generalized form of the augmented space formalism has been proposed by Mookerjee and Prasad (1993) and Saha *et al* (1994) to deal with correlated disorder.

The generalized augmented space theorem

If the set of random variables $\{n_k\}$ are correlated, the joint probability density does not break up into a product of the individual probability densities. However, we may still break up the joint probability density in terms of conditional probability densities.

$$P(n_1, n_2, \dots, n_p, \dots) = p(n_1) p(n_2|n_1) p(n_3|n_2, n_1) \dots p(n_p|n_{p-1}, n_{p-2}, \dots, n_1) \dots$$

Like the probability densities, the conditional probability densities are also positive definite, integrable functions. We shall assume that moments of the conditional probability densities are finite to all orders. We have shown earlier that such functions can be written as the diagonal resolvent of an operator in configuration space of the random variable. The probability density $p(n_1)$ may be written as :

$$p(n_1) = -(1/\pi) \Im m \langle \emptyset_1 | (n_1 I - M_1)^{-1} | \emptyset_1 \rangle$$

We have chosen a particular basis $|\emptyset_1\rangle, |1_1\rangle, \dots, |c_1\rangle$ in which the representation of M_1 is tridiagonal. c_1 is the cardinality of the configuration at the site labeled 1. We have also stated earlier that the actual values taken by n_1 are the eigenvalues $\{m_1^{k_1}\}$ of M_1 and these values are taken with probabilities ω_{k_1} . It is easy to check that the *average state* may be expressed in terms of the eigenstates of M_1 and the probabilities as

$$|\emptyset_1\rangle = \sum_{k_1} \sqrt{\omega_{k_1}} |m_1^{k_1}\rangle$$

Let us define :

$$\tilde{M}_1 = M_1 \otimes I \otimes I \otimes \dots$$

Similarly, we may express the conditional probability $p(n_2|n_1)$ as

$$p(n_2|n_1 = m_1^{k_1}) = -(1/\pi) \Im m \langle \emptyset_2 | (n_2 I - M_2^{k_1})^{-1} | \emptyset_2 \rangle$$

Exactly as before, we may express the *average state* in terms of the eigenstates of $M_2^{k_1}$ and the conditional probabilities $\{\omega_{k_2}^{k_1}\}$

$$|\emptyset_2\rangle = \sum_{k_2} \sqrt{\omega_{k_2}^{k_1}} |m_2^{k_2}\rangle$$

and define,

$$\tilde{M}_2 = \sum_{k_1} P_1^{k_1} \otimes M_2^{k_1} \otimes I \otimes I \otimes \dots$$

where $P_1^{k_1}$ the projection operator onto the state k_1 at the site labeled 1.

In general :

$$p(n_p|n_{p-1} = m_{p-1}^{k_{p-1}}, \dots, n_1 = m_1^{k_1}) = -(1/\pi) \Im m \langle \emptyset_p | (n_p I - M_p^{k_1, k_2, \dots, k_{p-1}})^{-1} | \emptyset_p \rangle$$

and,

$$|\emptyset_p\rangle = \sum_{k_{p-1}} \sum_{k_{p-2}} \dots \sum_{k_1} \sqrt{\omega_{k_p}^{k_1, k_2, \dots, k_{p-1}}} |m_p^{k_p}\rangle$$

$$\tilde{M}_p = \sum_{k_1} \sum_{k_2} \dots \sum_{k_{p-1}} P_1^{k_1} \otimes P_2^{k_2} \dots \otimes M_p^{k_1, k_2, \dots, k_{p-1}} \otimes I \otimes I \otimes \dots$$

The algebra of these operators is straightforward and we note the following :

$$\langle \emptyset_p | \{M_p^{k_1, k_2, \dots, k_{p-1}}\}^r P_p^{k_p} | \emptyset_p \rangle = (m_p^{k_p})^r \omega_{k_p}^{k_1, k_2, \dots, k_{p-1}}$$

We may now define the total average state $|\{\emptyset\}\rangle$ as $\prod_p^\otimes |\emptyset_p\rangle$.

$$\begin{aligned} \langle \{\emptyset\} | [\tilde{M}_1]^{r_1} \otimes [\tilde{M}_2]^{r_2} \otimes \dots | \emptyset \rangle &= \langle \emptyset | [(M_1)^{r_1} \otimes I \dots] \otimes \left[\sum_{k_1} P_1^{k_1} \otimes (M_2^{k_1})^{r_2} \right] \otimes \\ &\quad \left[\sum_{k_1} \sum_{k_2} P_1^{k_1} \otimes P_2^{k_2} \otimes \dots (M_3^{k_1, k_2})^{r_3} \otimes I \otimes \dots \right] \otimes \dots | \emptyset \rangle \end{aligned}$$

Expanding the terms in the brackets and using the fact that $P_n^k P_n^{k'} = \delta_{kk'} P_n^k$ we obtain

$$\langle \emptyset | [\tilde{M}_1]^{r_1} \otimes [\tilde{M}_2]^{r_2} \otimes \dots | \emptyset \rangle = \sum_{k_1} \sum_{k_2} \dots (m_1^{k_1})^{r_1} (m_2^{k_2})^{r_2} \dots \omega_{k_1} \omega_{k_2}^{k_1, k_2} \omega_{k_3}^{k_1, k_2} \dots$$

If we now define a well-behaved operator

$$\tilde{F}(\{\tilde{M}_p\}) = \sum_{r_1} \sum_{r_2} \dots \sum_{r_p} \dots B_{r_1, r_2, \dots} \tilde{M}_1^{r_1} \tilde{M}_2^{r_2} \dots$$

It follows that,

$$\begin{aligned} \langle \emptyset | \tilde{F}(\{\tilde{M}_p\}) | \emptyset \rangle &= \sum_{k_1} \sum_{k_2} \dots \omega_{k_1} \omega_{k_2}^{k_1, k_2} \dots \sum_{r_1} \sum_{r_2} \dots B_{r_1, r_2, \dots} (m_1^{k_1})^{r_1} (m_2^{k_2})^{r_2} \dots \\ &= \sum_{k_1} \sum_{k_2} \dots \omega_{k_1} \omega_{k_2}^{k_1, k_2} \omega_{k_3}^{k_1, k_2} F(m_1^{k_1}, m_2^{k_2}, \dots) \\ &= \ll F(\{n_p\} \gg \end{aligned} \quad (2.41)$$

The conclusion is that the average of a function of a set of correlated random variables is also the matrix element, taken between the average state, of the operator constructed by replacing the random variables by the operators related to the conditional probabilities. This is the *generalized augmented space theorem*.

For electronic structure calculations in a disordered system, F is chosen to be the matrix element of the Green function $(zI - H(\{n_R\}))^{-1}$, where H is the random Hamiltonian of the system and n_R are the site occupation variables .

We shall now assume that short-range order is restricted to the first nearest-neighbour shell *alone*. This is a reasonable assumption, based on the fact that short-range order decreases rapidly with distance . Hence the variables associated with sites beyond first neighbour shell will be assumed to be random with no correlation with the central site

The macroscopic state of order for a AB binary alloy is described in terms of the Warren-Cowley short-range order parameter

$$\alpha_r^{AB} = 1 - \frac{P_r^{AB}}{y} \quad (2.42)$$

with the B atom occupying the r th nearest neighbour site of the central A atom. $y = 1 - x$ is the macroscopic concentration of the species B and P_r^{AB} is the joint probability of finding a B atom anywhere in the r -th shell.

The probability density associated with the sites R' , belonging to the first nearest neighbour shell of R , is given by

$$\begin{aligned} p(n_{R'}|n_R = 0) &= (y + \alpha x)\delta(n_{R'}) + (1 - \alpha)x \delta(n_{R'} - 1) \\ p(n_{R'}|n_R = 1) &= (x + \alpha y)\delta(n_{R'} - 1) + (1 - \alpha)y \delta(n_{R'}) \end{aligned} \quad (2.43)$$

where n_R is the variable associated with central atom and $\alpha = \alpha_1^{AB}$

Following the augmented space procedure described earlier, we first generate the operators \tilde{M}_k for the binary distribution. The site R is associated with the label 1, and is the site at which the averaged Green function is calculated.

The augmented space operator associated with the independent probability density is given by,

$$\tilde{M}_R = \{x\mathcal{P}_R^0 + y\mathcal{P}_R^1 + \sqrt{xy}(T_R^{01} + xT_R^{10})\} \quad (2.44)$$

At the neighbouring sites R' , the operator associated with the conditional probability density is

$$\begin{aligned} \tilde{M}_{R'} &= x\mathcal{P}_R^0 \otimes \mathcal{P}_{R'}^0 + y\mathcal{P}_R^0 \otimes \mathcal{P}_{R'}^1 + X\mathcal{P}_R^1 \otimes \mathcal{P}_{R'}^0 + X'\mathcal{P}_R^1 \otimes \mathcal{P}_{R'}^1 \\ &+ B_1\mathcal{P}_R^0 \otimes (T_{R'}^{01} + T_{R'}^{10}) + B_2\mathcal{P}_R^1 \otimes (T_{R'}^{01} + T_{R'}^{10}) \\ &+ B_3(T_{R'}^{01} + T_{R'}^{10}) \otimes \mathcal{P}_{R'}^0 + B_4(T_{R'}^{01} + T_{R'}^{10}) \otimes \mathcal{P}_{R'}^1 \\ &+ B_5(T_{R'}^{01} + T_{R'}^{10}) \otimes (T_{R'}^{01} + T_{R'}^{10}) \end{aligned}$$

Various constants in the equation are defined through the following relations,

$$\begin{aligned} X &= x - \alpha(x - y) & X' &= y + \alpha(x - y) \\ B_1 &= x\sqrt{(1 - \alpha)y(x + \alpha y)} + y\sqrt{(1 - \alpha)x(y + \alpha x)} \\ B_2 &= y\sqrt{(1 - \alpha)y(x + \alpha y)} + x\sqrt{(1 - \alpha)x(y + \alpha x)} \\ B_3 &= \alpha\sqrt{xy} & B_4 &= -\alpha\sqrt{xy} \\ B_5 &= \sqrt{xy} \left(\sqrt{(1 - \alpha)y(x + \alpha y)} - x\sqrt{(1 - \alpha)x(y + \alpha x)} \right) \end{aligned}$$

We should note that if $\alpha = 0$ the operator $\tilde{M}_{R'}$ reduces to the same form as \tilde{M}_R . Uncorrelated disorder turns out to be a special case with α set to 0.

We make explicit use of these operators and the central theorem for correlated random variables in the augmented space recursion method. The TB-LMTO Hamiltonian in the most localized representation may now be transformed to the augmented space Hamiltonian exactly in the same way as we did for uncorrelated disorder. Once the effective Hamiltonian has been constructed, the generalized augmented space theorem gives the configuration averaged Green function to be

$$\ll G_{RL,RL}(z) \gg = \langle RL, \emptyset | (E\tilde{I} - \tilde{H})^{-1} | RL, \{\emptyset\} \rangle$$

2.3.3 The effective pair interactions

We start from a completely disordered alloy. Each site R has an occupation variable n_R associated with it. For a homogeneous perfect disorder $\langle n_R \rangle = x$, where x is the concentration of one of the components of the alloy. In this homogeneously disordered system we now introduce fluctuations in the occupation variable at each site : $\delta x_R = n_R - x$. Expanding the total energy in this configuration about the energy of the perfectly disordered state we get :

$$E(x) = E^{(0)} + \sum_{R=1}^N E_R^{(1)} \delta x_R + \sum_{RR'=1}^N E_{RR'}^{(2)} \delta x_R \delta x_{R'} + \dots \quad (2.45)$$

The coefficients $E^{(0)}$, $E_R^{(1)}$... are the effective renormalized cluster interactions. $E^{(0)}$ is the energy of the averaged disordered medium. If we embed atoms of the type A or B at R in the disordered background and the total energies are E_A and E_B , then by the above equation :

$$E_R^{(1)} = E_A - E_B$$

This one body interaction results from the interchange of a B atom with an A atom at site R in the alloy.

Similarly, $E_{RR'}^{(2)}$ is the effective renormalized pair interaction which is the difference in the one body interactions at R , when site R' ($\neq R$) is occupied either by an A or a B atom.

$$E_{RR'}^{(2)} = E_{AA} + E_{BB} - E_{AB} - E_{BA}$$

For magnetic pair interaction energy we take the averaged non magnetic disordered medium and embed two similar atoms with two different spins up and down and calculate

pair interaction energy as explained above. The same we repeat for other components with two different spins, up and down. Then we embed the different atoms with similar as well as two different spins, up and down. This procedure gives us the magnetic pair interaction energies which are given as:

$$J_{AA}^{(2)} = E_{AA}^{\uparrow\uparrow} + E_{AA}^{\downarrow\downarrow} - E_{AA}^{\uparrow\downarrow} - E_{AA}^{\downarrow\uparrow}$$

Similarly,

$$J_{BB}^{(2)} = E_{BB}^{\uparrow\uparrow} + E_{BB}^{\downarrow\downarrow} - E_{BB}^{\uparrow\downarrow} - E_{BB}^{\downarrow\uparrow}$$

And,

$$J_{AB}^{(2)} = E_{AB}^{\uparrow\uparrow} + E_{AB}^{\downarrow\downarrow} - E_{AB}^{\uparrow\downarrow} - E_{AB}^{\downarrow\uparrow}$$

Therefore the effective magnetic pair interaction energy is given as:

$$J^{(2)} = J_{AA}^{(2)} + J_{BB}^{(2)} - 2J_{AB}^{(2)}$$

Thus we can arrive at the relation of effective pair interaction energy including magnetism as:

$$E_{RR'}^{(2)} = E_{AA}^{(2)} + E_{BB}^{(2)} - 2E_{AB}^{(2)} + J_{AA}^{(2)} + J_{BB}^{(2)} - 2J_{AB}^{(2)} \quad (2.46)$$

We will retain terms up to pair interactions in the configuration energy expansion. Higher order interactions may be included for a more accurate and complete description. For the phase stability study, it is the pair interaction which plays the dominant role.

The total energy of a solid may be separated into two terms : a one-electron band contribution E_{BS} and the electrostatic contribution E_{ES} . The renormalized cluster interactions should, in principle, include both E_{BS} and E_{ES} contributions. Since the renormalized cluster interactions involve the difference of cluster energies, it is usually assumed that the electrostatic terms cancel out and only the band structure contribution is important. Such an assumption though is not rigorously true, has been shown to hold good in a number of alloy systems [Heine (1988)]. Considering only band structure contribution, the effective pair interactions may be written as :

$$E_{RR'}^{(2)} = - \int_{-\infty}^{E_F} dE \left\{ -\frac{1}{\pi} \Im m \log \sum_{IJ} \det (G^{IJ}(E)) \xi_{IJ} \right\} \quad (2.47)$$

where, G^{IJ} represents the configurationally averaged Green function corresponding to the disordered Hamiltonian whose R and R' sites are occupied by I-th and J-th type of atom, and

$$\xi_{IJ} = \begin{cases} +1 & \text{if } I=J \\ -1 & \text{if } I \neq J \end{cases}$$

The behavior of this function is quite complicated and hence the integration by standard routines (e.g. Simpson's rule or Chebyshev polynomials) is difficult, involving many iterations before convergence is achieved. Furthermore the integrand is multi-valued, being simply the phase of $\sum_{IJ} \det(G^{IJ}) \xi_{IJ}$. The way out for this was suggested by Burke Burke (1976) which relies on the repeated application of the partition theorem on the Hamiltonian H^{IJ} . The final result is given simply in terms of the zeroes and poles of the Green function in the region $E < E_F$

$$E_{RR'}^{(2)} = 2 \sum_{IJ} \xi_{IJ} \sum_{k=0}^{\ell_{max}} \left[\sum_{j=1}^{z^{k,IJ}} Z_j^{k,IJ} - \sum_{j=1}^{p^{k,IJ}} P_j^{k,IJ} + (p^{k,IJ} - z^{k,IJ}) E_F \right] \quad (2.48)$$

where $Z_j^{k,IJ}$ and $P_j^{k,IJ}$ are the zeros and poles of the peeled Green's function G_k^{IJ} of disordered Hamiltonian with occupancy at sites R and R' by I and J of which first (k-1) rows and columns has been deleted. $p^{k,IJ}$ and $z^{k,IJ}$ are the number of poles and zeroes in the energy region below E_F .

The Augmented Space Recursion

As discussed in the previous section, the calculation of the effective pair interaction with out magnetism as well as with magnetism taken into account in our formalism reduces to the determination of the peeled configuration averaged green functions $\langle G_k^{IJ} \rangle$. We shall employ the ASR coupled with the TB-LMTO introduced by Andersen and Jepsen (1984) for a first principles determination of these configuration averaged quantities. We shall take the most localized, sparse tight binding first order Hamiltonian derived systematically from the LMTO theory within the ASA and generalized to random alloys. The form of the effective Hamiltonian used for recursion in augmented space for the calculation of the peeled Green functions is given as :

$$H_k^{IJ} = \sum_{\ell=k}^{\ell_{max}} C_{R,\ell}^I a_R^\dagger a_R + \sum_{\ell=1}^{\ell_{max}} C_{R',\ell}^J a_{R'}^\dagger a_{R'} + \sum_{R'' \neq R, R'} \sum_{\ell=1}^{\ell_{max}} \left(C_{R'',\ell}^B + \delta C_\ell \tilde{M}^{R''} \right) a_{R''}^\dagger a_{R''} + \dots \\ + \sum_{R'' \neq R} \sum_{L=k} \sum_{L'} \Delta_{R,\ell}^{1/2,I} S_{LL'}^{R,R''} \left(\Delta_{R'',\ell'}^{1/2,B} + \delta \Delta_{\ell'}^{1/2} \tilde{M}^{R''} \right) a_R^\dagger a_{R''} + \dots$$

$$\begin{aligned}
& + \sum_{R'' \neq R'} \sum_L \sum_{L'} \Delta_{R',\ell}^{1/2,I} S_{LL'}^{R',R''} \left(\Delta_{R'',\ell'}^{1/2,B} + \delta \Delta_{\ell'}^{1/2} \widetilde{\mathbf{M}}^{R''} \right) a_{R'}^\dagger a_{R''} + \dots \\
& + \sum_{R'' \neq R} \sum_L \sum_{L'=k} \left(\Delta_{R'',\ell}^{1/2,B} + \delta \Delta_{\ell}^{1/2} \widetilde{\mathbf{M}}^{R''} \right) S_{LL'}^{R'',R} \Delta_{R,\ell'}^{1/2,I} a_{R''}^\dagger a_R + \dots \\
& + \sum_{R'' \neq R'} \sum_L \sum_{L'} \left(\Delta_{R'',\ell}^{1/2,B} + \delta \Delta_{\ell}^{1/2} \widetilde{\mathbf{M}}^{R''} \right) S_{LL'}^{R'',R'} \Delta_{R',\ell'}^{1/2,I} a_{R''}^\dagger a_{R'} + \dots \\
& + \sum_{R'' \neq R, R'} \sum_{R''' \neq R, R'} \sum_L \sum_{L'} \left(\Delta_{R'',\ell}^{1/2,B} + \delta \Delta_{\ell}^{1/2} \widetilde{\mathbf{M}}^{R''} \right) S_{LL'}^{R'',R'''} \left(\Delta_{R''',\ell'}^{1/2,B} + \delta \Delta_{\ell'}^{1/2} \widetilde{\mathbf{M}}^{R'''} \right) \dots \\
& \dots \left(a_{R''}^\dagger a_{R'''} + a_{R'''}^\dagger a_{R''} \right)
\end{aligned} \tag{2.49}$$

here, L is a composite index (lm). For a binary distribution $\widetilde{\mathbf{M}}^R$ is given by:

$$\widetilde{\mathbf{M}}^R = x b_{R\uparrow}^\dagger b_{R\uparrow} + (1-x) b_{R\downarrow}^\dagger b_{R\downarrow} + \sqrt{x(1-x)} \left(b_{R\uparrow}^\dagger b_{R\downarrow} + b_{R\downarrow}^\dagger b_{R\uparrow} \right) \tag{2.50}$$

For non-isochoric alloys, the difference in atomic radii of the constituents lead to change in the electronic density of states, as confirmed by experiment [Wright *et al* (1987)] and approximate theoretical techniques [Bose *et al* (1992)]. One thus expects that the mismatch of size produces, in addition to a relaxation energy E_R contribution, a change in the band structure. Within our ASR, off-diagonal disorder in the structure matrix $S^{\mathcal{P}}$ because of local lattice distortions due to size mismatch of the constituents, can be handled on the same footing as diagonal disorder in the potential parameters which is discussed Section 2.4.1.

The ASR with the TB-LMTO Hamiltonian coupled with orbital peeling allows us to compute configuration averaged pair-potentials directly, without resorting to any direct averaging over a finite number of configurations. Saha *et al* (2004) have discussed how one uses the local symmetries of the augmented space to reduce the Hamiltonian and carry out the recursion on a reducible subspace of much lower rank. If we fix the occupation of two sites, the local symmetry of the augmented space is lowered (this is very similar to the lowering of spherical symmetry to cylindrical symmetry when a preferred direction is introduced in an isotropic system). We may then carry out the recursion in a suitably reduced subspace.

Static concentration wave method

The static concentration wave (SCW) was proposed as a theory for ordering by Khachatryan (1978, 1983). The occupation probability $n(\vec{r})$ plays the key role in this theory. This function $n(\vec{r})$ that determines the distribution of solute atoms in an ordered phase can be

represented as a superposition of concentration waves:

$$n(\vec{r}) = x + \frac{1}{2} \sum_j [Q(\vec{k}_j) \exp(i\vec{k}_j \cdot \vec{r}) + Q^*(\vec{k}_j) \exp(-i\vec{k}_j \cdot \vec{r})] \quad (2.51)$$

where $\exp(i\vec{k}_j \cdot \vec{r})$ is a static concentration wave, \vec{k}_j is a non zero wave vector defined in the first Brillouin zone of the disordered alloy, \vec{r} is a site vector of the lattice $\{\vec{r}\}$, index j denotes the wave vectors in the Brillouin zone, $Q(\vec{k}_j)$ is static concentration wave amplitude and x is the atomic fraction of the alloying element.

The study of phase stability requires accurate approximations to the configurational energy as well as the use of statistical models to obtain the configurational entropy. The configurational energy within the pair interaction can be represented in Fourier space as the product of the Fourier transform of the effective pair interaction $V(\vec{k})$ and that of the pair correlation function $Q(\vec{k})$:

$$E \simeq \left(\frac{N}{2}\right) \sum_{\vec{k}} V(\vec{k}) Q(\vec{k})$$

where N is the number of atoms. Minimization of E will naturally occur for states of order characterized by maxima in the $Q(\vec{k})$ pair correlation spectrum located in the regions of the absolute minima of $V(\vec{k})$. Consequently, much can be predicted about the types of ordering to be expected from a study of the shape of $V(\vec{k})$, particularly from a search of its absolute minima (special points). At these points,

$$|\nabla_h V(h)| = 0$$

This was pointed out by Landau and Lifshitz (1969,1980), Krivoglaz and Smirnov (1964) and Khachaturyan (1978, 1983). Different types of ordered structures can be related directly to the minima of $V(\vec{k})$. In other words, given the knowledge of concentration wave vectors, one can readily predict the most stable ordered structure of the system at low temperatures. This is comparable to the knowledge derived from the studies like those based on X-ray, electron and neutron diffraction. A peak at the Γ point, $\mathbf{k} = (000)$, indicates the phase separation, while a peak at the Γ point, $\mathbf{k} = (100)$, in a FCC lattice suggests ordering. Peaks away from special points may correspond to the formation of long period superstructures. Within a simple mean field approximation, the instability can be obtained in the following way: If we add the expression for dominant quadratic term in the average energy to that of the configurational entropy under the simple mean field approximation we obtain an expression for the free energy:

$$F = \sum_{i,j} V_{ij}^2 (n_i - x)(n_j - x) + k_B T \sum_i [n_i \ln n_i + (1 - n_i) \ln(1 - n_i)]$$

where n_i is the concentration of the species A at the i -th site and c is the average concentration of that species. If we define a configuration variable γ_i^0 as $\langle \delta n_i \rangle_0$ (the symbol $\langle \dots \rangle_0$ denotes micro-canonical averaging), which is the variable relevant to the stability analysis, then the harmonic term in the Taylor expansion of the above free energy is

$$F^2 = \frac{N}{2} \sum_h \Gamma^*(\vec{k}(h)) F(\vec{k}(h)) \Gamma(\vec{k}(h)) \quad (2.52)$$

where, $\vec{k}(h) = 2\pi h_\alpha \vec{b}_\alpha$ and $\Gamma(\vec{k}(h)) = \mathcal{F}(n(\vec{r}) - x)$. The stability of a solid solution with respect to a small concentration wave of given wave vector $\vec{k}(h)$ is guaranteed as long as $F(\vec{k}(h))$ is positive definite. Instability sets in when $F(\vec{k}(h))$ vanishes i.e.

$$F(\vec{k}(h)) = k_B T^i + V(\vec{k}(h)) x (1 - x) = 0 \quad (2.53)$$

T^i being the temperature at which the instability sets in for the considered concentration wave. It appears from the above expression that under a simple mean field approximation the spinodal is always a parabola in the temperature-concentration (T,x) phase diagram, symmetric about $x = 0.5$. It is the concentration dependence of the effective pair interactions which brings about the asymmetry.

Experimentally the instability of the disordered phase to ordering may be seen in electron, x-ray or neutron scattering measurements. These are directly related to the Warren-Cowley short range order parameter $\alpha(\mathbf{k})$ which in turn is related to effective pair energies through [Ling *et al* (1994)]

$$\alpha(\mathbf{k}) = \frac{\beta x (1 - x)}{1 - \beta x (1 - x) V(\mathbf{k})} \quad (2.54)$$

Where $\beta = 1/(k_B T)$.

2.4 Computational details

We shall illustrate the applicability and accuracy of our various numerical details by taking the example Ni-Pt alloy systems.

2.4.1 Ordered alloys

We have performed the total energy density functional calculations for the ab-initio electronic structure description of alloys. The Kohn-Sham equations were solved in local spin density approximation (LSDA) with von Barth-Hedin (vBH) [von Barth and Hedin

(1972)] exchange correlations. The calculations have been performed in the basis of tight binding linear muffin-tin orbitals (TB-LMTO) in the atomic sphere approximation (TB-LMTO-ASA) [Andersen and Jepsen (1984), Andersen *et al* (1987, 1992), Andersen *et al* (1994), Das (2003)] including combined corrections. The calculations are semi-relativistic through inclusion of mass-velocity and Darwin correction terms.

Convergence with respect to Brillouin Zone k points

In Figure 2.1 we show the convergence of total energy and magnetic moments in Ni₃Pt alloy. This indicates that large Brillouin zone mesh resulting sufficiently large number of k points in the irreducible part of the Brillouin zone for k space integration is necessary to produce converged magnetic moments.

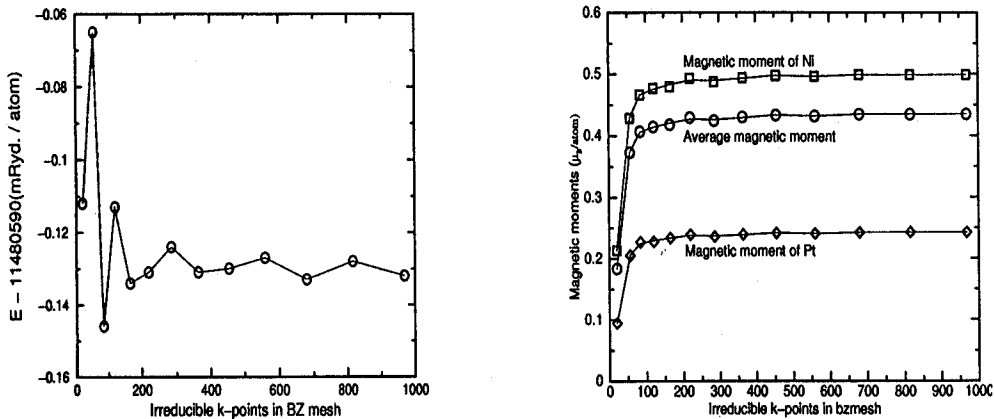


Figure 2.1: Variation of total energy and magnetic moments as a function number of k points in the Brillouin Zone (BZ) for Ni₃Pt alloy system.

Effect of tetragonal distortion in magnetism

Figure 2.2 shows the variation of total energy as well as magnetic moments in NiPt alloy as a function of tetragonal distortion. This shows that with the increase of tetragonal lattice distortion this alloy system slowly becomes paramagnetic. The LSDA calculation using TB-LMTO with von Barth and Hedin exchange correlation for NiPt ordered alloy reveals that at equilibrium lattice parameter ($c/a = 0.927$) this alloy system is paramagnetic. This agrees with the experimental prediction of Dahmani *et al* (1985).

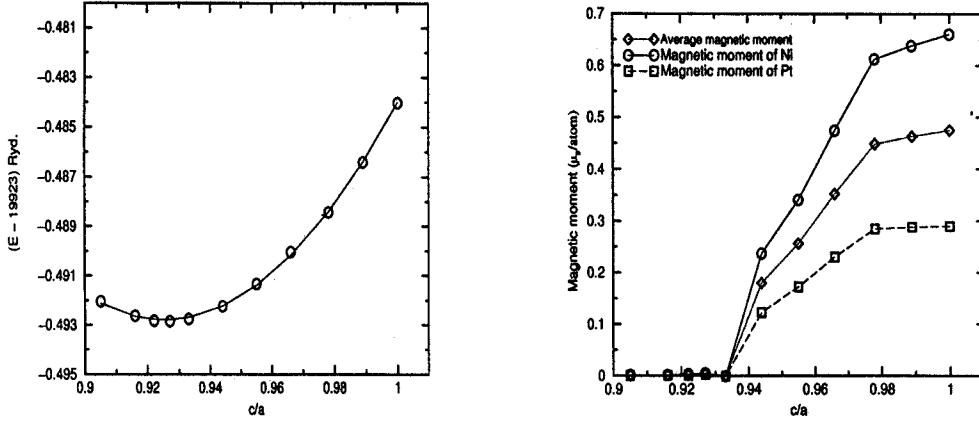


Figure 2.2: Variation of total energy and magnetic moments as a function of tetragonal distortion in NiPt alloy system.

2.4.2 Disordered alloys

In our present calculations using the example of Ni-Pt alloy system, we take the advantage of first principle TB-LMTO and calculate the self consistent relaxed potential parameters through a energy minimization procedure and then employ the charge neutrality procedure for the treatment of charge transfer effect. For 25 and 75% concentration of Pt in Ni-Pt alloy the energy minimization was done with varying total energies as a function of lattice parameter to get the equilibrium lattice parameter. In 50% concentration of Pt of ordered Ni-Pt alloy, it was experimentally observed that there is a tetragonal distortion. Since we are dealing with substitutional disorder, there may be a corresponding distortion in the disordered phase. In this case the energy minimization was done with varying total energies as a function of lattice distortion (c/a) to get equilibrium lattice distortion. Using this equilibrium lattice distortion we then applied the charge neutrality procedure for the treatment of charge transfer effect for this particular concentration.

In the following we discuss some of the issues related to electronic structure calculation of disordered alloys which need special attention.

Treatment of charge transfer

The treatment of charge transfer in disordered alloys has been a longstanding problem. This is because of the fact that to treat charge transfer in disordered alloys accurately one has to calculate the Madelung potential which is difficult as it depends upon the far environment in a given configuration. Therefore the calculation of Madelung potential is a challenging job for disordered alloys due to the absence of lattice periodicity. For the

treatment of the Madelung potential, we follow the procedure suggested by Andersen *et al* (1987, 1992) and further extended and implemented by [Kudrnovský and Drchal (1990)] for disordered alloys. We take the advantage of the flexibility of choice of atomic sphere radius in the TBLMTO-ASA to minimize the Madelung energy so as to make it negligible. We choose the atomic sphere radii of the components in such a way that they preserve the total volume on the average while the individual atomic spheres are almost charge neutral. The potential parameters in the alloy for the component Q(A or B) should be calculated at new radius $s_Q = (3V_Q/4\pi)^{1/3}$. The values of the potential parameters at the radii appropriate in the alloy phase s_Q can be obtained from the normal pressure radii s_Q^0 and the volume derivatives of the potential parameters using the logarithmic interpolation formulae.

$$\begin{aligned}
 C_Q^L &= C_Q^{0L} + \frac{dC_Q^L}{d \ln s_Q} \ln(s_Q/s_Q^0) \\
 \gamma_Q^L &= \gamma_Q^{0L} + \frac{d\gamma_Q^L}{d \ln s_Q} \ln(s_Q/s_Q^0) \\
 \Delta_Q^L &= \Delta_Q^{0L} \left[\frac{s_Q}{s_Q^0} \right]^{\frac{d \ln \Delta_Q^L}{d \ln s_Q}}
 \end{aligned}
 \tag{2.55}$$

The potential parameters Δ_Q^l and γ_Q^l of the constituent Q were then scaled by the factors $(s_Q/s^{alloy})^{2l+1}$. These potential parameters were used to parameterize the alloy Hamiltonian.

Lattice relaxation effect

(a) Deviation from Vegard's law :

Usual treatment of alloys with substitutional disorder place all atoms on a regular lattice whose lattice spacing is obtained by assuming Vegard's law. Vegard's law gives reasonably good results for those alloys made out of components with nearly equal atomic radii but fails for non isochoric alloys with components having large size mismatch. One therefore in general obtains equilibrium lattice constant from energy minimization with respect to the lattice constant. This approach takes into account differential expansion (contraction) around larger (smaller) atom for non-isochoric alloys. In Figure 2.3 we have shown the relative magnitudes of nearest neighbour distances for different concentrations of Pt in NiPt alloy system compared to Vegard's law values for average bond length. As the figure

shows, the nearest neighbour distances calculated using equilibrium lattice parameter is quite different than the Vegard's law values for average bond length.

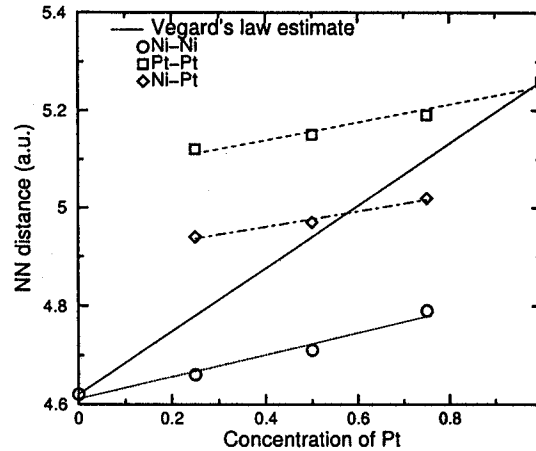


Figure 2.3: Nearest neighbour distance vs concentration of Pt with the choice of neutral charge spheres. For comparison the average bond length given by Vegard's law is shown in solid line.

(b) *Local lattice distortion :*

For non isochoric alloys whose constituents have large differences in atomic radii, one also has the possibility of local lattice distortions.

Various phenomenological theories of alloying such as the Hume-Rothery rules, state that size effects are significant for the study of phase stability. Local lattice distortions strongly influence mechanical properties of alloys like hardness and ductility. In magnetic alloys, local distortions may affect local magnetic moments.

Local lattice distortions essentially bring about disorder in the structure matrix and lead to off-diagonal disorder. An attempt to study the influence of lattice relaxation on electronic structure of concentrated alloys has been made by Kudrnovský and Drchal (1989) within the LMTO-CPA. They have suggested an approximate way of treating this through a mapping of the Hamiltonian onto an effective Hamiltonian with diagonal disorder alone. They assume a multiplicative form for the off-diagonal terms in the Hamiltonian. The random structure matrix is replaced by the non-random structure matrix of the undistorted lattice multiplied on two sides by site-diagonal random factors.

We wish to present the ASR as a formal way of dealing with off-diagonal disorder. There will be no need to assume a multiplicative form of the off-diagonal terms of the Hamiltonian. Structural disorder arising out of size mismatch is one candidate where a simple multiplicative form of an effective Hamiltonian may no longer be valid.

The random Hamiltonian for binary AB alloy described under the framework of the TB-LMTO is given by

$$\begin{aligned} \tilde{H} = & \sum \{C_L^A n_R + C_L^B (1 - n_R)\} \mathcal{P}_{RL} + \sum \sum \left\{ (\Delta_L^A)^{1/2} n_R + \dots \right. \\ & \left. (\Delta_L^B)^{1/2} (1 - n_R) \right\} S_{RL,R'L'} \left\{ (\Delta_{L'}^A)^{1/2} n_{R'} + (\Delta_{L'}^B)^{1/2} (1 - n_{R'}) \right\} \mathcal{T}_{RL,R'L'} \end{aligned}$$

where the potential parameters C and Δ at the site R can belong either to the A or the B atom depending upon which type of atom occupies R (i.e. n_R is 0 or 1). In absence of positional disorder, the structure matrix in the most localized representation is independent of the component atom type and is not random. However for non-isochoric alloys, the atoms get shifted from their undistorted positions.

The lattice distortion is essentially local and its effect on the structure matrix depends predominantly on the immediate environment. As an example, on a face-centered cubic lattice we can identify the smallest distorted tetrahedral units of nearest neighbour atoms. Possible configurations of A and B atoms occupying the corners of the units can be AAAA, AAAB, AABB, AB BB or BBBB. The AA and BB distances are different and the distance AB is the average of the two. The configurations obtained by rotation from other similar configurations have the same contribution to the structure matrix. Thus the structure matrix element between two points accruing in the unit will be given by

$$\begin{aligned} S_{RL,R'L'} = & S_{RL,R'L'}^{(AAAA)} n_R n_{R'} n_{R''} n_{R'''} + S_{RL,R'L'}^{(AAAB)} [n_R n_{R'} n_{R''} (1 - n_{R'''}) + \dots \\ & + (1 - n_R) n_{R'} n_{R''} n_{R'''} + n_R (1 - n_{R'}) n_{R''} n_{R'''} + n_R n_{R'} (1 - n_{R''}) n_{R'''}] + \dots \\ & + S_{RL,R'L'}^{(AABB)} [n_R n_{R'} (1 - n_{R''}) (1 - n_{R'''}) + (1 - n_R) n_{R'} (1 - n_{R''}) n_{R'''} + \dots \\ & + (1 - n_R) (1 - n_{R'}) n_{R''} n_{R'''} + (1 - n_R) n_{R'} n_{R''} (1 - n_{R'''}) + \dots \\ & + n_R (1 - n_{R'}) (1 - n_{R''}) n_{R'''} + n_R (1 - n_{R'}) n_{R''} (1 - n_{R'''})] + \dots \\ & + S_{RL,R'L'}^{(BBBA)} [n_R (1 - n_{R'}) (1 - n_{R''}) (1 - n_{R'''}) + (1 - n_R) n_{R'} (1 - n_{R''}) (1 - n_{R'''}) + \dots \\ & + (1 - n_R) (1 - n_{R'}) n_{R''} (1 - n_{R'''}) + (1 - n_R) (1 - n_{R'}) (1 - n_{R''}) n_{R'''}] + \dots \\ & + S_{RL,R'L'}^{(BBBB)} (1 - n_R) (1 - n_{R'}) (1 - n_{R''}) (1 - n_{R'''}) \end{aligned} \tag{2.56}$$

where $n_{R''}$ and $n_{R'''}$ describe the influence of the local environment on the structure matrix element connecting points R and R' . This description takes into account both the effect of distortions of the distance between R and R' and the angular distortion of the tetrahedron as we go from one configuration to another.

For the face-centered cubic lattice with structure matrix practically vanishing beyond the first nearest neighbour shell, number of such inequivalent configurations will be 144. Consideration of all these configurations will lead to an exact treatment of the distortion upto the first nearest-neighbour environment. However since, with the number of possible configurations increasing rapidly the computational effort very quickly becomes prohibitive, we shall assume that the dominant influence of off-diagonal disorder comes from the configurations of the two ends of the distorted bond extremities. This is the terminal point approximation. In this approximation only the bond stretchings or contractions are taken into account and all terms involving $n_{R''}$ and $n_{R'''}$ in the example of the tetrahedron are replaced by their averages. Thus, the effect of angular distortions is taken into account in an averaged sense. Invoking the terminal point approximation the number of inequivalent configurations of the bond become three : AA, AB and BB. The distribution of structure matrix is a tri-modal one.

$$S_{LL'}^{RR'} = S_{LL'}^{AA} n_R n_{R'} + S_{LL'}^{AB} [n_R (1 - n_{R'}) + (1 - n_R) n_{R'}] + S_{LL'}^{BB} (1 - n_R) (1 - n_{R'})$$

The Hamiltonian in the terminal point approximation is

$$\begin{aligned} H = & \sum (C_L^B + \delta C_L n_R) \mathcal{P}_{RL} + \sum \sum \left[(\Delta_L^B)^{1/2} (S_{RL,R'L'}^{BB} + (n_R + n_{R'}) S_{RL,R'L'}^{(1)} + \dots \right. \\ & \dots + n_R n_{R'} S_{RL,R'L'}^{(2)}) (\Delta_{L'}^B)^{1/2} + \delta \Delta_L (n_R S_{RL,R'L'}^{AB} + n_R n_{R'} S_{RL,R'L'}^{(3)}) (\Delta_{L'}^B)^{1/2} + \dots \\ & \left. \dots + (\Delta_L^B)^{1/2} (n_{R'} S_{RL,R'L'}^{AB} + n_R n_{R'} S_{RL,R'L'}^{(3)}) \delta \Delta_{L'} + \delta \Delta_L (n_R n_{R'} S_{RL,R'L'}^{(4)}) \delta \Delta_{L'} \right] \end{aligned} \quad (2.57)$$

where

$$\begin{aligned} \delta C_L &= C_L^B - C_L^A \\ \delta \Delta_L &= (\Delta_L^B)^{1/2} - (\Delta_L^A)^{1/2} \\ S_{RL,R'L'}^{(1)} &= S_{RL,R'L'}^{BB} - S_{RL,R'L'}^{AB} \\ S_{RL,R'L'}^{(2)} &= S_{RL,R'L'}^{AA} + S_{RL,R'L'}^{BB} - 2S_{RL,R'L'}^{AB} \\ S_{RL,R'L'}^{(3)} &= S_{RL,R'L'}^{AA} - S_{RL,R'L'}^{AB} \\ S_{RL,R'L'}^{(4)} &= S_{RL,R'L'}^{AA} + S_{RL,R'L'}^{BB} - S_{RL,R'L'}^{AB} \end{aligned}$$

The Hamiltonian in the augmented space is constructed by replacing the site occupation variables n_R by the operators M_R defined in configuration space. Once this Hamiltonian and its operations are defined, we apply the recursion method in augmented

space to obtain the continued fraction coefficients for the configuration averaged Green function. The degree of lattice distortion is however a delicate problem which calls for a first-principles treatment including minimization of the total energy with the degree of distortion. The corresponding calculations should provide both displacement of atoms and the electronic structure in the distorted lattice. Within the present computational implementation such calculation is still not possible. In our calculation, we therefore made further assumption concerning the degree of lattice distortion.

The calculation of the magnitude of lattice distortion has been carried out within the structural model given by rigid ion structure (RIS) [Mašek and Kudrnovský (1986)]. According to this model the lattice relaxes in such a way as to keep all the nearest neighbour distances close to the sum of the corresponding atomic radii for a particular concentration. This is found to be a reasonable model to deal with lattice relaxation effects in non-isochoric alloys [Saha and Mookerjee (1996)].

For a binary alloy of composition A_xB_y the volume V_{alloy} is written in terms of its constituents as

$$xV_A + yV_B = V_{alloy}. \quad (2.58)$$

The pressure volume relates the volume of the constituents in the alloy with their undistorted volume, V_A^0 and V_B^0 yields

$$\frac{(V_A - V_A^0)}{V_A^0} : \frac{(V_B - V_B^0)}{V_B^0} = \frac{\beta_B^0}{\beta_A^0} \quad (2.59)$$

where β_Q^0 ($Q = A, B$) are the bulk moduli of the components.

The solution of equations 2.58 and 2.59 yields the volumes of the constituents V_A and V_B as

$$V_A = \frac{\beta_B^0 V_{alloy} + yV_B^0(\beta_A^0 - \beta_B^0)}{xV_A^0\beta_B^0 + yV_B^0\beta_A^0} V_A^0 \quad (2.60)$$

$$V_B = \frac{\beta_A^0 V_{alloy} + yV_A^0(\beta_B^0 - \beta_A^0)}{xV_A^0\beta_B^0 + yV_B^0\beta_A^0} V_B^0 \quad (2.61)$$

This in turn gives the atomic radii of the constituents in a particular alloy system.

Considering the example of calculation of S_{LL}^{AB} , where B is the larger atom (*e.g.* Pt in the present case of Ni-Pt alloy), this matrix for a specific pair among 12 nearest neighbours connects an A atom at the site $(0, 0, 0)$ and a B atom. For example a B atom in the undistorted case would have been at the position $(\frac{a}{2}, \frac{a}{2}, 0)$ is now at $((\frac{a}{2} + d), (\frac{a}{2} + d), d)$,

where d is the displacement due to lattice distortion and a is the lattice constant. We have assumed that the lattice expands equally in the x , y and z directions. With these new coordinates and assuming that all other neighbouring coordinates are fixed at undistorted FCC positions, we compute the structure matrices S_{LL}^{AA} , S_{LL}^{AB} and S_{LL}^{BB} . This takes into account both the effect of radial distortion as well as angular distortion (the nearest neighbour is now $\sqrt{\frac{a^2}{2} + 2ad + 3d^2}$ instead of $\frac{a}{\sqrt{2}}$ and the nearest neighbour vector is $(\frac{a}{2} + d), (\frac{a}{2} + d), d$ instead of $(\frac{a}{2}, \frac{a}{2}, 0)$ in the above example). Consideration of rigid ion structure approximation and the knowledge of constituents atomic radii provides the value of d . The values of d for S_{LL}^{AB} came out to be $0.064 a$, $0.052 a$ and $0.054 a$ for 25%, 50% and 75% concentration of Pt in Ni-Pt alloy systems.

Effect of short range order

In most of the alloys there is either short range ordering or segregation tendency which actually determines the differences in phase stability properties. We have used the generalized augmented space recursion method which allows us to calculate the effect of short range order in the electronic structure of alloys. In augmented space recursion the Hamiltonian in the direct product space of real and configuration is written in terms of operator which replaces the local site occupation variables. In this case the joint probability distribution breaks up into individual probabilities. But in the case of generalized augmented space recursion the Hamiltonian which is written in terms of operator depends on the short range order parameter. In this case the joint probability is broken up into conditional probability densities. We perform recursion taking this generalized Hamiltonian to study the effect of the short range ordering in the electronic structure. In general the Warren Cowley short range order parameter decreases rapidly with distance. We have considered the correlation of central site with the sites of first neighbour.

Considering the example of Ni-Pt alloy system, the variation of total energy with a SRO parameter in this system shows a tendency towards ordering. In Figure 2.4 we show the variation of SRO parameter from segregation side to ordering side in particular for 55% concentration of Pt in Ni-Pt alloy. This tendency agrees with the experimental ordering behaviour of this system. The short range ordering is also found to have appreciable effect on the magnetic moments for NiPt alloy system. The value of magnetic moment including the SRO effect comes lower than the value without SRO effect and approaches the experimental value obtained by Parra and Cable (1980) which is discussed in detail in Chapter 3.

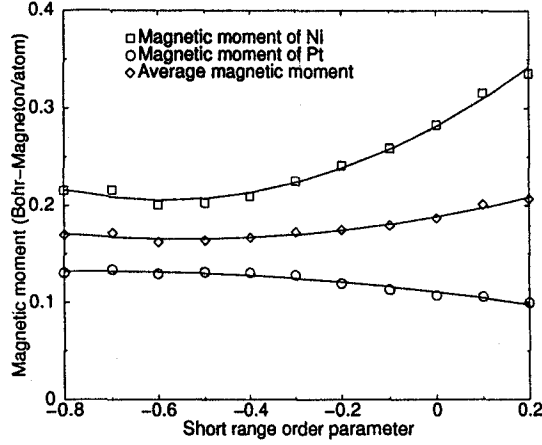


Figure 2.4: Variation of magnetic moments as a function of short range order parameter in $\text{Ni}_{45}\text{Pt}_{55}$ alloy system.

Convergence properties in augmented space recursion

For the calculation of physical properties of disordered alloys, the ASR coupled with first principle TB-LMTO has proved to be one of the successful and alternative to k-space integration methods. To establish the accuracy of the method one needs to carefully check errors in the recursion procedure in the augmented space and its convergence.

When we talk the convergence of the recursion method, we have to be careful in stating precisely what we mean. Finite space approximates to Green functions do not converge for real energy values. This problem arises in every computational method, as noted by Haydock *et al* (1972). The problem definitely arises in the usual k-space integration techniques, where methods using either complex energies or complex k-s have been attempted. The cause of this non-convergence is that an arbitrary small perturbation, like adding a single atom to a large but finite system, can shift all eigenvalues of the system. This causes an infinite change in the Green function near its corresponding poles. Thus, the precise meaning of the convergence of the recursion should imply rather the convergence of physical quantities built out of it. Most physical quantities are averages over the spectrum of the type :

$$F(E) = \int_{-\infty}^E f(E') n(E') dE'$$

It is the convergence of these quantities which will decide whether the recursion is convergent or not. For example, the Fermi energy is defined by

$$\int_{-\infty}^{E_F} n(E') dE' = n_e$$

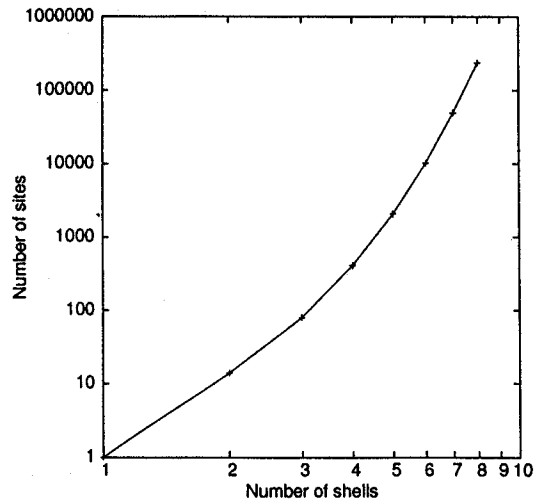


Figure 2.5: Log-log plot of the number of sites as we increase the number of shells in augmented space.

where n_e is the total number of electrons. While the band energy is

$$U = \int_{-\infty}^{E_F} E' n(E') dE'$$

We shall study in general the convergence of indefinite integrals of the kind

$$M_k(E) = \int_{-\infty}^E (E')^k n(E') dE'$$

The integrand E'^k is monotonic and well behaved within the integration range .

Errors can arise in the augmented space recursion because one can carry out only finite number of recursion steps and then terminate the continued fraction using available terminators. Also one chooses a large but finite part of the augmented space nearest neighbour map and ignores the part of the augmented space very far from the starting state. In Figure 2.5 we show how the number of sites increase as one increases the number of augmented space shells.

(a) *Error analysis on the continued fraction :*

We shall first carry out a simple error analysis of the continued fraction expression for the Green function because of errors created on the continued fraction coefficients. The procedure is similar to the one discussed by Haydock *et al* (1972)

The recursion is a two-term recurrence relation. We may therefore generate from this, a pair of linearly independent set of polynomials through the relations :

$$b_{n+1}X_{n+1}(E) = (E - a_n)X_n(E) - b_nX_{n-1} \quad (2.62)$$

where, X_n is either P_n or Q_n according to the initial conditions :

$$\begin{aligned} P_1(E) &= 1 & P_2(E) &= (E - a_1)/b_2 \\ Q_1(E) &= 0 & Q_2(E) &= 1 \end{aligned}$$

The approximated Green function in terms of the terminator $T(E)$ is given by :

$$G_N(E) = \frac{Q_{N+1}(E) - b_N Q_N(E)T(E)}{b_1 [P_{N+1}(E) - b_N P_N T(E)]}$$

The terminator determines entirely the essential singularities of the the spectrum. Haydock *et al* (1972) showed that a finite composition of fractional linear transformations like the one above can at most add a finite number of poles to the spectrum. The essential singularities of the exact $G(E)$ and $T(E)$ coincide. The fractional linear transformation redistributes the spectral weights over the spectrum.

Let us now assume that we make errors $\{\delta a_n, \delta b_n\}$ in the corresponding continued fraction coefficients. If we now start generating the orthogonal polynomials, starting from the exact initial conditions, but with the errors in the continued fraction coefficients, we shall obtain a pair of sets $\{\tilde{P}_n\}$ and $\{\tilde{Q}_n\}$. In general we shall have,

$$\tilde{P}_n(E) = (1 + A_n(E))P_n(E) + B_n(E)Q_n(E)$$

If we substitute this back into the recurrence relation and keep only the first order terms in the errors,

$$\begin{aligned} A_n(E) &= \{ \delta a_n [P_{n+1}(E)Q_{n+1}(E)] \\ &\quad + \delta b_n [P_n(E)Q_{n+1}(E) + P_{n+1}(E)Q_n(E)] \} / b_1 \\ B_n(E) &= \{ -\delta a_n P_{n+1}(E)^2 - \delta b_n [2 P_n(E)P_{n+1}(E)] \} / b_1 \end{aligned} \quad (2.63)$$

Using the above and the expression for the local density of states , we find that the first order relative error produced in the local density of states

$$\frac{\delta n(E)}{n(E)} = -2 \left[\left\{ \sum_{n=1}^{\infty} A_n(E) \right\} + b_1 R(E) \left\{ \sum_{n=0}^{\infty} B_n(E) \right\} \right]$$

where $R(E) = \text{Re } G(E)$. If we define the weighted Hilbert transforms of $P_n(E)$ as the so-called associated functions :

$$Q_n(E) = \text{Re} \left\{ \int_{-\infty}^{\infty} \frac{P_n(E')n(E')}{E - E'} dE' \right\}$$

These associated functions are also solutions of the three-term recursion. They are not polynomials, but are nevertheless orthogonal to the set $P_n(E)$. In terms of these, the error in the density of states is :

$$\frac{\delta n(E)}{n(E)} = \frac{2}{b_1} \left\{ \sum_{n=1}^{\infty} [\delta a_n P_{n+1}(E) Q_{n+1}(E) + 2 \delta b_{n+1} P_{n+1} Q_{n+2}] \right\} \quad (2.64)$$

The error in the Fermi energy will be given by :

$$\delta E_F = -\frac{1}{n(E_F)} \sum_{n=1}^{\infty} \left\{ \delta a_n A_n^{(0)}(E_F) + \delta b_{n+1} B_n^{(0)}(E_F) \right\} \quad (2.65)$$

While the error in the various moment functions are :

$$\delta M_k(E) = \delta E_F E_F^k n(E_F) + \sum_{n=1}^{\infty} \left\{ \delta a_n A_n^{(k)}(E_F) + \delta b_{n+1} B_n^{(k)}(E_F) \right\} \quad (2.66)$$

Where,

$$\begin{aligned} A_n^{(k)}(E) &= \frac{2}{b_1} \int_{-\infty}^E P_{n+1}(E') Q_{n+1}(E') (E')^k n(E') dE' \\ B_n^{(k)}(E) &= \frac{4}{b_1} \int_{-\infty}^E P_{n+1}(E') Q_{n+1}(E') (E')^k n(E') dE' \end{aligned} \quad (2.67)$$

(b) Termination Error :

In all computational calculations, the recursion can be carried out at most to a finite number of steps. After which the continued fraction is terminated by a terminator function $T(E)$ as discussed earlier. We have used the terminator of Luchini and Nex (1987) which smoothly joins onto the rest of the continued fraction and which reproduces the band widths, band weights and the essential singularities of the Green function at the band edges. Its spectral distribution is smooth, akin to a simple semicircular distribution.

Consider two situations, one in which we terminate at the N -th step, so that all coefficients for $n \leq N$ are free from the termination error; and another in which we terminate after $(N+r)$ steps. The recursive error in the Fermi energy and the band energy are :

$$\Delta E_F^{N+r,N} = -\frac{1}{n(E_F)} \sum_{n=N+1}^{N+r+1} (\delta a_n A_n^{(0)} + \delta b_{n+1} B_n^{(0)})$$

$$\Delta U^{N+r,N} = \sum_{n=N+1}^{N+r+1} \left\{ \delta a_n (A_n^{(1)} - E_F A_n^{(0)}) + \delta b_{n+1} (A_n^{(1)} - E_F A_n^{(0)}) \right\}$$

Here, $\Delta U^{N+r,N}$ is $\delta U^{N+r} - \delta U^N$ and δa_n and δb_{n+1} are the errors produced in these coefficients because of the termination where we replace the exact coefficients by the terminator coefficients. In case the coefficients converge, then if N is sufficiently large this recursive errors also converge. This is consistent with Haydock's criterion of the divergence of the series $\sum(1/b_n)$.

(c) *Finite size errors :*

The termination error is not always the predominant error in recursion calculations. Starting from a single state $|R_i, L, \{\emptyset\}\rangle$, the total number of states over which the subsequent recursively calculated basis spreads out, i.e. the rank of the subspace accessed by recursion, soon becomes prohibitively large. This is particularly true in the full augmented space. Not only are the lattice neighbours of the initial site accessed, but also all possible configurations of this cluster of sites. Figure 2.5 gives us some idea of the rank of the subspace accessed per recursion step of a binary alloy on a face centered cubic lattice. This can be tackled using the point group symmetries of the underlying lattice, the symmetry of the starting state, and the underlying symmetries of the configuration space (in case the disorder is homogeneous). This procedure drastically reduce the rank of the invariant subspace on which the recursion effectively acts. This is explained in great detail by Saha *et al* (2004).

In this section, we shall analyze the error made when the recursion hits a boundary and carries on further. Since we do not allow Hamiltonian elements within and without this subspace, the problem is that of a perfectly reflecting boundary.

The continued fraction coefficients can be expressed in terms of either Hänkel determinants of the Hamiltonian moments :

$$a_{n+1} = \frac{K_{n-2}}{K_{n-1}} \frac{H_n}{H_{n-1}} + \frac{K_n}{K_{n-1}} \frac{H_{n-1}}{H_n} \quad n \geq 1$$

and

$$b_{n+1}^2 = \frac{H_n H_{n-2}}{H_{n-1}^2} \quad n \geq 1$$

where

$$H_n = \begin{vmatrix} \mu_0 & \mu_1 & \dots & \mu_n \\ \mu_1 & \mu_2 & \dots & \mu_{n+1} \\ \dots & \dots & \dots & \dots \\ \mu_n & \mu_{n+1} & \dots & \mu_{2n} \end{vmatrix}$$

$$K_n = \begin{vmatrix} \mu_1 & \mu_2 & \dots & \mu_{n+1} \\ \mu_2 & \mu_3 & \dots & \mu_{n+2} \\ \dots & \dots & \dots & \dots \\ \mu_{n+1} & \mu_{n+2} & \dots & \mu_{2n+1} \end{vmatrix}$$

Thus if we make sure that the rank of the accessed subspace is sufficiently large that its boundary is not hit by recursion up to M steps, then up to $2M$ moments of the density of states are exactly reproduced, errors occur only from moment $2M+1$. For the coherent potential approximation for diagonal disorder, we know that the first eight moments are exact and the subsequent moments of the order $O((1/Z)^n)$, Z being the connectivity of the lattice. To obtain comparatively accurate results with recursion we must go at least four steps of recursion and make sure our estimate of errors in the subsequent recursion coefficients and the terminator are comparable with the CPA which is also used to study the physical properties within single site mean field approximation.

To illustrate our results we have carried out the calculations using energy dependent formulation of augmented space recursion in which the disordered Hamiltonian with diagonal as well as off-diagonal disorder is recast into an energy dependent Hamiltonian having only diagonal disorder. This allows one to sample more shells in the augmented space. Though this formulation reduces the computational burden, the recursion becomes energy dependent and it is not suitable to carry out one recursion per energy point. This is tackled by choosing a few seed points across the energy spectrum uniformly and then carry out recursion on those points and spline fit the coefficients of recursion through out the whole spectrum. This enabled us to carry out large number of recursion steps since the configuration space grows significantly less faster for diagonal as compared to off diagonal disorder. Using this formulation and convergence procedure, we have checked the convergence of Fermi energy along with the band energy and magnetic moments with

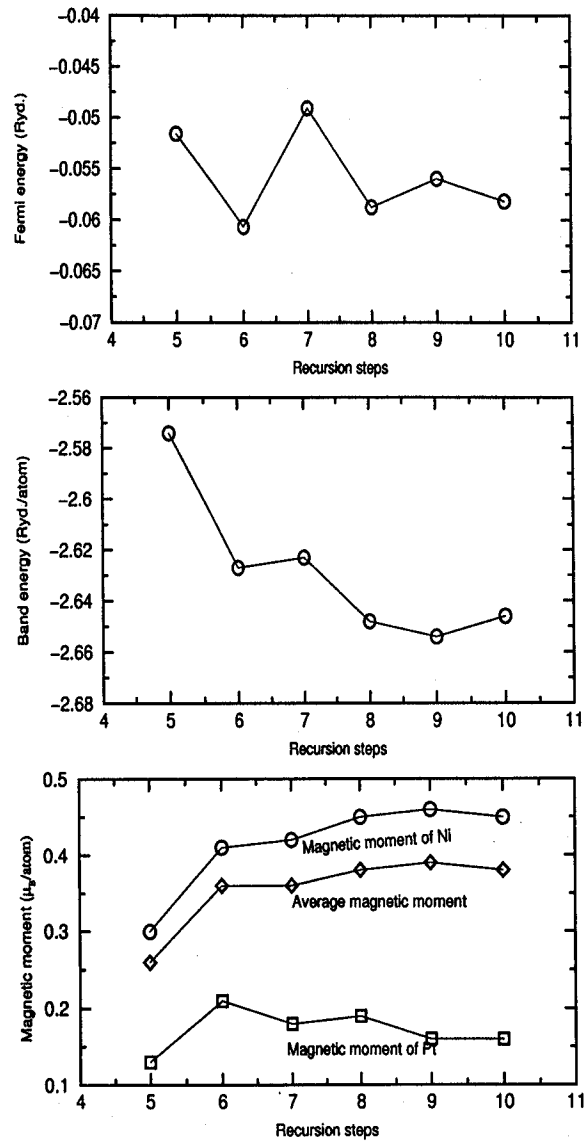


Figure 2.6: Fermi energy, band energy and magnetic moments as a function of recursion steps in Ni_3Pt .

respect to recursion steps before termination in Ni_3Pt . Figure 2.6 shows the convergence beyond seven step recursion. However, to have better convergence we may have to go more steps of recursions with equally more number of augmented space shells. Since the augmented space recursion is performed in the TB-LMTO basis the errors in the recursion procedure should be within the ambit of TB-LMTO itself.

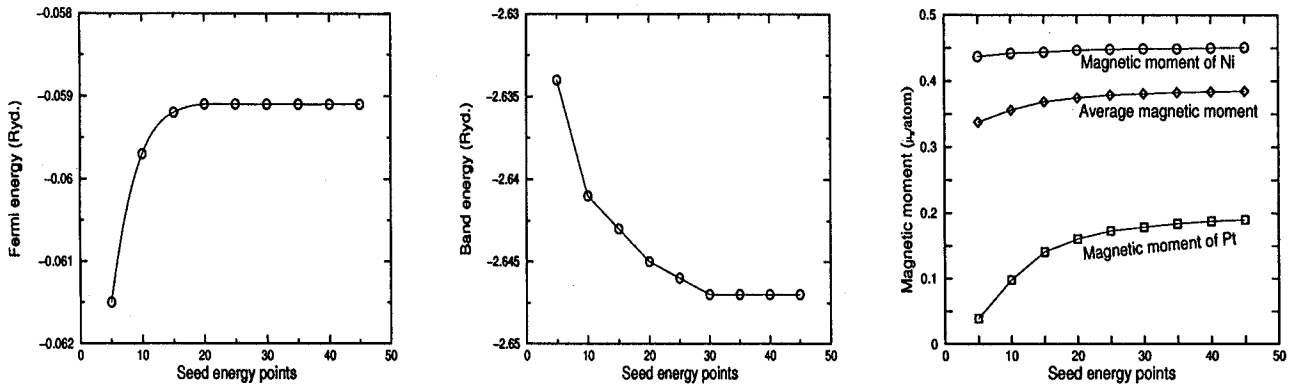


Figure 2.7: Fermi energy, band energy and magnetic moments as a function of seed energy points in Ni_3Pt .

In Figure 2.7 we show the convergence of Fermi energy along with the band energy and magnetic moments as a function of seed energy points in Ni_3Pt . These quantities converge beyond thirty five seed energy points.

In Figure 2.8 we show the variation of first nearest neighbour pair interaction energy as a function of number of recursion steps in NiPt_3 alloy system. These interaction energies are calculated using the augmented space recursion method coupling with orbital peeling technique in the basis of TB-LMTO as discussed in 2.3.3. Interaction energies are calculated at the Fermi energy which is obtained using diagonal formulation of the procedure pointed out above. We clearly see the convergence of pair interaction energy beyond seven step recursion. Since the pair interaction energies are used to study the chemical ordering or segregation and phase stability coupling it with statistical models like concentration wave approach in binary alloys, it is important to check their convergence.

These systematic studies indicate that such convergence analysis is essential for every case under study using the augmented space based recursion method.

2.4.3 Phase stability analysis

The pair interaction energies obtained from the electronic structure calculations (ASR coupled with orbital peeling technique in TB-LMTO basis) are now used as the inputs for

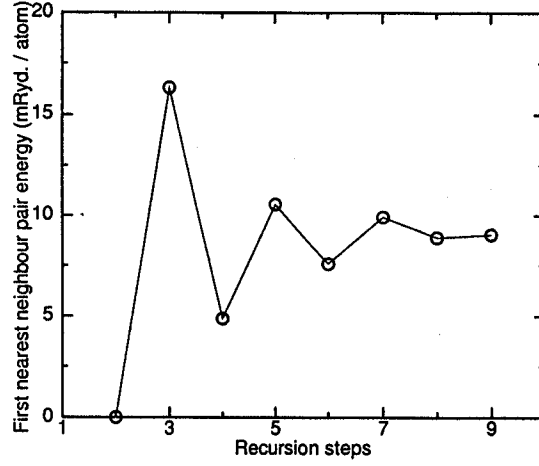


Figure 2.8: First nearest neighbour pair interaction energy as a function of recursion steps in NiPt₃ alloy system.

the calculation of differences in the formation energies of ordered and disordered phases (ordering energies), relative stability of the ordered phases in terms of calculation of anti phase boundary (APB) energy and the determination of ordering vectors (known as ordering stars).

Ordering energy

The ordering energy is defined as the difference between the formation energy of ordered alloy and the corresponding formation energy of disordered alloy. Since we are dealing with the effective pair potentials, the ordering energy can be calculated using these pair potentials. The relation for ordering energy using pair potentials is given as [Turchi *et al* (1988)]:

$$E^{ord} = \frac{1}{2} \sum_k V_k \delta x_o \delta x_k \quad (2.68)$$

where, δx_o (δx_k) = x_o (x_k) - x , x_o (x_k) = 1 if the site o/k is occupied by A atom and x_o = 0 if the site o/k is occupied by B atom. For $L1_2$ structure (as for examples Ni₃Pt and NiPt₃) the expression for ordering energy per atom in terms of pair potentials considering only up to fourth nearest neighbours is given as:

$$E_{Ni_3Pt}^{ord} = -\frac{3}{32} [V_1 - \frac{1}{3} V_2 + V_3 - \frac{1}{3} V_4] \quad (2.69)$$

For $L1_0$ structure for NiPt the expression for ordering energy per atom considering up to fourth nearest neighbour pair potentials is given as:

$$E_{NiPt}^{ord} = -\frac{1}{8} [V_1 - V_2 + V_3 - V_4] \quad (2.70)$$

Using these two relations we have found the ordering energy for Ni_3Pt , NiPt and NiPt_3 which are discussed in detail in Chapter 4.

Antiphase boundary energy

Kanamori and Kakehasi (1977) used the method of geometrical inequalities which is capable of searching for ground structure. They considered the energy of the three dimensional Ising like model:

$$E_c = \sum_k V_k P_k \quad (2.71)$$

where, V_k is the interaction constant of the k -th nearest neighbour interaction and P_k is the total number of k^{th} neighboring pairs in the given configuration. Defining the anti-phase boundary energy ξ by

$$\xi = -V_2 + 4 V_3 - 4 V_4 , \quad (2.72)$$

the authors proved rigorously that for $\xi > 0$, $L1_2$ and $L1_0$ are the corresponding superstructures possible at concentration 25 % and 50 % while for $\xi < 0$, one has the DO_{22} and A_2B_2 superstructures. We have applied these conditions in our calculations to find out the relative stability between DO_{22} and $L1_2$ structures in Ni_3Pt and NiPt_3 that between A_2B_2 and $L1_0$ in NiPt . The details of relative stability analysis in Ni-Pt systems is discussed in Chapter 4.

Special-point ordering

A wide range of phenomena related to order-disorder and magnetic transitions can be explained using the symmetry properties of the pair potentials (V_{ij}). If a symmetry element (rotation, rotation-inversion or mirror plane) of the space group in k -space is located at point h , the vector representing the gradient $\nabla_h V(h)$ of an arbitrary potential energy function $V(h)$ at that point must lie along or within the symmetry element. If two or more symmetry elements intersect at point h , one must necessarily have

$$|\nabla_h V(h)| = 0 \quad (2.73)$$

since a finite magnitude vector can not lie simultaneously in intersecting straight lines having only a point in common. At these so-called special points, the potential energy function $V(h)$ represents an extremum regardless of the choice of the pair interaction energies. Thus special points play an important role in the search for lowest energy ordered structures. The points which differ by a vector of a reciprocal lattice are considered

Table 2.1: The special points and stars of the *FCC* structure.

k-vector Star	Members	Brillouin zone points	Ordering structure
$\langle 000 \rangle$	[000]	Γ	
$\langle 100 \rangle$	[100] [010] [001]	X	L1 ₂ , L1 ₀
$\langle 1\frac{1}{2}0 \rangle$	$[1\frac{1}{2}0]$ $[\frac{1}{2}01]$ $[01\frac{1}{2}]$ $[\bar{1}\bar{\frac{1}{2}}0]$ $[\frac{1}{2}0\bar{1}]$ $[0\bar{1}\bar{\frac{1}{2}}0]$	W	A ₂ B ₂ , DO ₂₂
$\langle \frac{1}{2}\frac{1}{2}\frac{1}{2} \rangle$	$[\frac{1}{2}\frac{1}{2}\frac{1}{2}]$ $[\frac{1}{2}\frac{1}{2}\bar{\frac{1}{2}}]$ $[\frac{1}{2}\frac{1}{2}\frac{1}{2}]$ $[\frac{1}{2}\frac{1}{2}\bar{\frac{1}{2}}]$	L	L1 ₁

equivalent. In the case of simple structures with a single atom per unit cell, it is sufficient that two symmetry elements intersect at special points. These special points are listed in the crystallographic tables. They are always located at the surface of the Brillouin zone. The ‘star’ of a special point vector \mathbf{k} is obtained by applying all the rotations and rotation-inversion of the space group on the vector \mathbf{k} . All these vectors of a star are also considered equivalent. The special points of the *FCC* structure are located at the points Γ , X, W and L of the Brillouin zone as shown in Table 2.1.

2.5 Summary

The theoretical methods presented in this chapter along with the computational details taking the example of Ni-Pt alloy systems demonstrates ASR coupled with first principle TB-LMTO is able to tackle charge transfer, lattice relaxation, short range order effects in disordered alloys. The study of convergence properties shows that the errors in this method can be made compatible with the errors inherent in the TB-LMTO. This gives us confidence about the reliability of our computation results.

Chapter 3

Electronic and magnetic properties of X-Pt (X=Fe,Co,Ni) alloy systems

The magnetic and chemical interactions in solid solutions, their interdependence and the role they play in determining the electronic and magnetic properties of transition metal alloys have been the subject of extensive research since many years. The interplay between magnetism and spatial order in transition metal alloy systems has been extensively studied both experimentally [Cadeville and Morán-López (1987), Mirebeau *et al* (1982), Pierron-Bohnes *et al* (1985), Mirebeau *et al* (1984), Pierron-Bohnes *et al* (1983)] and using phenomenological models based on statistical thermodynamics [Sato *et al* (1959), Swalin (1962), Vonsovskii (1974), Bieber *et al* (1981), Bieber and Gautier (1981), Bieber and Gautier (1986), Hennion (1983), Marshall (1968), Hicks (1970), Hasegawa and Kanamori (1971), Buttler (1973), Jo and Miwa (1976), Jo (1976), Hasegawa (1979), Hamada (1979), Kakehashi (1982)]. In this chapter, we studied the electronic and magnetic properties of ordered as well as disordered phase of the Fe-Pt, Co-Pt and Ni-Pt. Many studies on optical and magneto-optical characterization of these systems are available in recent literatures [Uba *et al* (1998), Greets *et al* (1994), Weller *et al* (1994)] Nevertheless, a systematic first-principles study bringing out the interdependence of the magnetic and chemical ordering and the trend in this alloy series is lacking. The present chapter aims at a systematic and comparative first principles study of the electronic structure and magnetism in these systems, using techniques based on the local spin density approximation (LSDA) of the density functional theory.

Considering the case of ordered alloys, we have carried out a thorough study including careful investigation of the influence of various local as well as non-local exchange

Contents of this chapter has been published in Durga Paudyal, T. Saha-Dasgupta and A. Mookerjee, *J. Phys.: Condens. Matter* **16** 2317 (2004)

correlation functionals on the value of the equilibrium lattice parameters and magnetic moments of ordered Fe-Pt, Co-Pt and Ni-Pt alloy systems.

The calculational scheme used for our calculations of disordered alloys is based on augmented space recursion (ASR) technique. As already discussed in chapter 2, among the various advantages of the ASR in going beyond the single-site approximation is the possibility of inclusion of local lattice distortions [Saha and Mookerjee (1996)] which is important in the case of alloys with size mismatch between components as in the case of Fe-Pt, Co-Pt and Ni-Pt.

An important aspect in understanding the interplay between magnetism and ordering in disordered transition metal alloys involves investigation of the influence of local environment, namely the short-range ordering (SRO) effect, on electronic and magnetic properties of these alloys. There have been determination of SRO parameters for different degrees of disorder using first principles techniques [Lu *et al* (1994), Staunton *et al* (1994), Johnson *et al* (1994)] or extraction of these parameters from experiments and analysis of their effect on electronic structure and properties [Borici-Kuqo *et al* (1998), Wolverton *et al* (1998), Abrikosov *et al* (1996)]. SRO for a disordered binary alloy A_xB_{1-x} is described, for example, by the Warren-Cowley parameter [Cowley (1950)]. In present chapter we have carried out charge-self-consistent calculations based on generalized ASR technique to examine the short range ordering effect in Fe-Pt, Co-Pt and Ni-Pt systems. The results show good agreements with available experimental values.

Another important ingredient for proper description of electronic and magnetic structure of these alloys is the relativistic effect due to presence of heavy mass element, Pt. All calculations described in this chapter are done with scalar relativistic corrections. The importance of relativistic effect has been explained in great detail in chapter 4 taking the example of phase stability of Ni-Pt alloy system.

3.1 Results and discussions

3.1.1 Lattice parameters

In Table 3.1, we quote the values of equilibrium lattice parameters, obtained by minimizing the total energy with respect to the lattice parameters for $L1_2$ superstructures at 25 and 75% and $L1_0$ superstructure at 50% concentration of Pt in Fe-Pt, Co-Pt and Ni-Pt alloy systems with different choice of local (von Barth-Hedin (vBH) [von Barth and Hedin (1972)] and Vosko-Wilk-Nusair (VWN) [Vosko *et al* (1980)]) as well as non-local (Langreth-Mehl-Hu (LMH) [Langreth *et al* (1981)] and Perdew-Wang (PW) [Perdew and

Table 3.1: The equilibrium lattice parameters in a.u. of FePt, CoPt and NiPt systems in ordered structures with various choices of exchange correlation functionals. See text for various abbreviations.

x	vBH	VWN	LMH	PW	Expt.
Fe_{1-x}Pt_x					
0.00 (BCC)	5.28	5.30	5.36	5.54	5.406 [Pearson (1958)]
(FCC)	6.47	6.47	6.53	6.63	6.877 [Pearson (1958)]
0.25(L1 ₂)	6.71	6.91	6.99	7.21	7.049 [Kashyap <i>et al</i> (1995)]
0.50(L1 ₀)	a = 7.16 c = 6.94	a = 7.18 c = 6.94	a = 7.22 c = 7.02	a = 7.46 c = 7.26	a = 7.253 [Pearson (1958)] c = 7.020 [Pearson (1958)]
0.75(L1 ₂)	7.25	7.27	7.30	7.54	7.313 [Podgórný (1991, 1992)]
Co_{1-x}Pt_x					
0.00 (hex)	a = 4.65 c = 7.48	a = 4.66 c = 7.49	a = 4.70 c = 7.59	4.83 7.78	4.728 [Pearson (1958)] 7.675 [Pearson (1958)]
(FCC)	6.55	6.56	6.63	6.81	6.684 [Pearson (1958)]
0.25(L1 ₂)	6.78	6.80	6.86	7.06	6.923 [Kashyap <i>et al</i> (1999)]
0.50(L1 ₀)	a = 7.14 c = 6.78	a = 7.14 c = 6.78	a = 7.18 c = 6.86	a = 7.40 c = 7.08	a = 7.204 [Pearson (1958)] c = 7.007 [Pearson (1958)]
0.75(L1 ₂)	7.21	7.22	7.25	7.50	7.240 [Pearson (1958)]
Ni_{1-x}Pt_x					
0.00 (FCC)	6.54	6.55	6.61	6.80	6.646 [Pearson (1958)]
0.25(L1 ₂)	6.77	6.78	6.84	7.05	6.890 [Pisanty <i>et al</i> (1990)]
0.50(L1 ₀)	a = 7.16 c = 6.63	a = 7.16 c = 6.64	a = 7.18 c = 6.74	a = 7.42 c = 6.96	a = 7.209 [Pearson (1958)] c = 6.769 [Pearson (1958)]
0.75(L1 ₂)	7.20	7.21	7.24	7.49	7.251 [Pisanty <i>et al</i> (1990)]
1.00 (FCC)	7.37	7.38	7.40	7.66	7.400 [Pearson (1958)]

Wang (1986)) exchange correlation potentials. The non-local exchange correlation potentials seem to decrease overbinding and predict larger equilibrium lattice parameters than the local ones. The PW seems to go overboard and give estimates of the equilibrium lattice parameters which are *larger* than the experimental values. The best agreement with experiment is found to be LMH.

3.1.2 Magnetism of Fe-Pt alloys

Ordered alloys :

In Table 3.2, we show results for two sets of calculations for magnetic moments in ordered Fe-Pt alloys. In first set of calculations, we have calculated local as well as average magnetic moments corresponding to the theoretically estimated lattice parameters obtained via energy minimization procedure. In second set, calculations were done using experimental lattice parameters.

For Fe₃Pt alloy in L1₂ super-structure the use of non-local exchange correlation functionals LMH appear to give better agreement with experimental values [Kashyap *et al* (1995)] for local and average magnetic moments as compared to local exchange correlation functionals. This holds good for both the choices of lattice parameters. The results for average and local magnetic moments from previous works by Kashyap *et al* (1995) and Podgórný (1991, 1992), both using TB-LMTO, are in agreement with our corresponding results as can be seen from Table 3.2. The differences seen with these results are primarily due to different computational details. Both these authors have used frozen core approximation in their calculations without taking into account of *f* states for Pt. Podgorny and Kashyap *et al* in their calculations used 286 and 84 k points in the irreducible part of the Brillouin Zone (BZ) respectively. On the other hand, our calculations are all electron calculations taking a *spdf* minimal basis for Pt and using 969 k points in irreducible part of BZ. The local magnetic moment on Pt sites obtained by Hasegawa and Kanamori (1971) using augmented plane wave (APW) method is in exact agreement to the corresponding experimental value though their average magnetic moment and local magnetic moment on Fe sites are lower (by 0.20 μ_B for average and 0.15 μ_B for Fe sites) than the corresponding experimental estimates [Kashyap *et al* (1995)]. Our calculation using the vBH functional for the exchange correlation potential and theoretically estimated lattice parameter leads to the conclusion of a non-magnetic ground state which is in agreement with that found in a previous study by Uhl *et al* (1994). This once again emphasizes that magnetic moments are very sensitively dependent on the particular exchange-correlation functional used and the detailed accuracy of the numerical calculations.

Table 3.2: The local and average magnetic moments of Fe-Pt system in ordered structures with various choices of exchange correlation functionals.

conc. of Pt	XC used/Expt/ Ref.	magnetic moment (μ_B /atom) of					
		with eq. lat. par.			with expt. lat. par.		
		Fe	Pt	av.	Fe	Pt	av.
0.00(BCC)	vBH(this work)	2.15			2.25		
	VWN(this work)	2.21			2.30		
	LMH(this work)	2.29			2.33		
	PW(this work)	2.55			2.35		
	(Expt.) [Lide (2000)]				2.22		
0.25(L1 ₂)	vBH(this work)	0.00	0.00	0.00	2.57	0.32	2.01
	VWN(this work)	2.46	0.29	1.92	2.64	0.34	2.06
	LMH(this work)	2.63	0.33	2.06	2.70	0.35	2.11
	PW(this work)	2.78	0.35	2.17	2.68	0.37	2.10
	(vBH) [Kashyap <i>et al</i> (1995)]				2.56	0.26	1.99
	(VWN) [Podgórný (1991, 1992)]	2.51	0.26	1.95			
	[Hasegawa and Kanamori (1971)]				2.50	0.50	2.0
(Expt.) [Kashyap <i>et al</i> (1995)]				2.70	0.50	2.15	
0.50(L1 ₀)	vBH(this work)	2.73	0.35	1.54	2.81	0.35	1.58
	VWN(this work)	2.79	0.35	1.57	2.85	0.35	1.60
	LMH(this work)	2.88	0.35	1.61	2.90	0.35	1.63
	PW(this work)	3.01	0.36	1.69	2.86	0.36	1.61
	[Osterloh <i>et al</i> (1994)]				2.92	0.38	
	(VWN) [Podgórný (1991, 1992)]	2.85	0.30	1.57			
(Expt.) [Osterloh <i>et al</i> (1994)]				2.80		0.77	
0.75(L1 ₂) FM AFM	vBH(this work)	2.99	0.31	0.98	3.10	0.32	1.02
	VWN(this work)	3.12	0.32	1.02	3.15	0.33	1.03
	LMH(this work)	3.19	0.34	1.05	3.20	0.34	1.06
	PW(this work)	3.24	0.39	1.11	3.12	0.37	1.06
	[Podgórný (1991, 1992)]	3.22	0.34	1.06			
	[Tohyama <i>et al</i> (1989)]				4.21	0.33	
	vBH(this work)	3.11	0.15		3.16	0.15	
	VWN(this work)	3.17	0.15		3.20	0.15	
	LMH(this work)	3.24	0.15		3.25	0.16	
	PW(this work)	3.31	0.17		3.18	0.16	
	[Podgórný (1991, 1992)]	3.46	0.16				
	[Tohyama <i>et al</i> (1989)]				4.13	0.00	
	(Expt.) [Kulikov <i>et al</i> (1985)]				3.3		

For FePt alloys the local magnetic moment of Fe site in $L1_0$ superstructure calculated using vBH exchange correlation potential and experimental lattice parameter shows closest agreement with experimental value [Osterloh *et al* (1994)]. The LMH based estimates of the local magnetic moment on Fe sites are rather large as compared with the available experimental data [Osterloh *et al* (1994)]. The experimental value for local magnetic moment of Pt in this concentration is not available. The experimentally estimated average magnetic moment is significantly lower than that of the calculated values using both local as well as non local exchange correlations. However all the available theoretical estimates by different groups [Podgórný (1991, 1992), Osterloh *et al* (1994)] are significantly high, just like ours as compared to the experimental estimate quoted by Osterloh *et al* (1994). The experimental result may be interpreted assuming the magnetic moment at the Fe and Pt sites to be arranged antiparallely giving rise to ferri-magnetic ground state. However, we were unable to show any theoretical evidence for this and our calculations do predict a stable ferromagnetic alignment as pointed out by Osterloh *et al* (1994). As in the case of Fe_3Pt , the slight difference between the values obtained by Podgórný (1991, 1992) and by us is again due to the difference in the calculational details. In addition to using frozen core approximation and neglect of f states in Pt site, Podgórný has assumed the cubic crystal structure for FePt in $L1_0$ structure while in reality it is tetragonal. In our calculations, we have assumed the experimentally observed tetragonal structure. The local magnetic moments obtained by Osterloh *et al* (1994) using augmented spherical wave method are higher than ours as well as calculations by Podgórný (1991, 1992).

The experimental ground state ordered magnetic phase $FePt_3$ is antiferromagnetic. We have carried out calculations on this alloy both in the ferromagnetic as well as the antiferromagnetic structures. We have found the total energy in the case of antiferromagnetic structure is indeed lower than that of ferromagnetic structure. In the ferromagnetic calculation, the local as well as average magnetic moment obtained by Podgórný (1991, 1992) using VWN exchange correlation potential with theoretical estimates of lattice parameter is in close agreement with our corresponding value. The calculated local magnetic moment on Fe sites by Tohyama *et al* (1989) using an empirical tight binding model is significantly higher than both ours and that of Podgórný (1991, 1992). Our calculated magnetic moment on Fe site for the antiferromagnetic structure using PW non local exchange correlation with theoretically estimated lattice parameter is in closest agreement with the experimental value [Kulikov *et al* (1985)]. This is the one case where LMH underestimates the staggered magnetization.

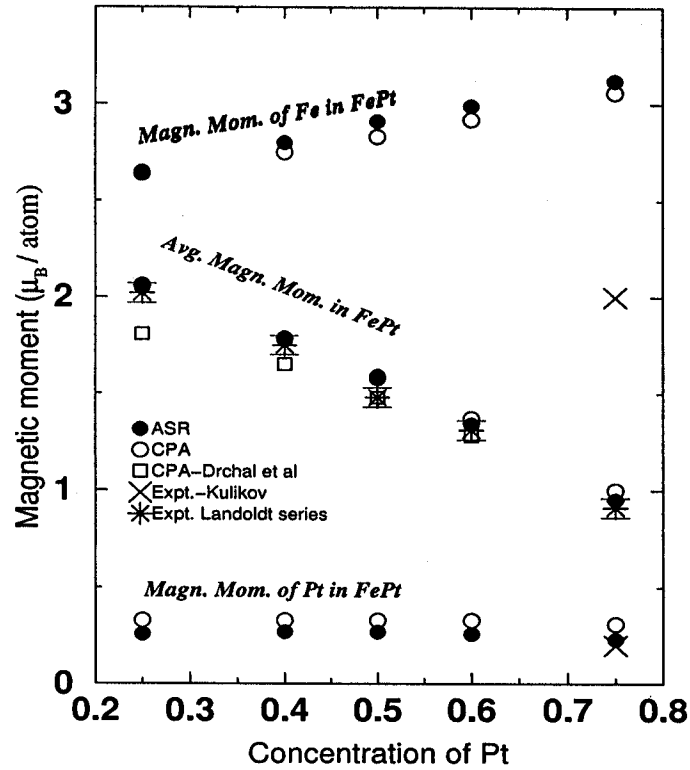


Figure 3.1: Magnetic moments in disordered Fe-Pt alloy systems using two different configuration averaging methods namely augmented space recursion (ASR) and coherent potential approximation (CPA) as compared to available experimental values given in Landoldt series [Wijn (1986)].

Disordered alloys :

In Figure 3.1, we compare our calculated disordered magnetic moments using augmented space recursion with the available experimental values taken from Landoldt series [Wijn (1986)] as well as with CPA calculations. The average magnetic moments agree quite well with the corresponding experimental values in all concentrations. The numerical values of local as well as average magnetic moments calculated using LMTO-CPA are in agreement with those obtained using the ASR. This shows that the single site approximation like CPA works well for the Fe-Pt disordered alloys. The average magnetic moments obtained by Hayn and Drchal (1998) using CPA matches well for most concentrations though they deviate a bit at low concentrations of Pt. Our calculations uses charge neutral spheres to reduce the effect of Madelung contribution whereas Hayn and Drchal (1998) have used equal Wigner Seitz radii of both constituents and the effect of Madelung due to charge transfer was taken into account using screened impurity model [Hayn and Drchal

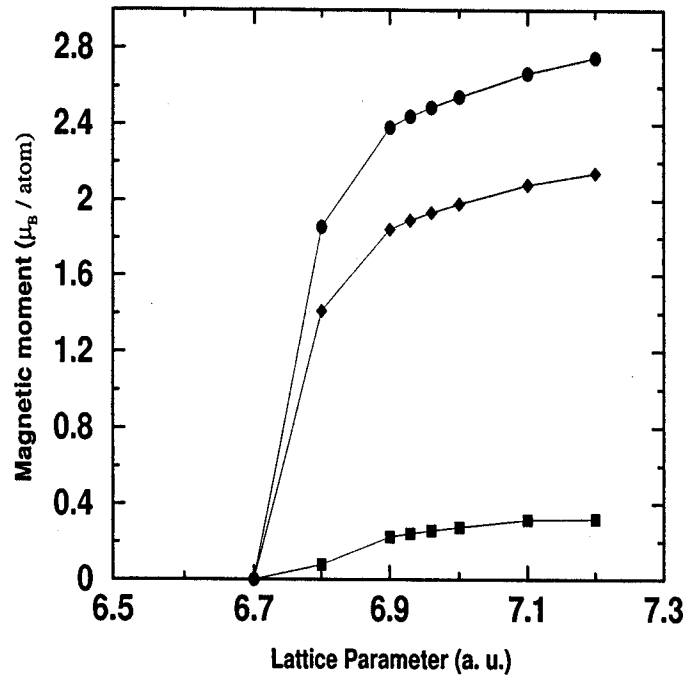


Figure 3.2: Magnetic moments as a function of lattice parameters for 25% concentration of Pt in disordered Fe-Pt alloy. Circles and squares denote local magnetic moment on Fe site and Pt site respectively. Diamonds represent average magnetic moment.

(1998)]. The local moment on the Fe sites increases towards the isolated Fe moment as the concentration of Pt increases. This is an indication of the fact that local environmental effects are unimportant and consequently the CPA and ASR results agree closely.

In 25% concentration of Pt there is invar effect which shows anomalies in the thermal expansion. We have observed two minima of total energy one with a high moment and a large lattice constant 6.93 au and the other with a zero moment and small lattice constant 6.71 au. The total energy difference between the magnetic and non magnetic states is 2.4 mRyd/atom which is higher than the calculations by Drchal *et al* (0.7 mRyd/atom) and lower than that of Staunton *et al* (15.7mRyd/atom). In Figure 3.2, we show the behaviour of magnetic moment as a function of lattice parameter which shows non magnetic to ferromagnetic transition at 6.71 a.u. Our calculated average as well as local magnetic moment on Fe and Pt sites corresponding to theoretically estimated lattice parameter (6.93 a.u.) on magnetic state are 1.89, 2.44 and 0.24 μ_B respectively.

Table 3.3 summarizes the known experimental and earlier theoretical results on disordered FePt with 25% Pt. Two reported experimental results in this case differ to each other. The localized components of the magnetic moments for Fe ($2.03 \pm 0.02 \mu_B$) and

Pt ($0.34 \pm 0.08 \mu_B$) were estimated from spin polarized neutron diffraction measurements by Ito *et al* (1974) , while the magnetization measurements of Caporaletti and Graham (1980) indicated moments of 2.75 and $0.45 \mu_B$ for Fe and Pt respectively. The values of average magnetic moments quoted in Landoldt series for different experiments are 2.02 and $2.27 \mu_B$. The theoretical estimates based on different methods also differ between each other. These differences are mainly due to the differences in the computational details chosen in each framework and also different approximations being used in each method.

Table 3.3: Various estimates of the local and averaged magnetic moments in Bohr-magneton for disordered $\text{Fe}_{75}\text{Pt}_{25}$ alloy.

Author	Fe	Pt	Average
Expt. [Ito <i>et al</i> (1974)]	2.03 ± 0.02	0.34 ± 0.08	1.61 ± 0.03
Expt. [Caporaletti and Graham (1980)]	2.75	0.45	2.20
Expt. (a) [Wijn (1986)]			2.02
Expt. (b) [Wijn (1986)]			2.27
LMTO-CPA [Hayn and Drchal (1998)]			1.81
KKR-CPA [Major <i>et al</i> (2003)]	2.80	0.23	2.16
LCAO-CPA [Koepernik <i>et al</i> (1997)]			2.17
ASR (this work)	2.44	0.24	1.89

For the 75% concentration of Pt our estimate of the magnetic moment on Fe sites is higher than that measured by Kulikov *et al* (1985) (which is about $2\mu_B$).

In order to check the possible short range order effect, we have checked the variation of total energy as a function of short range order and found that the total energy decreases as short range order goes from positive (segregation side) to negative (ordering side) confirming this system as an ordering system. In Figure 3.3 we show the variation of the magnetic moments as functions of the SRO parameter for 75% concentration of Pt. We find that both the local and average magnetic moments show an increasing tendency as the SRO parameters goes from the segregating to the ordering side. This is justified by the fact that the magnetic moment of Fe is enhanced when it is surrounded by Pt as we have seen in the ordered alloys. We therefore conclude that the discrepancy with the experimental data of Kulikov *et al* (1985) can not be due to the short range ordering

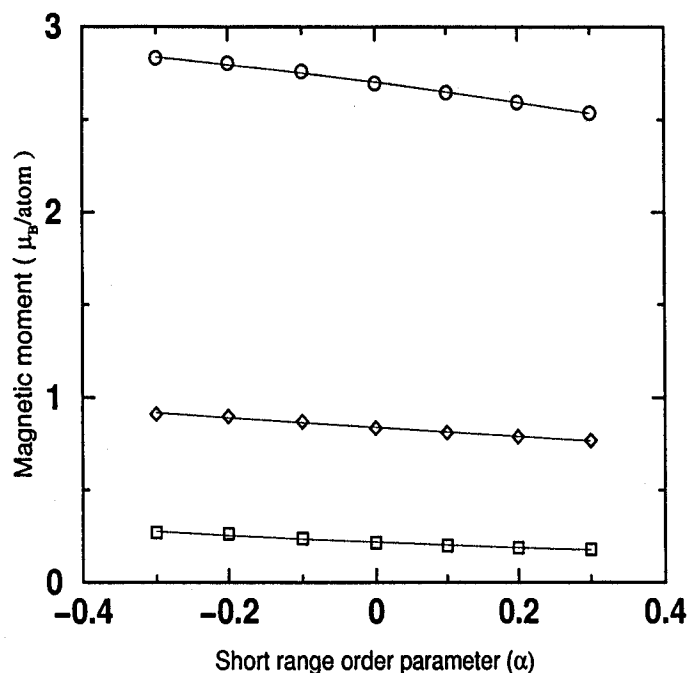


Figure 3.3: Variation of magnetic moments as a function of short range order parameter (α) for 75% in Fe-Pt system. Circles, squares and diamonds denote the local magnetic moments on Fe sites, on Pt sites and average magnetic moments respectively.

effect, probably the other possible factors influencing the experimental results need to be considered.

3.1.3 Magnetism in Co-Pt alloys

Ordered alloys :

Table 3.4 shows the calculated and experimental magnetic moments for ordered Co-Pt alloys. No experimental result is available for 25% of concentration of Pt in ordered case. The local as well as average magnetic moments obtained by Kashyap *et al* (1999) using vBH exchange correlation potential with experimental lattice parameter are lower (by $0.30 \mu_B$ for Co site, $0.01 \mu_B$ for Pt site and $0.23 \mu_B$ for average) than our corresponding values which could be due to differences in computational details as mentioned in the case of Fe-Pt. The local as well as average magnetic moments obtained by Kootte *et al* (1991) using localized spherical wave method using vBH exchange correlation and experimental lattice parameters are in agreement with our corresponding values.

For 50% concentration of Pt, our results agree well with the previous theoretical

Table 3.4: The local and average magnetic moments of Co-Pt system in ordered structures with various choices of exchange correlation functionals.

conc. of Pt	XC used/Expt/ Ref.	magnetic moment (μ_B /atom) of					
		with eq. lat. par.			with expt. lat. par.		
		Co	Pt	av.	Co	Pt	av.
0.00 Hex. (FCC)	vBH(this work)	1.55 (1.57)			1.60 (1.62)		
	VWN(this work)	1.58 (1.60)			1.62 (1.64)		
	LMH(this work)	1.62 (1.65)			1.64 (1.67)		
	PW (this work)	1.67 (1.70)			1.63 (1.66)		
	Expt. Hex. [Kootte <i>et al</i> (1991)]				1.58 [1.61]		
0.25 (L1 ₂)	vBH(this work)	1.56	0.35	1.26	1.69	0.39	1.37
	VWN(this work)	1.63	0.37	1.32	1.73	0.40	1.40
	LMH(this work)	1.73	0.40	1.40	1.76	0.39	1.42
	PW(this work)	1.80	0.39	1.45	1.74	0.41	1.41
	[Kashyap <i>et al</i> (1999)] [Kootte <i>et al</i> (1991)]				1.39 1.64	0.38 0.36	1.14 1.32
0.50 (L1 ₀)	vBH(this work)	1.69	0.38	1.03	1.79	0.38	1.09
	VWN(this work)	1.74	0.39	1.07	1.83	0.39	1.11
	LMH(this work)	1.82	0.40	1.11	1.87	0.39	1.13
	PW(this work)	1.91	0.42	1.16	1.83	0.40	1.12
	[Kashyap <i>et al</i> (1999)] [Kootte <i>et al</i> (1991)]				1.85 1.69	0.38 0.37	1.12 1.03
	[Uba <i>et al</i> (2001)]				1.60	0.30	
	Expt.[Kootte <i>et al</i> (1991)] Expt.[Kootte <i>et al</i> (1991)]				1.70 1.60	0.25 0.30	0.98 0.95
0.75 (L1 ₂)	vBH(this work)	1.71	0.25	0.62	1.74	0.26	0.64
	VWN(this work)	1.75	0.26	0.63	1.82	0.27	0.65
	LMH(this work)	1.83	0.28	0.67	1.87	0.28	0.68
	PW(this work)	1.95	0.36	0.76	1.82	0.31	0.69
	[Kashyap <i>et al</i> (1999)] [Kootte <i>et al</i> (1991)]				1.85 1.69	0.25 0.27	0.65 0.63
	[Tohyama <i>et al</i> (1989)]				2.88	0.38	
	[Lange <i>et al</i> (1998)] [Uba <i>et al</i> (2001)]	1.72	0.25	0.62	1.74	0.24	
	Expt.[Kootte <i>et al</i> (1991)]				1.64	0.26	0.61
	Expt.[Lange <i>et al</i> (1998)]						0.70

results [Kashyap *et al* (1999), Kootte *et al* (1991), Uba *et al* (2001)] within the errorbars of different calculational schemes and are in reasonable agreement with the observed magnetic moments [Kootte *et al* (1991)] as summarized in Table 3.4.

For 75% concentration of Pt, the calculated local magnetic moments on Co site and that of average magnetic moments using possible exchange correlations with both theoretically estimated as well as experimental lattice parameters are on higher side as compared to the experimental estimates [Kootte *et al* (1991)]. The calculated local moment of Pt using vBH exchange correlation and theoretically estimated lattice parameter is close to the experimental value [Kootte *et al* (1991)]. The theoretical estimates for local as well as average magnetic moments by Kashyap *et al* (1999) and Kootte *et al* (1991) as in 50% concentration of Pt are in agreement with our corresponding estimates as can be seen from Table 3.4. The slight differences seen are again due to the differences in computational details. The local magnetic moments calculated by Tohyama *et al* (1989) using tight-binding method are significantly higher than ours as well as experimental estimates which can be seen from Table 3.4. The recent work by Lange *et al* (1998) using fully relativistic TB-LMTO with vBH exchange correlation and theoretically estimated lattice parameter report the local as well as average magnetic moment close to our corresponding values. Their experimental value for average magnetic moment matches with our corresponding calculated value using non local exchange correlation potentials and experimentally estimated lattice parameter. The supercell calculation of Uba *et al* (2001) with LMTO using vBH exchange correlation potential and experimental lattice parameter matches well with our corresponding value.

Disordered alloys :

In Figure 3.4, we show the comparison of local magnetic moments of Co and Pt as well as average magnetic moment of disordered Co-Pt system. Calculations have been done both within ASR and CPA schemes using vBH exchange correlations. The comparison with experimental results for average magnetic moment taken from Landoldt series [Wijn (1986)] matches well with our calculations. The calculated magnetic moments with augmented space recursion method are in better agreement with experimental results than that of coherent potential approximation method. From this Figure we can see that the local moment of Co obtained by ASR calculation is almost constant with the increase of concentration of Pt which is the signature of weak local environmental effect on Co site. This finding is in agreement with that of Sanchez *et al* (1988) who also pointed out almost constant magnetic moment at Co site as a function of Pt concentration. The average magnetic moments obtained by Koepernik *et al* (1997) using linear combination

of atomic orbitals combined with coherent potential approximation (LCAO-CPA) method taking into account both diagonal and off diagonal disorder effects show close agreement with our results (except 20% concentration of Pt where the value obtained by Koepernik *et al* (1997) is in higher side than ours) using augmented space recursion (ASR).

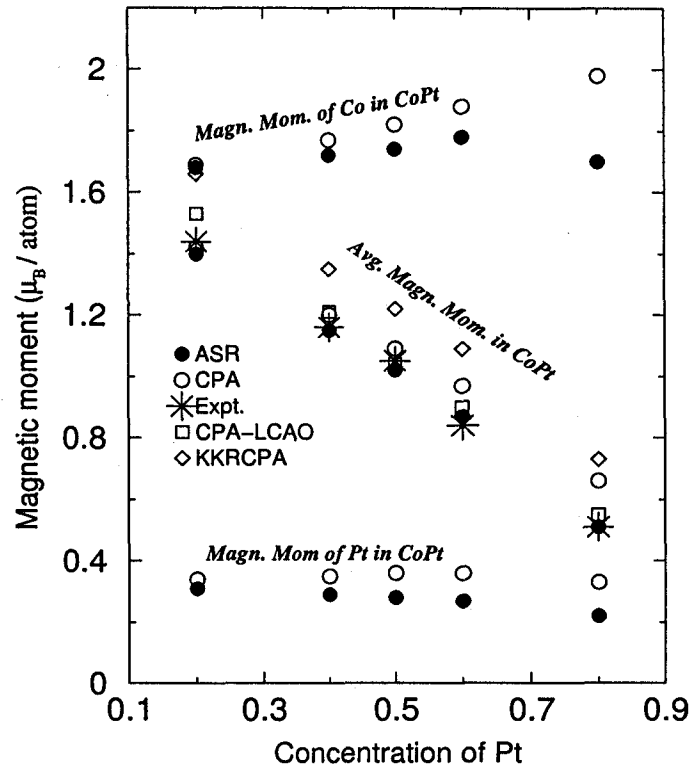


Figure 3.4: Magnetic moments in disordered Co-Pt alloy systems using two different linearized muffin-tin orbital (LMTO) based configuration averaging methods namely augmented space recursion (ASR) and coherent potential approximation (CPA) as compared to available experimental values given in Landoldt series [Wijn (1986)]. CPA-LCAO and KKR-CPA denote coherent potential approximation based linear combination of atomic orbitals method of Koepernik *et al* (1997) and Korringa Kohn Rostoker coherent potential approximation method of Ebert *et al* (1992) respectively.

The results obtained by Ebert *et al* (1992) using Korringa-Kohn-Rostoker coherent potential approximation (KKR-CPA) are higher than ours as well as experimental values. The calculations by Ebert *et al* (1992) using KKR-CPA with single site approximation were though fully relativistic did not take into account lattice relaxation and off diagonal disorder effects. Therefore it is not surprising that our calculations show better agreement with experiments. According to the calculation of Shick *et al* (1996) using fully relativis-

tic linearized muffin-tin orbital based coherent potential approximation (LMTO-CPA) method the average and partial magnetic moments of Co and Pt in $\text{Co}_{50}\text{Pt}_{50}$ are 1.07, 1.79 and $0.35 \mu_B$ respectively while the value of Ghosh *et al* (2001) using ASR are 1.05, 1.85 and $0.24 \mu_B$ for the same. Our values in this case are 1.05, 1.80 and 0.29. The reason behind the differences seen in between LMTO-CPA of Shick *et al* (1996) and ASR is again same as explained above in the connection with KKR-CPA and ASR. Though the calculations by Ghosh *et al* (2001) (using theoretically estimated lattice parameter) and ours (using experimental lattice parameter) used same ASR method, ours being charge neutral and self consistent show better agreement for local magnetic moments with corresponding charge neutral and self consistent calculations.

In order to investigate the possible influence of short range order on the disordered magnetic moments, we have performed a complete investigation in terms of the total energy calculations as a function of short range order parameter. Like Fe-Pt, Co-Pt also shows a tendency to order. We find that short range order has very little effect on magnetism. As for example in Figure 3.5, we show the variation of magnetic moments with respect to short range order for 20 and 80% concentration of Pt. This indicates almost constant magnetic moment as a function of short range order.

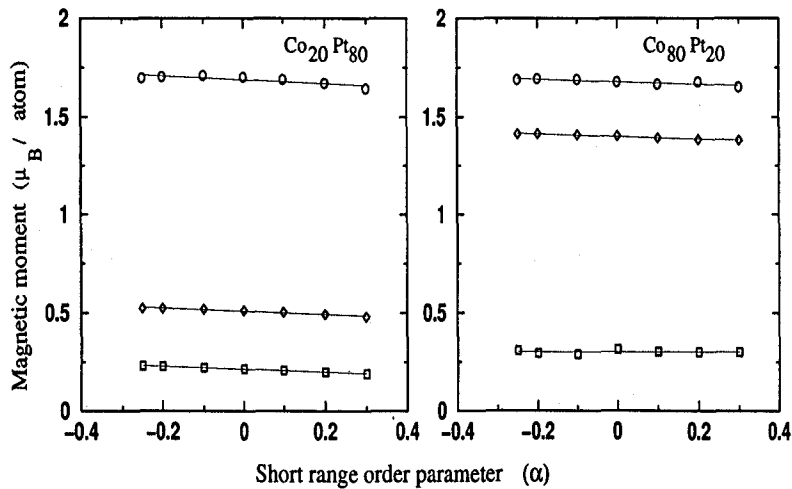


Figure 3.5: Variation of magnetic moments as a function of short range order parameter (α) in Co-Pt systems. Circles, squares and diamonds denote the local magnetic moments on Co sites, on Pt sites and average magnetic moments respectively.

Table 3.5: The local and average magnetic moments of Ni-Pt system in ordered structures with various choices of exchange correlation functionals.

Concentration of Pt	XC used/Expt/ Ref.	magnetic moment (μ_B /atom) of					
		with eq. lat. par.			with expt. lat. par.		
		Ni	Pt	average	Ni	Pt	average
0.00(FCC)	vBH(this work)	0.61			0.62		
	VWN(this work)	0.62			0.64		
	LMH(this work)	0.64			0.65		
	PW(this work)	0.66			0.64		
	Expt. [Lide (2000)]	0.62					
0.25(L1 ₂)	vBH(this work)	0.50	0.24	0.43	0.57	0.27	0.49
	VWN(this work)	0.54	0.26	0.47	0.60	0.29	0.52
	LMH(this work)	0.62	0.29	0.53	0.65	0.30	0.56
	PW(this work)	0.71	0.36	0.63	0.63	0.32	0.56
	[Singh (2003)]	0.58	0.27	0.50			
	[Expt.] [Parra and Cable (1980)]				0.49	0.25	0.43
0.50(L1 ₀)	vBH(this work)	0.00	0.00	0.00	0.33	0.17	0.25
	VWN(this work)	0.06	0.03	0.05	0.46	0.23	0.34
	LMH(this work)	0.55	0.27	0.41	0.65	0.31	0.48
	PW(this work)	0.72	0.34	0.53	0.63	0.32	0.48
	[Singh (2003)]	0.60	0.27	0.44			
	[Expt.] [Parra and Cable (1980)]				0.28	0.17	0.22
0.75(L1 ₂)	vBH(this work)	0.47	0.09	0.18	0.55	0.10	0.21
	VWN(this work)	0.50	0.09	0.20	0.57	0.11	0.22
	LMH(this work)	0.55	0.11	0.22	0.61	0.12	0.24
	PW(this work)	0.65	0.16	0.28	0.58	0.12	0.24
	[Singh (2003)]	0.58	0.10	0.22			

3.1.4 Magnetism in Ni-Pt alloys

Ordered alloys :

In Table 3.5, we show results of two sets of ordered calculations in Ni-Pt alloys using possible local as well as non local exchange correlation potentials one with theoretically

calculated lattice constants via energy minimization procedure and other using experimental lattice parameters.

For 25% concentration of Pt, the calculated local as well as average magnetic moments in ordered Ni-Pt alloys obtained using vBH local exchange correlation potential in theoretically calculated lattice parameter show very good agreement with experimental values [Parra and Cable (1980)]. The values obtained by Singh (2003) in the same case are higher in comparison to ours and experimental estimate [Parra and Cable (1980)]. Singh (2003)'s calculations seemingly did not include the f states in Pt in the TB-LMTO basis. Our test calculations without including f states of Pt also show higher values of magnetic moments for this concentration of Ni-Pt alloy.

For 50% concentration of Pt in $L1_0$ structure calculated local as well as average magnetic moments using vBH exchange correlation potential with the use of experimental lattice parameter is closest to the experimental estimate [Parra and Cable (1980)]. Our calculations with the use of local exchange correlations and theoretically estimated lattice parameters lead to non magnetic ground state which is in agreement with that found in previous study by Dahmani *et al* (1985). In our calculations we have taken into account the tetragonal distortion as in the case of Fe-Pt and Co-Pt alloys in $L1_0$ structure.

For 75% concentration of Pt, for $NiPt_3$ alloy in $L1_2$ structure there is no experimental result available. For this concentration we have got higher local magnetic moment of Ni than at the 50% concentration of Pt. This was obtained while using local exchange correlations. In this case if we use non local exchange correlations then we get the decrease of local magnetic moment of Ni on going from 50% to 75% concentration of Pt. The average as well as local magnetic moments on Pt sites show the decreasing tendency using both local as well as non local exchange correlations with theoretically as well as experimentally estimated lattice constants.

The calculations by Singh (2003) using vBH exchange correlations and theoretically estimated lattice parameters show that the local magnetic moment of Ni increases while going from 25% to 50% and decreases while going from 50% to 75% concentration of Pt. The calculations by Singh (2003) did not take into account the tetragonal distortion for 50% concentration of Pt which means putting lattice parameters $a = c$ which is not the right ground state structure. For a test we also repeated our calculation without taking into account the tetragonal distortion for 50% concentration of Pt using vBH local exchange correlation potentials and theoretically estimated lattice constants and we also observed same trend as Singh obtained. However, for the calculation taking into account the degrees of freedom for tetragonal distortion we found that the magnetic moments vanish with the use of local exchange correlation potentials in theoretically estimated

lattice parameters.

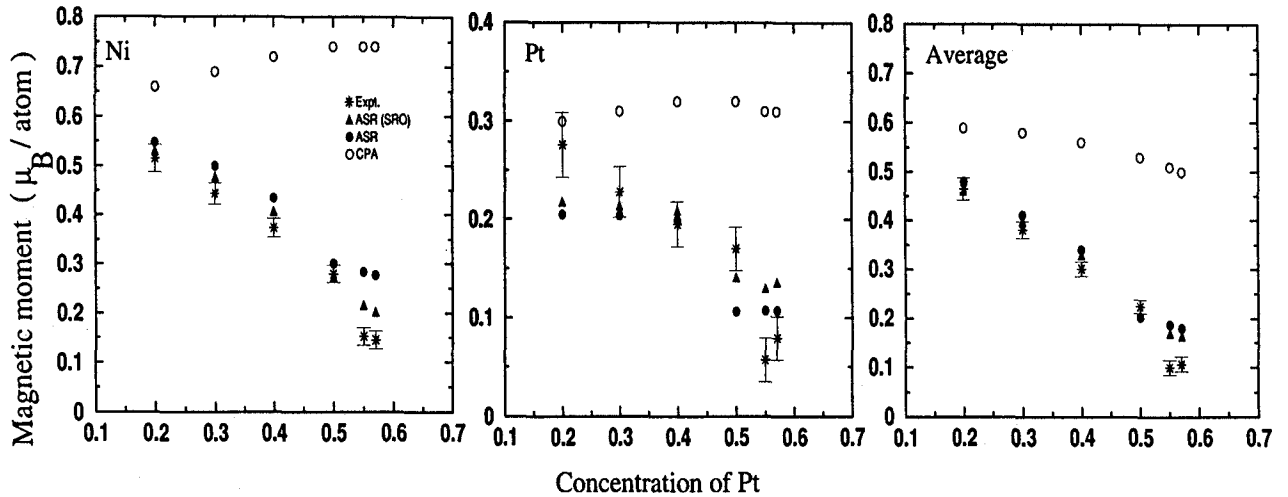


Figure 3.6: Magnetic moments in disordered Ni-Pt alloy systems using two different configuration averaging methods namely augmented space recursion (ASR) and coherent potential approximation (CPA) as compared to experimental values given by Parra and Cable (1980). ASR (SRO) denotes the results taking short range ordering effect into account.

Disordered alloys :

We have plotted the local and average magnetic moments of disordered Ni-Pt system in Figure 3.6. The comparison of calculated disordered magnetic moments using augmented space recursion (ASR) method with vBH exchange correlation potentials and experimental lattice parameter matches well with experimental values [Parra and Cable (1980)] in all concentrations except 55% and 57% of Pt. Our calculations of magnetic moments using coherent potential approximation (CPA) method using vBH exchange correlation potential and experimental lattice parameters are very different than the calculations using ASR method and experimental estimates [Parra and Cable (1980)]. Using CPA the local magnetic moments of Ni do not even follow the trend of corresponding experimental estimates. ASR being capable to go beyond single site approximation taking into account lattice relaxation and off diagonal disorder effect which is very important in NiPt alloys provides better agreement with experiment than CPA. Our calculated values for 55% and 57% concentration of Pt using ASR method are in higher side in comparison to the experimental estimates which leads us to suspect the presence of short range ordering effect. We performed calculations incorporating short range order for all concentration of

Pt in this system and found that the magnetic moments of Ni decreases by appreciable fraction for 55% and 57% concentration of Pt. The moment of Pt increases slightly. These give rise to the decrease of average magnetic moment in these concentrations. Calculations incorporating the effect of short range order agrees well with experimental estimate of Parra and Cable (1980).

3.2 Summary

To summarize, our study for ordered alloys to investigate the role played by different possible exchange correlation functionals shows that choice of the exchange-correlation potential has considerable effect on the values of the equilibrium lattice constants as well as magnetic moments.

The present study on disordered alloys shows that the single site approximation based methods work reasonably well for Fe-Pt systems and is in close agreement with our ASR predictions. For the Co-Pt system, the CPA begins to deviate from the ASR. CPA based calculations show slight increase in the local magnetic moment of Co with increasing Pt concentration, while the ASR shows almost constant behaviour.

It is in the Ni-Pt alloy that CPA shows the largest deviation from the ASR. The CPA estimates of the magnetic moments are quite different from the experimental values. It predicts increase of the local magnetic moment on Ni with increasing Pt concentration, whereas experimentally the reverse behaviour is observed. In the absence of local environment effects, increase of Pt concentration in Ni-Pt should lead to increase in the local Ni moment, since isolated clusters of Ni in Pt become more probable. This leads to narrowing of the local density of states on Ni and consequently according to the Stoner picture, an increase in the local Ni moment. Finally in the dilute limit, this local moment should approach the moment of an isolated Ni atom. This behaviour is certainly seen in Fe-Pt alloys. However, the fragile moment on Ni seems to need at least 50% Ni atoms in its nearest neighbour environment, otherwise it loses its local moment. This is indeed what one sees in experiment and is a strong indicator of large local environmental effect in Ni-Pt. The CPA predicts increase of the local magnetic moment on Ni with increasing Pt concentration. This is expected, since the CPA does not take into account the effect of local environment. The ASR, however, predicts the correct trend with increasing Pt concentration. The estimates of the actual value of the local magnetic moments are also much better.

Our total energy calculation as a function of short range order confirms the ordering tendency in these systems. The calculation of magnetic moments as a function of short

range order shows that its effect is small on the magnetism in Fe-Pt and Co-Pt disordered alloys but significant on the magnetism of disordered Ni-Pt.

Finally, the numerical details of calculations, convergence with the number of k-points in the Brillouin zone integrations, choice of atomic sphere radii, proper convergences in the the ASR, the proper choice of the minimal basis set in the TB-LMTO, all of these affect the actual values of the estimated magnetic moments.

Chapter 4

Study of phase stability in NiPt systems

In the present chapter we focus on the application of the augmented space recursion method for phase stability study in Ni-Pt alloys. This system of alloys is of importance because of the possible need for relativistic corrections due to the heavy mass of Pt as well as the effects due to charge transfer and size mismatch between Ni and Pt. This therefore forms a perfect candidate for testing the applicability and limitations of our formalism, bringing in the relative importance of various effects for the accurate description of phase formation in this system. All calculations have been done in the nonmagnetic phase of Ni-Pt alloys. The phase diagram of this [Dahmani *et al* (1985)] alloy system shows that the magnetic transition temperature is below the chemical order-disorder transition temperature. Considering the fragile magnetic moment of Ni, one would therefore expect the influence of magnetism to be negligible on the chemical order in this system.

The previous studies of ordered and substitutionally disordered NiPt alloy systems have shown the importance of inclusion of relativistic effects. Treglia and Ducastelle (1987) had shown that late transition metal alloys should exhibit phase separating tendencies but they argue that the exceptional ordering behavior of NiPt is due to the relativistic corrections. In a first principle study, Pinski *et al* (1991, 1992) found that the disordered fcc $\text{Ni}_{1-x}\text{Pt}_x$ alloy at $x = 0.5$, calculated by means of the single site KKR-CPA, becomes unstable at low temperatures, to a perturbation by a $\langle 100 \rangle$ ordering wave and concluded that the corresponding long range ordered state (LRO) i.e. the $L1_0$ structure should be the predicted ground state for which the large size mismatch between Ni and Pt plays the main role and the effect of relativity can be neglected. However, Lu *et al* (1991, 1992) pointed out that a local ordering tendency determined by perturbation analysis, doesn't necessarily predict the correct LRO ground state if the size mismatch of the two elements is large, as is the case for Ni and Pt and concluded that relativity is the

The contents of this chapter has been published in Durga Paudyal, T. Saha-Dasgupta and A. Mookerjee, *J. Phys.: Condens. Matter* 15 1029 (2003)

sole reason for long range order in NiPt. The work of Singh *et al* (1993) demonstrated that the relativistic effects do stabilize the ordered structures over the disordered solid solution. Recently Ruban *et al* (2002) have studied the problem of phase stability in NiPt alloy system based on ordered calculations with the inclusion of Madelung energy with multipole corrections. In this chapter, we examine the relativistic treatment of the Hamiltonian and charge transfer and lattice relaxation effects on the electronic structure and phase stability of face-centered cubic NiPt system at 25%, 50% and 75% of concentration of Pt. As mentioned already, the augmented space recursion (ASR) technique, which we use here, is capable of taking into account environmental effects, effects of short range order and local lattice relaxation effects due to size mismatches. To circumvent the problem of calculation of Madelung energy contribution for disordered system, we have used the appropriate effective atomic sphere radii for each of the constituents so that the spheres are neutral on the average and this has been done with precision at each concentration [Kudrnovský and Drchal (1990)]. We have shown that without inclusion of relativistic effects the formation energy comes out to be positive which contradicts experimental results. With the scalar relativistic corrections, involving mass-velocity and Darwin terms, the formation energy comes out negative indicating that the relativistic effects play an important role in NiPt alloys in agreement with earlier studies. We find that the charge transfer effects have also an important role to play in deciding on the correct ground state structure, particularly when the concentration of Pt is high. Our study on transition temperatures based on a mean field theory could reproduce the qualitative experimental trends.

4.1 Results and discussions

We have applied our formalism discussed in Chapter 2 in calculating the effective pair potentials for the FCC based NiPt alloys for concentrations $x = 0.25, 0.5$ and 0.75 of Pt. The calculation of the effective pair potentials has been restricted up to fourth nearest neighbour interactions. Total energy density functional calculations were performed at the concentration $x = 0.25, 0.5$ and 0.75 of Pt. The Kohn-Sham equations were solved in the local density approximation (LDA). The LDA was treated with in the context of tight binding linear muffin tin orbitals (TB-LMTO) in the atomic sphere approximation (ASA). The calculations were performed non relativistically as well as scalar relativistically and the exchange correlation potential of Von Barth and Hedin was used. We have theoretically calculated lattice constants via energy minimization procedure in both nonrelativistic as well as scalar relativistic cases and used them in the corresponding calculations of formation energies as well as pair interactions in these alloy systems. Two sets

of calculations were performed, one with the same Wigner-Seitz radius (charged spheres) for Ni and Pt. In the other set we followed the procedure introduced by Andersen *et al* (1987, 1992) and extended by Kudrnovský and Drchal (1990), which allows us flexibility in the choice of ASA radii for the constituents. The idea is to choose ASA radii of atomic species in such a way that the spheres are charge neutral on the average. The potential parameters Δ_i^I and γ_i^I of the constituent I were then scaled by the factors $(s^I/s^{alloy})^{2l+1}$ to account for the fact that the Wigner-Seitz radius of constituent I, s^I , is different from that of the alloy, s^{alloy} . These potential parameters were used to parameterize the alloy Hamiltonian. For the purpose of augmented space recursion, seven shell map was generated and thirty five seed energy point recursion was performed, as explained in Chapter 2, to calculate the Fermi energy with the second order LMTO-ASA Hamiltonian through the recursion method using eight level of recursion and analytical terminator of Luchini and Nex. For the effective pair potentials, we used the orbital peeling method within the frame work of ASR for the calculation of peeled averaged Green function described in detail in Chapter 2.

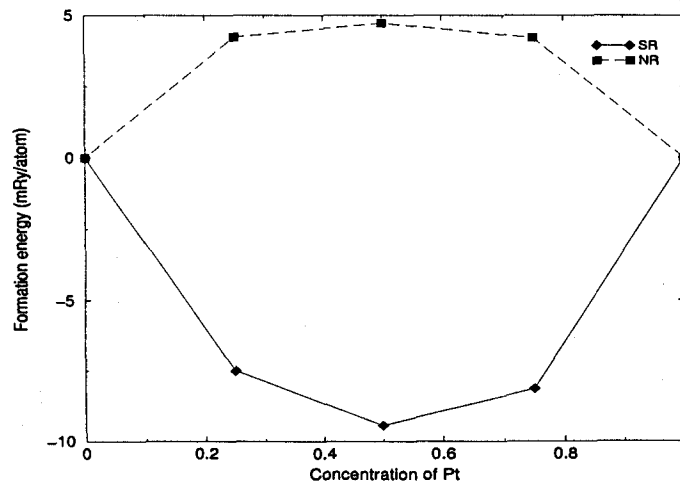


Figure 4.1: Formation energy vs concentration of Pt with the choice of neutral charge spheres.

In Figure 4.1 we have shown the formation energy of NiPt alloy system with various Pt concentrations based on ordered calculations. It shows that without inclusion of relativistic effects the formation energy comes out to be positive which contradicts experimental results. With the inclusion of scalar relativistic corrections the formation energy comes out to be negative. This indicates that relativistic effects play an important role in the stability of NiPt alloys, in agreement with earlier studies. Our results are in closer agreement with previous works based on the Full-Potential LMTO and the Connolly-Williams

Table 4.1: Formation energies for Ni_xPt_y with the choice of neutral charge spheres including scalar relativistic corrections. The values in brackets are without relativistic corrections. The corresponding estimate for charged sphere calculations are shown with *'s. ** refers to calculations without combined correction. *** refers to disordered formation energy.

y	Reference	Formation energy in mRyd/atom SR (NR)
0.25	this work	-7.50(4.25)
	this work	-7.59*(4.17)*
	Expt.[Amador <i>et al</i> (1993)]	-5.16
	FPLMTO + CWM[Amador <i>et al</i> (1993)]	-6.30
	LMTO[Amador <i>et al</i> (1993)]	-7.17
	LMTO + CWM [Ruban <i>et al</i> (1995)]	-6.66
0.50	this work	-9.44(4.74)
	this work	-9.02*(4.85)*
	Expt.[Amador <i>et al</i> (1993)]	-7.06
	FPLMTO + CWM[Amador <i>et al</i> (1993)]	-8.69
	LMTO[Amador <i>et al</i> (1993)]	-8.5
	LMTO + CWM [Ruban <i>et al</i> (1995)]	-8.95
	KKR-ASA[Singh <i>et al</i> (1993)]	-12.00**
	KKR-ASA[Singh and Gonis (1994)]	-8.10
KKR-CPA[Singh <i>et al</i> (1993)]	-7.7***	
0.75	this work	-8.15(4.22)
	this work	-3.97*(6.65)*
	Expt.[Amador <i>et al</i> (1993)]	-4.78
	FPLMTO + CWM[Amador <i>et al</i> (1993)]	-6.40
	LMTO[Amador <i>et al</i> (1993)]	-6.70
	LMTO + CWM [Ruban <i>et al</i> (1995)]	-9.12

technique [Amador *et al* (1993), Ruban *et al* (1995), de Fontaine (1994)] and with experimental estimate. Singh *et al* (1993) have also calculated the formation energy for 50% of Pt. Their results for the formation energy obtained from ordered calculations without combined correction deviates quite a bit from ours as well as other results based on the Full-Potential LMTO and the Connolly-Williams technique [Amador *et al* (1993), Ruban *et al* (1995), de Fontaine (1994)], which is presumably due to the neglect of the combined correction in reference Singh *et al* (1993). Singh and Gonis (1994) have also done the calculation with combined correction which shows better agreement. The full-potential methods are expected to provide better estimates than other methods. The full comparison of present and previous available results on formation energies are compiled in Table 4.1

We next approached the problem from the disordered end. We started from a completely disordered alloy and set up concentration wave fluctuations in it to see when this destabilizes the disordered phase as suggested by Khachatryan (1978, 1983). The calculation of the lattice distortion for disordered alloys has been carried out within the structural model given by rigid ion structure (RIS) [Mašek and Kudrnovský (1986)] which is explained in Chapter 2.

We have computed the effective pair potentials for two sets of potential parameters with charged and charge neutral spheres which are compared with available previous results in Tables 4.2 and 4.3. Figure 4.2 shows that the effective pair potentials for NiPt₃ is very small in magnitude using potential parameters with charged spheres. We used these pair potentials to calculate the anti-phase boundary energy. The anti-phase boundary energy comes out to be negative for NiPt₃ and NiPt indicating stability of DO₂₂ over L₁₂ for NiPt₃ and A₂B₂ over L₁₀ for NiPt. Further we calculated the minima of the special points according to the prescription described in Chapter 2. In the case of NiPt₃ and NiPt shown in Figure 4.4, we could not get the minima at $\langle 100 \rangle$ which is not quite correct because experiments show NiPt₃ has L₁₂ and NiPt has L₁₀ ordering. But in the case of Ni₃Pt we could get the positive anti-phase boundary energy as well as minima at $\langle 100 \rangle$ correctly showing the ordering L₁₂. In Figure 4.5 we have plotted the effective pair potentials as a function of energy relative to Fermi energy and number of neighboring shells with charge neutral potential parameters including scalar relativistic corrections which shows that the first nearest neighbor pair potentials are larger in magnitude than the second, third and fourth nearest neighbour pair potentials. With potential parameters from neutral sphere calculations including scalar relativistic corrections for NiPt₃ and NiPt the anti-phase boundary energies come out to be positive and the minima of special points are at $\langle 100 \rangle$ correctly showing L₁₂ and L₁₀ orderings. If we use charge neutral

Table 4.2: The effective pair potentials for NiPt alloy system calculated with potential parameters taken from calculations with the choice of charged spheres and including scalar relativistic corrections. (O-L) refers to calculations without multipole corrections, M refers to calculations with multipole corrections and SCI to calculations with screened Coulomb interactions. US-PP refers to ultrasoft pseudo-potentials. * refers to non-relativistic calculations.

Reference	v_1 (mRy/atom)	v_2 (mRy/atom)	v_3 (mRy/atom)	v_4 (mRy/atom)
Concentration of Pt = 25%				
Present work	11.36	-0.05	-0.07	-0.41
	11.972*	0.015*	0.054*	0.046*
Concentration of Pt = 50%				
Present work	7.832	0.114	-0.129	-0.057
	8.597*	0.10*	0.053*	0.263*
Singh <i>et al</i> (1993)	4.22	1.14	0.22	-1.04
	4.94*	0.52*	0.32*	-0.18*
Pinski <i>et al</i> (1991, 1992)	9.4*	0.8*	0.4*	-0.2*
Pourovskii <i>et al</i> (2001) CWM-ASA+M SGPM	5.00	0.25	0.19	-0.28
	5.28	0.06	-0.82	-0.66
Ruban <i>et al</i> (2002) with SGPM ASA+M (O-L)(SCI) ASA (SCI)	14.05(15.44)	0.32(-0.10)	-1.09(-1.22)	-1.76(-0.84)
	12.26(14.35)	0.53(-0.15)	-1.31(-1.48)	-2.14(-0.98)
With Connolly Williams ASA+M ASA+M (O-L)	12.68	1.31	-0.02	-0.73
	13.70	0.49	-0.86	-1.39
ASA	14.33	0.28	-1.72	-1.92
US(PP)	12.81	1.30	0.69	-0.40
Direct calculation(SCI) ASA+M	12.45	0.47	-0.49	-0.65
Concentration of Pt = 75%				
Present work	2.785	0.236	-0.116	0.276
	3.813*	0.361*	-0.175*	0.366*

Table 4.3: The effective pair potentials for NiPt alloys with potential parameters taken from calculations with the choice of charge neutral spheres including scalar relativistic corrections. The corresponding estimate for non relativistic calculations are shown with *'s.

Reference	v_1 (mRy/atom)	v_2 (mRy/atom)	v_3 (mRy/atom)	v_4 (mRy/atom)
Concentration of Pt = 25%				
Present work	12.34	-0.092	-0.046	-0.54
	13.08*	-0.021*	0.152*	-0.041*
Concentration of Pt = 50%				
Present work	10.08	0.1	0.004	-0.24
	10.111*	0.126*	0.246*	0.175*
Singh <i>et al</i> (1993)	16.02	1.34	0.06	-1.58
	11.96*	0.66*	0.28*	-0.46*
Ruban <i>et al</i> (2002) Neutral(GPM)	5.49	1.22	0.01	-0.73
Concentration of Pt = 75%				
Present work	8.9	0.26	0.1	0.02
	7.874*	0.297*	0.276*	0.34*

potential parameters without including scalar relativistic effect the anti-phase boundary energies come out to be positive for Ni₃Pt and NiPt but negative for NiPt₃. This shows for NiPt₃ both scalar relativistic as well as charge transfer effects play important role to predict correct ground state.

So, we argue that on increasing the concentration of Pt atom the careful treatment to take into account of charge transfer effect becomes increasingly important. In Figure 4.3, we have also shown the effective pair potentials without scalar relativistic corrections. For NiPt₃ it is clearly seen that the effective pair potentials with scalar relativistic corrections are larger in magnitude than the non relativistic ones.

In Figure 4.5 we have plotted that the effective pair potentials vs concentration of Pt with charge neutral potential parameters including scalar relativistic corrections which shows that the first nearest neighbour effective pair potentials decrease with the increase of the Pt concentration. Singh *et al* (1993) and Singh (1996) have also calculated the

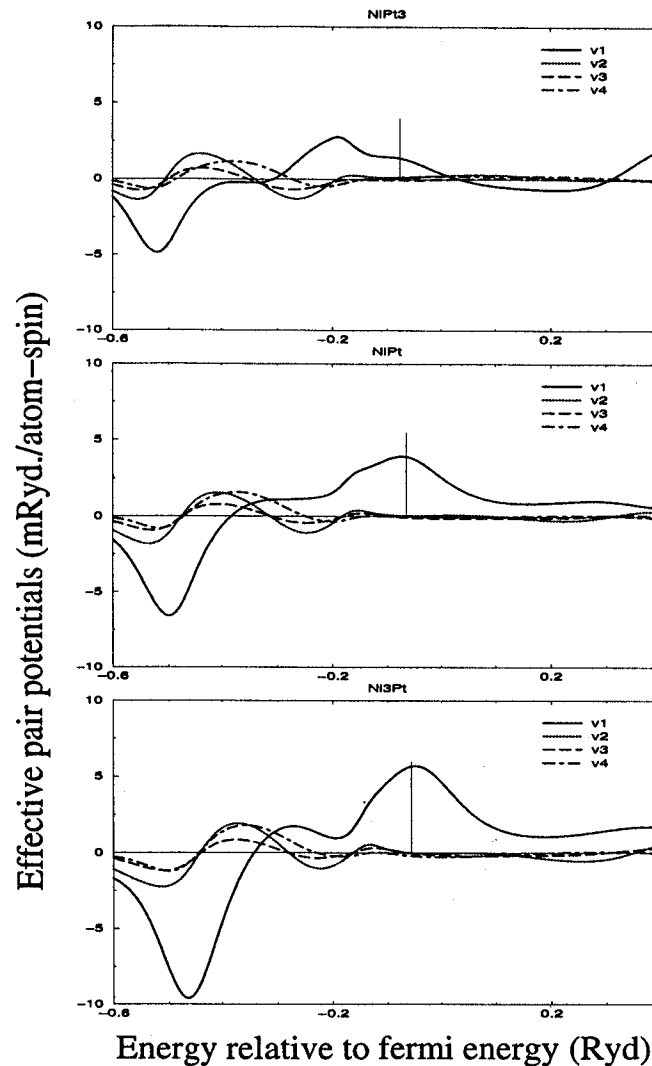


Figure 4.2: (i) The effective pair potentials calculated with the choice of charged spheres including scalar relativistic corrections.

effective pair potentials using KKR-CPA-GPM method. Their values of effective pair potentials are much larger than ours. They pointed out that due to the large values of effective pair potentials the ordering energy and ordering temperatures (transition temperatures) are much higher than that observed experimentally. Our estimates give rise to instability temperatures which are closer to the experimental results (shown in Figure 4.7). For example, our estimate for the instability temperature for the 50% alloy is 1683°K, whereas the estimate from the KKR-CPA is around 2979°K. The experimental estimates of the transition temperature is 950°K [Dahmani *et al* (1985)]. In KKR-CPA-

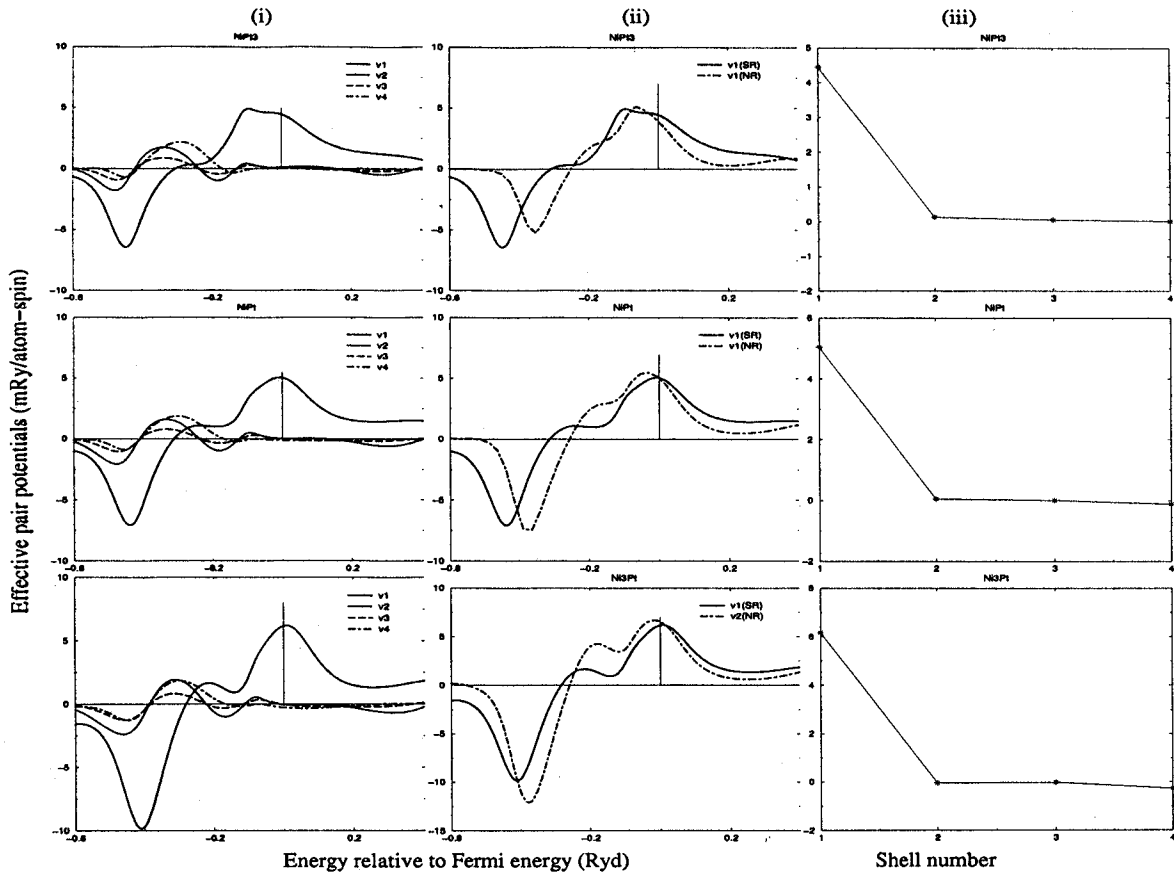


Figure 4.3: (i) The effective pair potentials as a function of energy, calculated with charge neutral potential parameters including scalar relativistic corrections. (ii) Comparison between the first nearest neighbour effective pair potentials with scalar relativistic corrections and without scalar relativistic corrections by taking charge neutral potential parameters. (iii) The effective pair potentials as a function of shell numbers with charge neutral potential parameters including scalar relativistic corrections.

GPM method one considers only the single site approximation and one does not take into account any off diagonal disorder which may arise because of size mismatch of the constituent atoms. The ASR, on the other hand, as discussed earlier can do this with facility. Our test calculation for NiPt (50% concentration of Pt) without taking into account lattice relaxation due to size mismatch effect gives an estimate of instability temperature of 2363⁰K which is indeed higher than that of our original estimate with taking into account lattice relaxation due to size mismatch effect. The calculations of Pinski *et al* (1991, 1992) were carried out without scalar relativistic effects. Their values are consequently rather large as compared to ours. Ruban *et al* (2002) have calculated pair

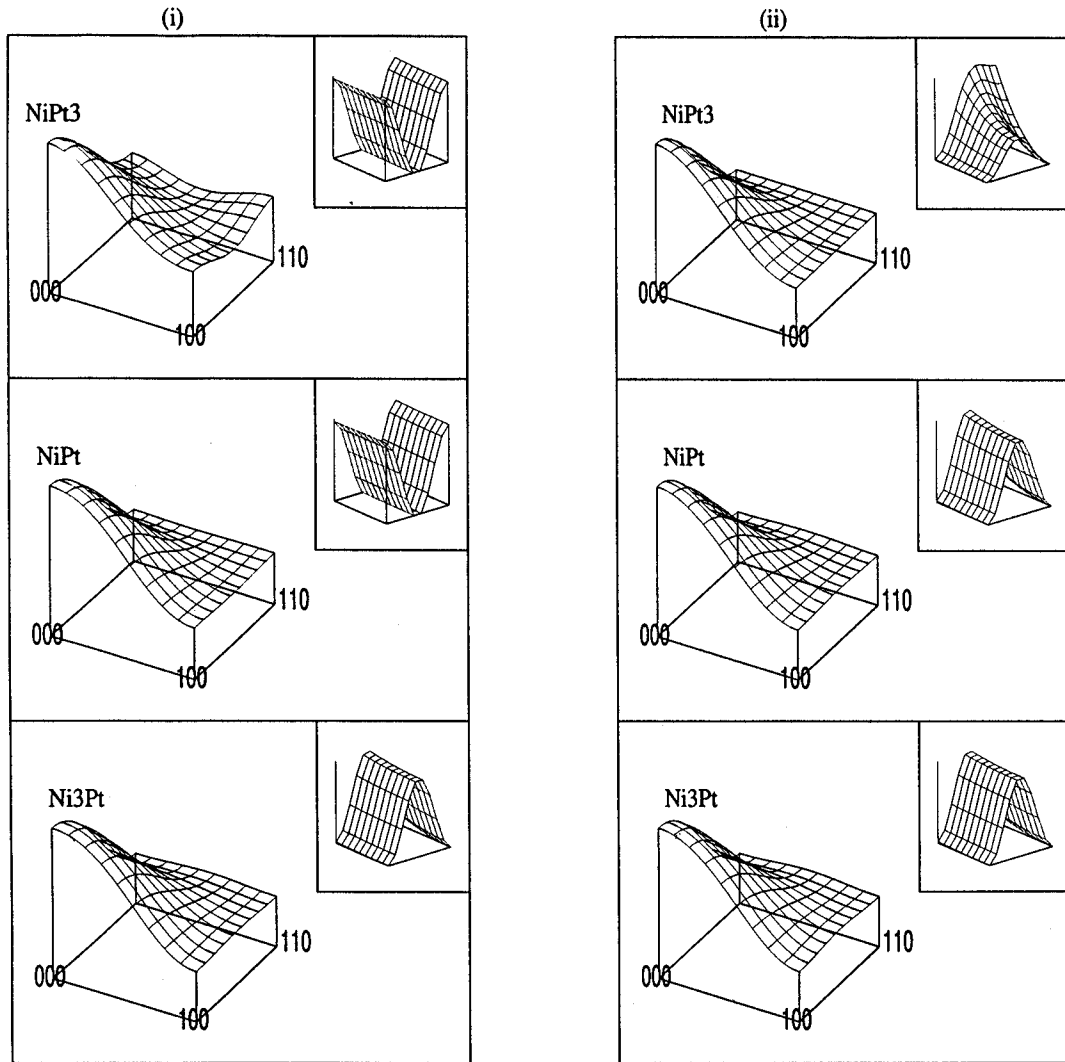


Figure 4.4: The $V(\vec{k})$ surface for NiPt alloy system with potential parameters calculated with the choice of (i) charged spheres (ii) charge neutral spheres, on $k_z = 0$ plane. The figures in inset show the enlarged view of the corresponding $V(\vec{k})$ surfaces on $k_z = 0$ plane in the vicinity of the (100) to (110) direction.

potentials for 50% concentration of Pt using different methods and showed that different methods give different values of pair potentials. Their nearest neighbor pair-potential is slightly higher than ours. The effective pair potentials obtained by Pourouvkii *et al* (2001) from the neutral charge spheres GPM method are similar to the estimates of Ruban *et al* (2002).

In Figure 4.6 we have shown the ordering energy, anti-phase boundary energy and

Table 4.4: The anti-phase boundary energies for Ni_xPt_y alloys from charged and neutral sphere calculations. The values in brackets are without relativistic corrections.

concentration of Pt	APB energy (mRy/atom)	
	Charged spheres	Neutral spheres
0.25	1.41(0.017)	2.07(0.793)
0.50	-0.402(-0.94)	0.876(0.158)
0.75	-1.804(-2.525)	0.06(-0.553)

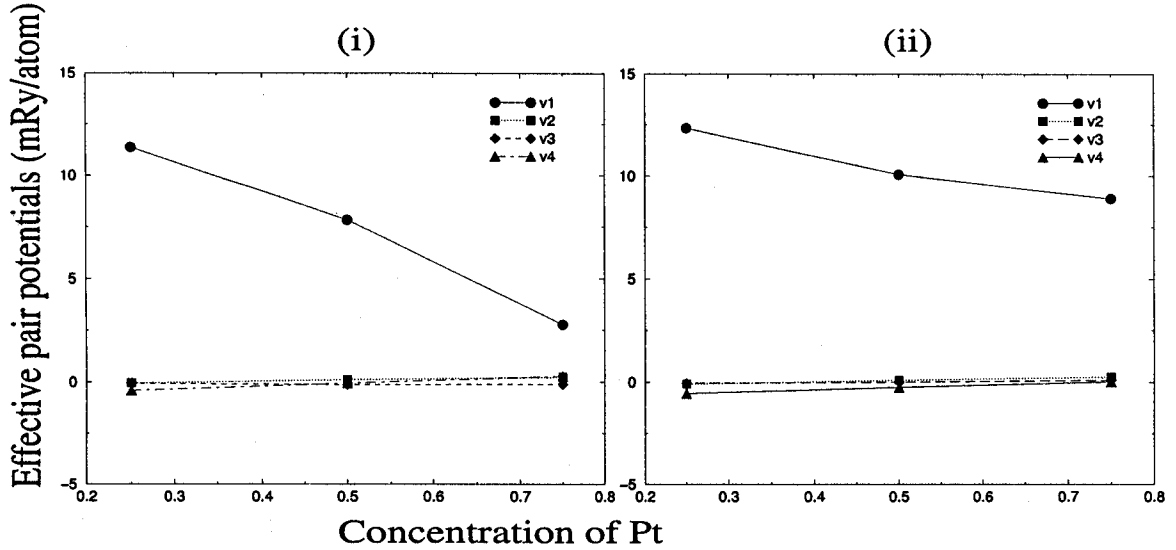


Figure 4.5: The effective pair potentials vs concentration of Pt with the choice of potential parameters with (i) charged spheres including scalar relativistic corrections and (ii) charge neutral spheres including scalar relativistic corrections.

instability temperatures vs concentration of Pt with charge neutral potential parameters including scalar relativistic correction. The ordering energy in all three cases Ni_3Pt , NiPt and $NiPt_3$ is negative showing the stability of ordered structures compared to disordered solution. Among all three concentrations, NiPt attains maximum value of ordering energy which confirms that $L1_0$ in NiPt system is the most stable structure. The anti-phase boundary energy in all these cases Ni_3Pt , NiPt and $NiPt_3$ comes out to be positive showing the ordering structures $L1_2$ for Ni_3Pt , $L1_0$ for NiPt and $L1_2$ for $NiPt_3$ as described

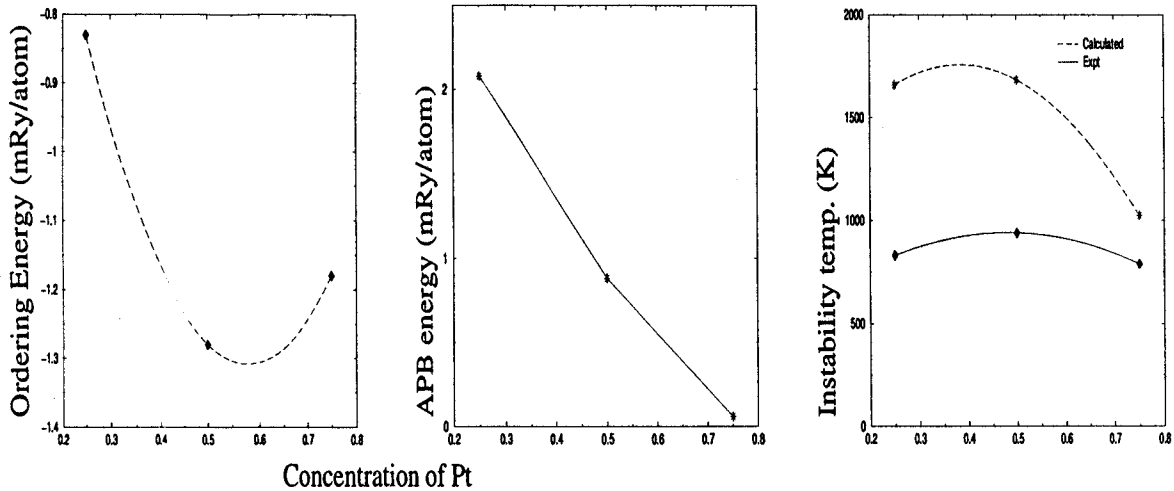


Figure 4.6: Ordering energy, anti-phase boundary energy and instability temperatures vs concentration of Pt with the choice of charge neutral potential parameters including scalar relativistic correction.

above. The magnitude of instability temperatures using the charge neutral potential parameters comes out to be larger than the experimental transition temperatures. However, the qualitative trend of the change of the instability temperatures with changing concentration of Pt comes out to be correct. Amador *et al* (1993) also reported the phase diagram (instability temperature vs concentration of Pt) of this system described by the nearest neighbour tetrahedron effective interactions from clusters with appropriate effective volume. Their values for transition temperatures are smaller than ours but the trend is not same as experimental findings and ours.

4.2 Summary

Our total energy calculations for the ordered alloys indicate that in order to have the correct sign for the formation energy, it is essential to include relativistic corrections. Our analysis of the concentration wave approach indicates that for Ni₃Pt neither relativistic correction nor the charge transfer effect is essential for the correct prediction of the $L1_2$ ground state. For NiPt although scalar relativistic correction is not essential, careful treatment of charge transfer effect is a must to predict the correct ground state ($L1_0$). For NiPt₃ both these corrections are essential to predict the correct ground state $L1_2$.

Although it seems that qualitatively the relativistic corrections and charge transfer effect plays the essential role only for the high Pt content alloys, for quantitative prediction

of the instability temperature both these corrections are required across the concentration range.

The main conclusions of this Chapter are :

- We have demonstrated that for accurate prediction of the ground state structures and instability temperatures for alloys with components with large atomic size differences like NiPt, it is essential to take into account both relativistic corrections and averaged charge neutrality of the atomic spheres.
- We have also demonstrated the augmented space recursion combined with the first-principles tight-binding linear muffin-tin orbitals (TB-LMTO) and the orbital peeling are both computationally feasible and suitable techniques for such studies as described above.

These techniques will form the basis of our further study into similar alloy systems, but with magnetic effects included.

Chapter 5

Phase stability analysis in Fe-Pt and Co-Pt alloy systems

Study of alloy phase stability in general is complicated and modeling of all the relevant effects active in a particular alloy system is a challenge by itself. One needs to take into account systematically the effects like the on-site and off-site disorder, charge-transfer effect, the effect of local lattice distortions, the short range ordering effect, relevant for a given alloy system as already demonstrated in the case of Ni-Pt. For alloys with magnetic component, a further ingredient, namely magnetism is added to the problem. One might naively think that one needs to be concerned with magnetism only if one is interested in magnetic properties of materials. This is however not the case. Rather the formation of stable ordered structures can depend on properly taking into account magnetism, which can strongly effect the phase stability. The most illustrative example is that of the strong ferromagnet Ni-rich Fe-Ni alloys, where the ordering is entirely driven by magnetism and absence of spin-polarization in calculation leads to wrong ground state with phase-segregated rather than phase-ordered configuration [Ducastelle (1991)]. There are also many other magnetic alloy systems which are not so strong ferromagnets as in the case of Ni-rich Fe-Ni with completely full majority spin d-states but possess similar attributes.

In our present study, we considered the problem of phase stability in Fe-Pt and Co-Pt alloys. We have already discussed at length the electronic and magnetic properties of Fe-Pt and Co-Pt systems in Chapter 3. In this chapter we take the task of systematic first-principles study on chemical ordering tendency in these alloy systems. The phase diagrams of Fe-Pt [Stahl *et al* (2003)] and Co-Pt [Sanchez *et al* (1988)] alloy systems show that the magnetic transition temperature is below the chemical order-disorder transition

The contents of this chapter has been published in Durga Paudyal, T. Saha-Dasgupta and A. Mookerjee, *J. Phys.: Condens. Matter* 16 7247 (2004)

temperature in most part of the phase diagram except in the region of high concentration of Co (above 60%) in Co-Pt alloys. In this region one would therefore expect a strong influence of magnetism on the chemical order. In our approach, the magnetism part is dealt within Stoner theory with rigidly exchange-split, spin-polarized band. Within this approach the paramagnetic phase has “no exchange-splitting” and the magnetization in the paramagnetic phase is lost via Stoner particle-hole excitations. However, the other point of view of describing the paramagnetic phase could be that of the local-moment formation where the average over the local moment’s orientations produce zero overall magnetization but nevertheless there exists a local-moment disorder [Staunton *et al* (1997)]. Whether such description is necessary or not depends on the time-scale associated with the rate of change of orientation of the local moments as compared to the time scale of electronic motion. Staunton *et al* (1997) have shown that consideration of such local moment formation can be important in describing properly the atomic short-range order data in FeV system. We are yet to explore the effect of such local moment formations for the paramagnetic Fe-Pt and Co-Pt alloys. However our results obtained within Stoner approach already show reasonable agreement with experimental results, suggesting the necessity of inclusion of such effect in a second level. Our calculational scheme is that of augmented space recursion coupled with orbital peeling technique implemented within the framework of first-principles electronic structure calculation of TB-LMTO as the method of calculation of pair interaction energies. In particular, we have generalized our earlier technique to take into account of magnetic effects for the cases where the magnetic transition is higher than the order disorder chemical transition temperature as in the case of Co_3Pt . Our scheme has been already proved to be efficient to handle the issues of off-diagonal disorder, large charge transfer effect, local lattice distortion which are important for alloys with large size mismatch between components and components with very different valences as is the case in Fe-Pt and Co-Pt. Due to the presence of the high-mass element Pt, relativistic effect also turn out to be crucial, which has been dealt within the scalar relativistic theory. We perform a thorough analysis of the phase stability in terms of pair interaction, effective pair potential surfaces, instability temperatures and atomic short range order maps. Our theoretical results obtained within this framework successfully reproduce the experimentally observed trends.

Table 5.1: Pair interaction energies upto fourth nearest neighbour in mRyd/atom. The values inside bracket in the case of 25% concentration of Pt in Co-Pt are with the magnetic contribution.

Conc. of Pt (x)	V ₁	V ₂	V ₃	V ₄
Fe_{1-x}Pt_x				
0.25	5.98[4.73]	-0.12[-0.15]	0.39[0.15]	-0.15[-0.33]
0.50	5.80	-0.15	0.28	-0.48
0.75	4.14	-0.03	0.20	-0.13
Co_{1-x}Pt_x				
0.25 1*	9.97[8.00] [4.06]	-0.11[-0.13] [-1.83]	0.24[0.17] [0.39]	-0.30[-0.21] [-0.22]
0.50	8.04	-0.01	0.15	-0.12
0.75 2*	7.07 1.11	0.08 -2.27	0.10 0.33	-0.18 -0.93

1* : Capitan *et al* (1999); 2* : Kentzinger *et al* (2000)

5.1 Results and discussions

5.1.1 Pair interaction energies

The pair interaction energies calculated for 25, 50 and 75% concentration of Pt in Fe-Pt and Co-Pt alloy systems using above explained formalism are shown in the Table 5.1. In all cases we have obtained positive first nearest neighbour pair interaction energies which indicate the ordering tendency in these alloys in accordance with the experimentally predicted ordering tendencies. These calculations are carried out using experimental lattice parameters shown in Chapter 3.

From the Figure 5.1 we see the increase in first nearest neighbour pair interaction energies when one goes from Fe-Pt to Co-Pt. Figure 5.1 also shows the strong concentration dependence of pair interaction.

For 25% concentration of Pt in Co-Pt alloys, we have included the effect of magnetism since the Curie temperature lies above the order disorder transition temperature in the experimental phase diagram [Sanchez *et al* (1988)]. The first nearest neighbour pair interaction energy calculated with the inclusion of magnetic contribution comes out to be

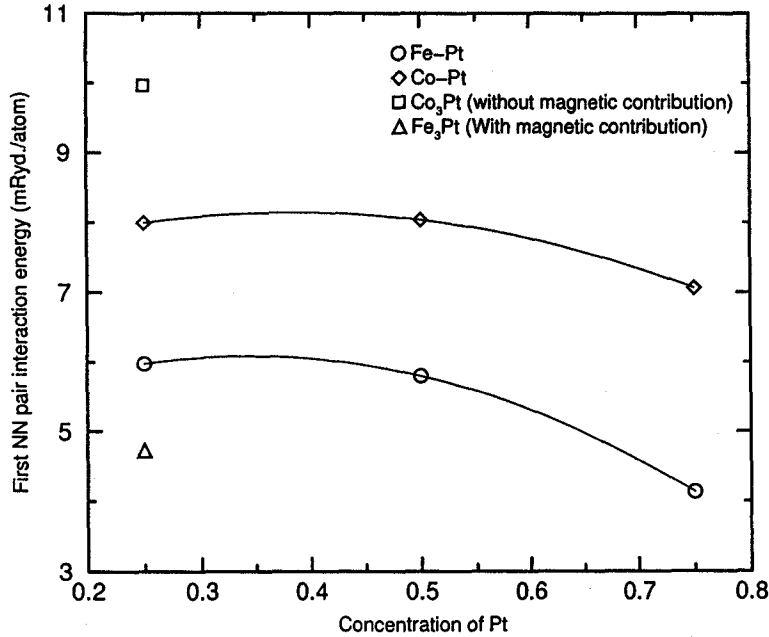


Figure 5.1: Plot of first nearest neighbour pair interaction energies (V_1) in Fe-Pt and Co-Pt alloys showing the concentration dependence.

lower than the corresponding value obtained without magnetic contribution.

In the experimental phase diagram of Fe-Pt alloy system [Stahl *et al* (2003)], the magnetic transition temperature (Curie temperature) for Fe₃Pt lies much below the order disorder chemical transition temperature. So it is not necessary to include the magnetic effect to study the chemical ordering problem. However to compare it with the Co₃Pt case we have carried out the calculation for Fe₃Pt alloy too. Our calculation shows the same trend as Co₃Pt, namely the dominant V_1 interaction decreases on including magnetic effect.

In Figure 5.2, we show the density of states with and without magnetic contribution for 25% concentration of Pt in Co-Pt system. In magnetic case we see that the majority spin band almost full. The contribution to the pair interaction energy in this case mainly comes from the partially filled band. There is little decrease in the Fermi energy in magnetic case as compared to non magnetic case. This shifting of Fermi energy slightly reduces the pair interaction energy. The low value of first neighbour pair interaction energy in magnetic case is primarily due to the negative value of magnetic pair interaction energy between two Co atoms.

In Figure 5.3, taking the example of 25% concentration of Pt in Co-Pt with magnetic contribution, we show the variation of pair interaction energy as a function of nearest

neighbour shells. The pair interaction energy decreases rapidly while going from first nearest neighbour to second nearest neighbour shell. For comparison we have also plotted the pair interaction energies extracted by Capitan *et al* (1999) from their experimentally measured short range order using inverse cluster variation method. Our calculated first and second nearest neighbour pair interaction energies are higher than that of Capitan *et al* (1999). But there is agreement in the third and fourth nearest neighbour pair interaction energies. Though there are differences in the first and second nearest neighbour pair interaction energies between Capitan *et al* (1999)'s and ours, the trend of pair interaction energy as a function of nearest neighbour shells is similar as is seen from the Figure 5.3.

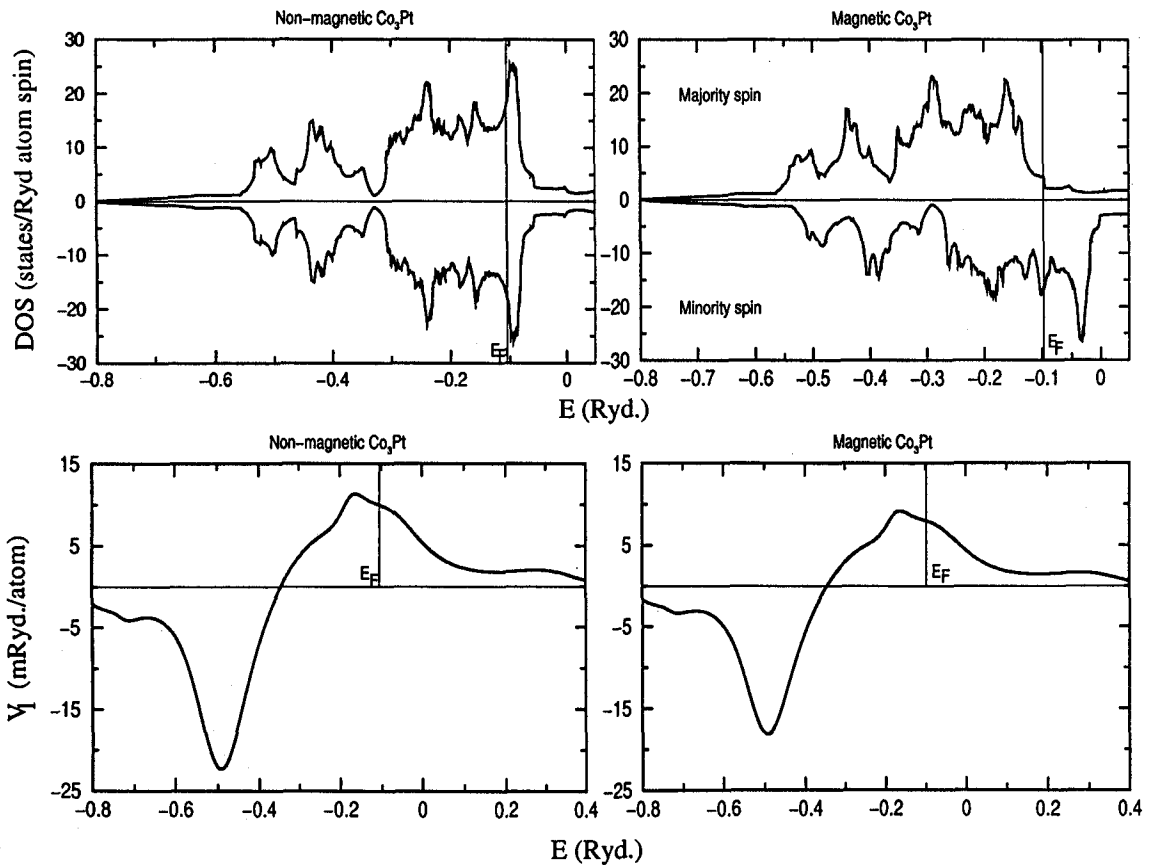


Figure 5.2: Density of states and first nearest neighbour pair interaction energy as a function of energy in Co₃Pt alloy system.

The pair interaction energies extracted by Kentzinger *et al* (2000) from their experiment on short range order using inverse cluster variation method for 75% concentration of Pt in Co-Pt are tabulated in Table 5.1. Their first neighbour pair energy is lower in magnitude than that of second neighbour pair interaction energy. Our calculated pair

interaction energies instead follow usual trend of having higher magnitude of first neighbour pair energy than that of second neighbour pair energy. Though there is substantial difference in the trend of pair interaction energies, the instability temperatures computed using both sets of pair interaction energies turn out to be almost same as shown in the Section 5.1.3.

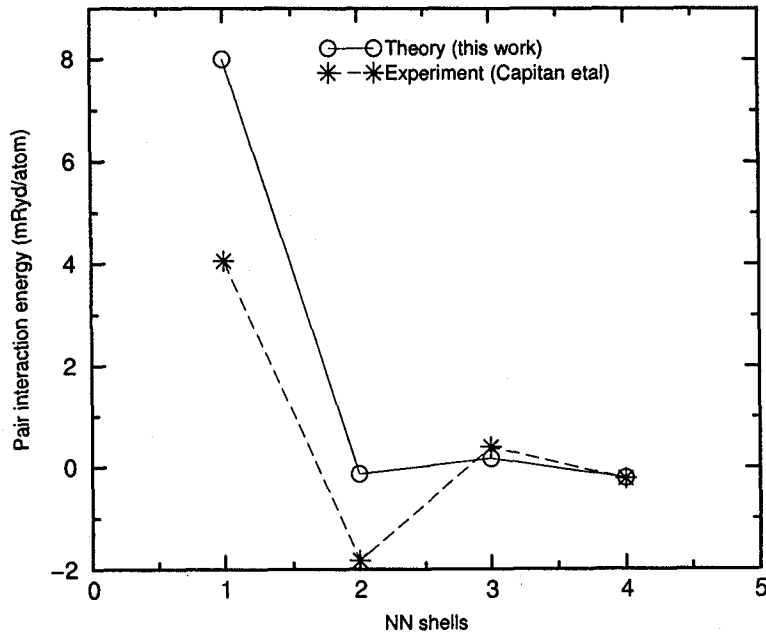


Figure 5.3: The calculated pair interaction energies as a function of shell numbers in Co_3Pt as compared to experimental estimates of Capitan *et al* (1999).

5.1.2 Effective pair potential surfaces

The effective pair potentials $V(\mathbf{k})$ calculated using pair interaction energies ($T = 0$) for Fe-Pt and Co-Pt alloys at 25, 50 and 75% concentration of Pt are shown in the Table 5.2. These effective pair potentials were obtained by the Fourier transform of above explained first four nearest neighbour pair interaction energies. The values of $V(\mathbf{k})$ for different ordering stars are compared in the Table 5.2. From the Table the minima are seen at the position $\langle 100 \rangle$. These minima clearly show the $L1_2$ chemical ordering for 25 and 75% and $L1_0$ chemical ordering for 50% concentration of Pt in these alloy systems. The value for $V(100)$ increases when one goes from 25 to 50% and then decreases while going from 50 to 75% concentration of Pt in Fe-Pt alloys. In Co-Pt alloys The value for $V(100)$ systematically decreases while going from 25 to 50 and then to 75% concentration of Pt.

Table 5.2: Effective potentials $V < \mathbf{hkl} >$. The values inside bracket in the case of 25% concentration of Pt in Co-Pt are with the magnetic contribution.

Conc. of Pt(x)	Expt. ordering	$V < 000 >$	$V < 100 >$	$V < 1\frac{1}{2}0 >$	$V < \frac{1}{2}\frac{1}{2}\frac{1}{2} >$
$\text{Fe}_{1-x}\text{Pt}_x$					
0.25	$< 100 > L1_2$	78.60	-29.56	-20.44	-1.08
0.50	$< 100 > L1_0$	69.66	-32.10	-19.34	-4.86
0.75	$< 100 > L1_2$	52.74	-19.90	-14.5	-1.38
$\text{Co}_{1-x}\text{Pt}_x$					
0.25 1*	$< 100 > L1_2$	121.14[96.78]	-46.06[-36.66]	-36.98[-30.06]	-2.94[-1.74]
	$< 100 > L1_2$	[44.46]	[-32.98]	[-15.90]	[8.34]
0.50	$< 100 > L1_0$	98.58	-34.86	-30.5	-1.38
0.75 2*	$< 100 > L1_2$	85.56	-30.76	-26.60	-2.64
	$< 100 > L1_2$	-3.54	-31.86	-2.62	2.46

1* : Capitan *et al* (1999); 2* : Kentzinger *et al* (2000)

In 25 % concentration of Pt in Co-Pt alloy, the magnetic transition temperature is higher than the order disorder transition temperature. Therefore we have included the effect of magnetism in the chemical order in this particular alloy. The comparison of $V(\mathbf{k})$ minima shown in the Figure 5.4 with magnetic contribution indeed matches with the minima obtained using the pair interaction energies extracted from the experimentally measured short range order parameters using inverse cluster variation method by Capitan *et al* (1999). This experimental measurement was done in ferromagnetic state. If we compare with the non-magnetic $V(100)$ surfaces we see that there is decrease in the chemical ordering which indicates that the magnetism actually reduces the chemical ordering in this alloy allowing to order in lower temperature. As a comparison the “artificial” magnetic $V(100)$ surface of Fe_3Pt alloy system shows that taking into account the effect of V_n farther than first nearest neighbour, magnetism increases slightly the tendency to chemical order over that of the non magnetic case.

The $V(100)$ minima obtained for CoPt_3 using our theoretically calculated pair interaction energies and that of extracted pair interaction energies from the experimentally measured short range order parameters using inverse cluster variation method by Kentzinger *et al* (2000) match well which is shown in Figure 5.5 The differences seen in the patterns of $V(\mathbf{k})$ is due to the differences in individual pair interaction energies in real

space. Though there is difference in $V(\mathbf{k})$ surface patterns, the value of $V(100)$ minima in both cases are very similar.

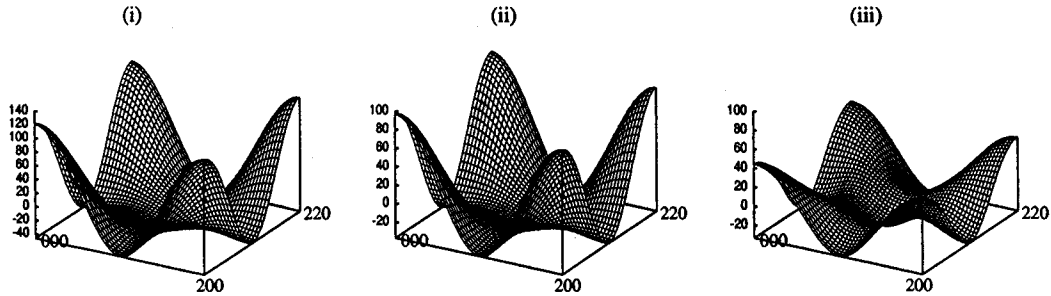


Figure 5.4: Effective pair potential $V(\mathbf{k})$ surfaces for Co_3Pt alloy system in the $(\mathbf{hk0})$ plane using our theoretically calculated pair interaction energies (i) without magnetic contribution and (ii) with magnetic contribution and (iii) using extracted pair interaction energies by Capitan *et al* (1999) from their experiment.

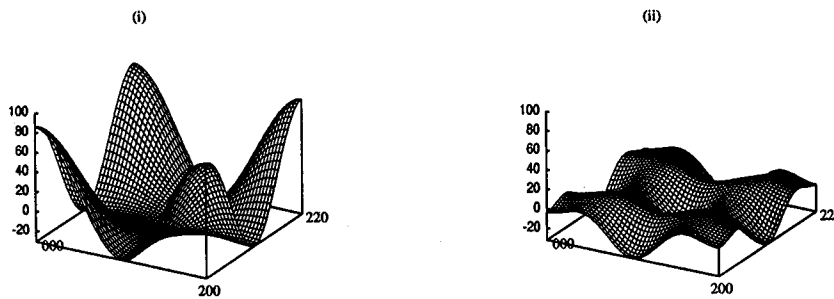


Figure 5.5: Effective pair potential $V(\mathbf{k})$ surfaces for CoPt_3 alloy system in the $(\mathbf{hk0})$ plane using (i) our theoretically calculated pair interaction energies and (ii) extracted pair interaction energies by Kentzinger *et al* (2000) from their experiment.

5.1.3 Instability temperatures

Using the pair interaction energies obtained by us, we have calculated the instability temperatures in Fe-Pt and Co-Pt alloys within Khachatryan's concentration wave approach as explained in Chapter 2. The results are shown in Figure 5.6. In Fe-Pt system the calculated order disorder transition temperatures are lower than that of corresponding experimental order disorder transition temperatures. We however clearly see the correct trend of calculated instability temperature with experimentally predicted transition temperature.

Our calculation with the inclusion of effect of magnetism for 25% concentration of Pt in Co-Pt alloys shows the instability temperature closer to experimental order disorder transition temperature than that of the calculated instability temperature with out magnetic effect. This is also in good agreement with the value obtained using the pair interaction energies extracted from the experimentally measured short range order parameters using inverse cluster variation method by Capitan *et al* (1999). For 50% concentration of Pt our calculated instability temperature matches with the calculation by Staunton's group [Razee *et al* (2001)] using KKR-CPA based method. The calculated values of instability temperature are much higher than the experimentally predicted order disorder transition temperatures. The values of instability temperatures obtained by us and Staunton's group [Razee *et al* (2001)] and that of Sanchez's group [Kentzinger *et al* (2000)] (using extracted pair interaction energies upto fourth nearest neighbour from the experimentally measured short range order parameters using inverse cluster variation method) for 75% concentration of Pt are almost similar and slightly lower than the experimental predictions of order disorder transition temperatures.

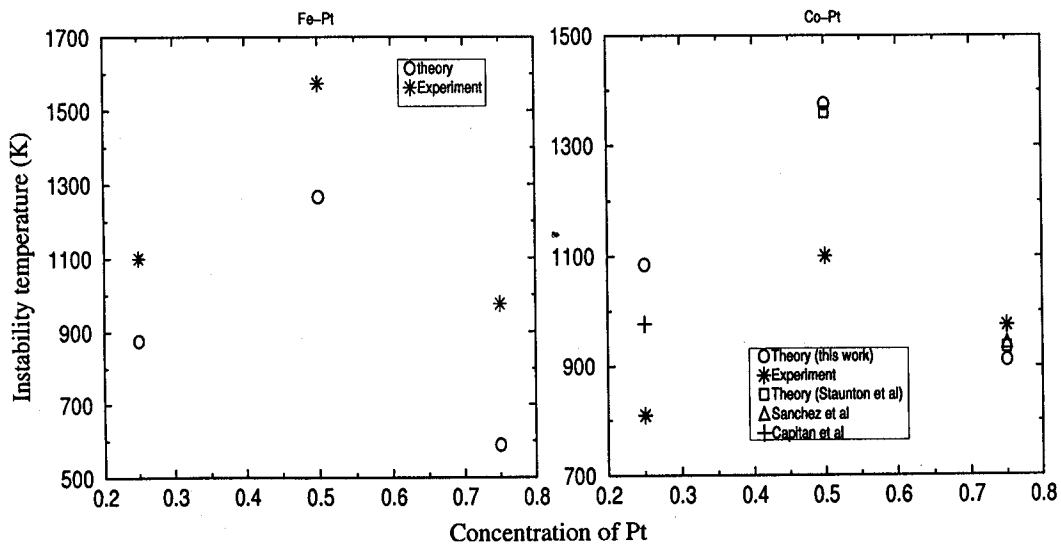


Figure 5.6: Theoretically calculated instability temperatures as compared to experimentally measured order disorder transition temperatures.

The experimental phase diagram of Co-Pt shows that the order disorder transition temperature for 75% concentration of Pt higher than 25% concentration of Pt. But the experimental phase diagrams of Fe-Pt and Ni-Pt show the order disorder transition temperature for 25% concentration of Pt higher than 75% concentration of Pt. Our calculation for Fe-Pt and Ni-Pt (shown in chapter 4) show the similar trend of instability temperature as that of experimental trend of order disorder transition temperature. In Co-

Pt our calculated instability temperature at 25% concentration of Pt is higher than that of 75% concentration of Pt. But the experimental order disorder transition temperature is otherwayround as pointed out above. This calls the need for further investigation in terms of important effects that might have been overlooked. One important effect among these could have been the neglect of possible local moment formations in the paramagnetic CoPt and CoPt₃ alloy systems which might be relatively more important than that in Fe-Pt systems. The next important effect to be taken into account in general for all alloy systems studied is the effect of electrostatic contribution in the effective pair interaction energies and the effect of multisite interactions in addition to the pair interaction.

Our comparison of calculated transition temperatures for Fe-Pt and Co-Pt shows that the transition temperatures for corresponding concentrations of Pt in these alloys increase as we go from Fe-Pt to Co-Pt (and then to Ni-Pt (shown in chapter 3)).

5.1.4 Short range order

The SRO parameters $\alpha(\mathbf{k})$ for different ordering stars calculated using pair interaction energies ($T = 0$) for Fe-Pt and Co-Pt alloys at 25, 50 and 75% concentration of Pt are shown in the Table 5.3. These SRO values were calculated at 10 K above the instability temperatures using above explained first four nearest neighbour pair interaction energies to see the effect of SRO in the disordered phase. These SRO values show the peak positions at $\langle 100 \rangle$. These peak positions correspond to the diffused scattering peaks which clearly show the L1₂ short range ordering for 25 and 75% and L1₀ short range ordering for 50% concentration of Pt in the disordered phase of these alloy systems. In Figure 5.7 we show the concentration dependence of SRO peaks $\alpha \langle 100 \rangle$. For 50% concentration of Pt in Fe-Pt and Co-Pt the magnitude of SRO peak is maximum. Next higher peak magnitude is for 25% concentration of Pt in these alloys and the least is for 75% concentration of Pt. The trend matches with the trend of experimental order disorder transition temperature.

The SRO patterns for Co₃Pt with magnetic contribution match with the patterns obtained by the Fourier transform of Capitan *et al* (1999)'s experimental real space SRO parameters which is shown in the Figure 5.8. If we compare with the non-magnetic SRO $\langle 100 \rangle$ patterns we see there is enhancement in the SRO peak which indicates that the magnetism actually enhances the short range ordering in the disordered phase of this alloy.

The SRO patterns obtained for CoPt₃ using our theoretically calculated pair interaction energies and that the patterns obtained by the Fourier transform of Kentzinger *et al* (2000)'s real space SRO parameters agree reasonably well (shown in Figure 5.9), although

Table 5.3: Short range order $\alpha < \mathbf{hkl} >$. The values inside bracket in the case of 25% concentration of Pt in Co-Pt are with the magnetic contribution.

Conc. of Pt (x)	Expt. ordering	$\alpha < \mathbf{000} >$	$\alpha < \mathbf{100} >$	$\alpha < \mathbf{1\frac{1}{2}0} >$	$\alpha < \mathbf{\frac{1}{2}\frac{1}{2}\frac{1}{2}} >$
Fe_{1-x}Pt_x					
0.25	$< \mathbf{100} > L1_2$	0.009	2.987	0.106	0.035
0.50	$< \mathbf{100} > L1_0$	0.010	3.965	0.077	0.036
0.75	$< \mathbf{100} > L1_2$	0.014	2.720	0.173	0.053
Co_{1-x}Pt_x					
0.25 1*	$< \mathbf{100} > L1_2$	0.006[0.004]	2.834[3.045]	0.106[0.144]	0.023[0.028]
	$< \mathbf{100} > L1_2$	[0.013]	[3.063]	[0.057]	[0.024]
0.50	$< \mathbf{100} > L1_0$	0.007	3.943	0.217	0.030
0.75 2*	$< \mathbf{100} > L1_2$	0.009	2.851	0.222	0.035
	$< \mathbf{100} > L1_2$	0.035	3.014	0.034	0.025

1* : Capitan *et al* (1999); 2* : Kentzinger *et al* (2000)

the effective pair potential surfaces have been shown to differ quite a bit as discussed in Section 5.1.2. This in turn points to nonuniqueness of the scheme to extract the pair interaction energies from experimentally measured SRO data.

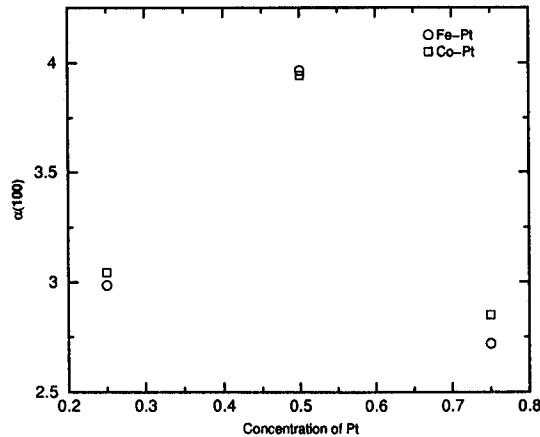


Figure 5.7: Plot of SRO, $\alpha(100)$ values in Fe-Pt and Co-Pt alloys which shows the concentration dependence in the short range order.

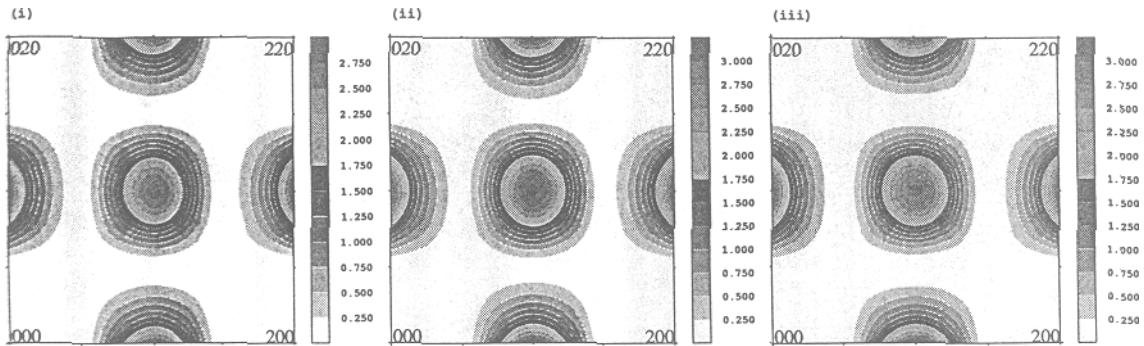


Figure 5.8: SRO ($\alpha(\mathbf{k})$) patterns for Co_3Pt alloy system in the $(\mathbf{hk0})$ plane using our theoretically calculated pair interaction energies (i) without magnetic contribution and (ii) with magnetic contribution and (iii) using real space SRO parameters from the ferromagnetic experimental measurement of Capitan Capitan *et al* (1999). The peaks in the contour plots locate the peaks in the short range order patterns. The plots were drawn at 10 K above the calculated instability temperature.

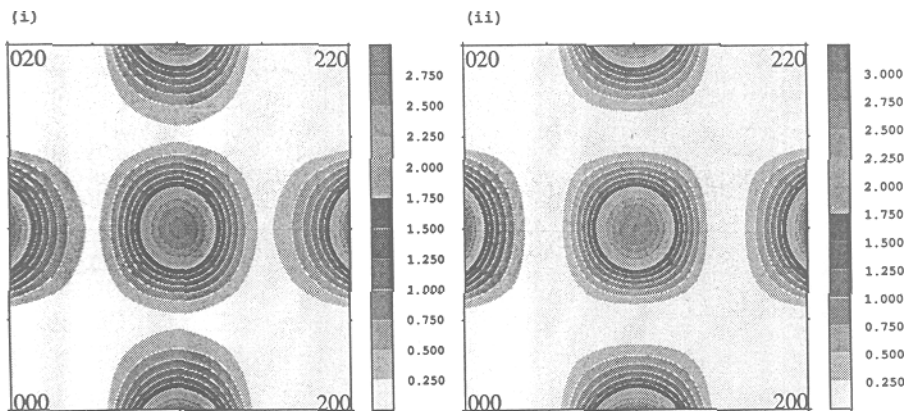


Figure 5.9: SRO ($\alpha(\mathbf{k})$) patterns for CoPt_3 alloy system in the $(\mathbf{hk0})$ plane using (i) our theoretically calculated pair interaction energies and (ii) experimentally measured real space SRO values by Kentzinger *et al* (2000). The peaks in the contour plots locate the peaks in the short range order patterns. The plots were drawn at 10 K above the calculated instability temperature.

5.2 Summary

We have applied our theory for chemical order in metallic alloys for Fe-Pt and Co-Pt systems. Our investigation indicates the chemical ordering tendency in these alloys. There

is short range ordering tendency in the disordered phase of these alloys. Taking the example of Co_3Pt we have demonstrated how the magnetism plays a role in chemical order within the Stoner approach. We have compared our calculations of atomic short range order in Co_3Pt and CoPt_3 with diffuse x-ray and neutron scattering experiments and obtained fair agreements. In this study of Fe-Pt and Co-Pt alloys we have demonstrated that our augmented space recursion method coupled with orbital peeling in the basis of linear muffin tin orbital is capable for accurate prediction of chemical order.

Chapter 6

Ordering in $3d-5d$ (CuAu) and segregation in $3d-4d$ (CuAg) Systems

Recently Wang and Zunger (2003) have studied ordered CuAu and CuAg alloys and pointed out the effect of relativistic corrections in the formation energies in these alloys. In this chapter we shall show, through a first-principle calculation, that in binary alloys of CuAu the relativistic shift of the $5d$ band of Au brings it closer to the $3d$ band of Cu greatly enhancing $3d-5d$ hybridization. In addition, the relativistic contraction of s -orbital leads to a reduction of the equilibrium lattice constant around Au, thus lowering the size mismatch with Cu. This reduces the strain energy associated with packing $3d$ and $5d$ atoms of dissimilar sizes onto a given lattice. The amount of both the enhanced $d-d$ hybridization and the reduced packing strain are larger in CuAu than in CuAg. This explains why CuAu forms stable ordered alloys, while the isovalent CuAg, made of elements from the same columns in the periodic table, phase separates. Simple arguments, such as atomic size-mismatch or electro-negativity differences, do not explain these contrasting behaviours between CuAg and CuAu. In fact, the constituent elements in the stable CuAu alloys have larger atomic size mismatch than the unstable CuAg.

We extend the study made by Wang and Zunger (2003) to disordered alloys. We show the differences in the stability of $3d-5d$ (CuAu) and $3d-4d$ (CuAg) alloys arise mainly due to relativistic corrections. We examine the effect of relativistic corrections to the pair energies and order disorder transition temperatures in these alloys. The short-ranged order or segregation patterns in CuAu/CuAg alloys is also studied within the Krivoglaz-Moss-Clapp model.

¹The contents of this chapter has been submitted to *Physica B : Condensed Matter* (2004)

Table 6.1: Formation energies in mRyd/atom. The values shown in the brackets are without relativistic corrections.

Alloy system	ΔH_{form}	ΔH_{elast}	ΔH_{chem}
CuAg (this work)	6.21 (8.13)	16.30 (17.49)	-10.09 (-9.36)
Wang and Zunger (2003)	7.51 (9.34)	18.74 (19.66)	-11.23 (-10.32)
CuAu (this work)	-5.97 (10.72)	19.20 (28.99)	-25.17 (-18.27)
Wang and Zunger (2003)	-3.64 (12.16)	27.43 (35.13)	-31.07 (-22.97)

6.1 Results and discussions

6.1.1 Calculations on ordered alloys

Formation energies :

In Table 6.1, we show the formation energies of the L1₀ structure of CuAg and CuAu alloys calculated relativistically (including mass velocity and Darwin correction but without spin orbit couplings) as well as non-relativistically. The calculations were performed taking the same lattice parameters that calculated by Wang and Zunger (2003). The relativistically calculated formation energies (in mRyd/atom) are 6.21 and -5.97 for CuAg and CuAu. We see the clear trend of ordered alloy formation in the case of CuAu as contrasted with the phase-separating tendency of CuAg. To gain better insight into those trends following the argument of Wang and Zunger (2003), we have decomposed the total formation energies into the chemical formation energy and the elastic formation energy. The elastic energy of formation is the energy needed to deform the elemental solids A and B from their respective equilibrium lattice constants to the lattice constants of the final AB alloy.

$$\Delta H_{elast} = x[E_A(a) - E_A(a_A^0)] + (1 - x)[E_B(a) - E_B(a_B^0)]$$

The chemical energy of formation is simply the difference between the (fully relaxed) total energy of the alloy and the energies of the de-formed constituents.

$$\Delta H_{chem} = E(A_x B_{1-x}; a) - xE_A(a) - (1 - x)E_B(a)$$

where a is equilibrium lattice constant of alloy, a_A^0 and a_B^0 are equilibrium lattice constants of the constituents and x is the concentration of one of the constituents.

Thus ΔH_{elast} is a volume deformation energy of the constituents, and ΔH_{chem} is the constant volume energy change between the prepared constituents and the compound, which consists of any chemical effect such as hybridization, charge transfer, altered band occupation etc. Since a deformation of equilibrium structures is involved, one expects $\Delta H_{elast} > 0$. In general the chemical formation energy is negative. The sum gives the conventional definition of alloy formation energy and the system is stable only if this formation energy is negative.

$$\Delta H = \Delta H_{elast} + \Delta H_{chem} \quad (6.1)$$

Table 6.1, shows that the relativistic effect significantly reduces the elastic energy of formation of 3d-5d alloys (e.g. from 28.99 to 19.20 mRyd/atom in CuAu). This effect is much smaller in the 3d-4d systems (e.g. 17.49 to 16.30 mRyd/atom in CuAg). The reason for this can also be appreciated by inspecting the non-relativistically-and relativistically-calculated equilibrium lattice constants of the FCC elements as already shown by Wang and Zunger (2003).

Table 6.2: Potential parameters (Δ_d) in mRyd/atom. The values shown in the brackets are without relativistic corrections.

Alloy system	Site (A/B)	Δ_d
CuAg	Cu	7.2 (6.6)
	Ag	15.7 (14.0)
CuAu	Cu	7.0 (5.9)
	Au	22.2 (17.3)

In addition to reduction in the magnitude of elastic energy of formation, Table 6.1 also shows that relativistic corrections enhance the magnitude of chemical energy of formation (e.g. from -18.27 to -25.17 mRyd/atom in CuAu). This effect is much smaller in 3d-4d alloys (e.g. from -9.36 to -10.09 mRyd/atom in CuAg). There are two effects that explain this relativistic chemical stabilization. First the relativistic raising of the energy of the 5d state reduces the 3d-5d energy difference and thus improve the 3d-5d hybridization. Table 6.2 shows the potential parameter (Δ) for d orbitals of Cu, Ag and Au in CuAg and CuAu alloys. This parameter (Δ) measures the hopping strength (t_{ij}), via the relation

$$t_{ij}^{dd} \sim \Delta_d^{1/2} S_{ij} \Delta_d^{1/2}$$

where S_{ij} denotes the structure matrix which is same for alloys having same lattice structure. From Table 6.2, it is seen that the the difference in hopping strength between 3d and 5d are higher than that of 3d and 4d in relativistic case which is the signature of higher overlap and hence the stability in CuAu alloys with relativistic corrections. The second effect is the relativistic lowering of the s band and raising of the d band leads to an increased occupation of the bonding s band and a decreased occupation of the anti-bonding d bands. These effects can be appreciated by integrated orbital charges shown in Table 6.3. From Table 6.3 we also see that Au gain significant sp occupation (0.26e in CuAu) and lose d occupation (-0.28e in CuAu) due to the relativistic effect. The opposing trends in sp and d charge arrangement leads to a small net change in the total charge. Since the sp band increases its occupation, whereas the upper antibonding edge of d band is depleted, these relativistic effects increase the stability of CuAu alloys. In contrast, the relativistic gain in sp occupation and loss of d occupation in Ag is much smaller.

Table 6.3: Integrated number of electrons (n) of each angular momentum type within the atomic spheres of Cu, Ag and Au in CuAg and CuAu alloys. The values shown in the brackets are without relativistic corrections. The table also shows the difference $\Delta n = n_{rel} - n_{nonrel}$.

Alloy system	Site (A/B)	s orbital	p orbital	d orbital
CuAg	Cu	0.69 (0.68)	0.69 (0.66)	9.62 (9.66)
	Ag	0.69 (0.65)	0.74 (0.71)	9.47 (9.55)
CuAu	Cu	0.64 (0.66)	0.72 (0.65)	9.64 (9.68)
	Au	0.86 (0.68)	0.83 (0.75)	9.18 (9.46)
Δn				
CuAg	Cu	0.01	0.03	-0.04
	Ag	0.04	0.03	-0.08
CuAu	Cu	-0.02	0.07	-0.04
	Au	0.18	0.08	-0.28

Our results for formation energies are comparable, within the error window of our calculational method, to the results obtained by Wang and Zunger (2003). These authors used full potential linearized augmented plane wave method with exchange correlation functional of Ceperley and Alder (1980) parametrized by Perdew and Zunger (1981). They have carried out k space integration with $8 \times 8 \times 8$ mesh resulting 60 special k points. On the other hand we have in our TB-LMTO calculation used von Barth and Hedin exchange correlation functional and we have carried out the k space integration with

Table 6.4: Pair energies in mRyd/atom. The values shown in the brackets are without relativistic corrections. $V_n = E_{RR'}^{(2)}$ where R' is a n-th nearest neighbour of R .

Alloy system	V_1	V_2	V_3	V_4
CuAg	-0.63 (-0.90)	0.09 (0.05)	-0.02 (0.00)	0.12 (0.10)
CuAu	2.29 (-0.23)	0.19 (0.20)	0.06 (0.11)	0.21 (0.17)

32×32×32 mesh resulting 2601 special k points to ensure the convergence of total energy.

6.1.2 Calculations on disordered alloys

Effective pair energies :

In Table 6.4, we show the effective pair energies up to fourth nearest neighbour in 3d-4d CuAg and 3d-5d CuAu alloys.

The first nearest neighbour pair interaction of CuAg shows segregation behaviour which matches with the positive value of formation energy of the ordered calculations.

In CuAu alloy the pair interaction calculations without relativistic correction shows segregation tendency. Inclusion of these corrections lead to the correct conclusion of an ordering behaviour. Our relativistic calculation in ordered CuAu shows that the with L1₀ structure has lower total energy than the A₂B₂ superstructure. This confirms a stable L1₀ low temperature structure of CuAu. However, the antiphase boundary energy has the wrong sign. This could be due to the fact that in CuAu the APB energies are long ranged and more than the fourth nearest neighbour values need to be taken.

Order disorder transition temperatures :

Using these pair interactions obtained by us, we have calculated the instability temperatures in CuAu alloys with relativistic corrections. For the entropy part we have taken a simple mean-field Bragg-Williams expression. Our calculation in CuAu alloy shows an instability temperature (246°K) slightly higher than the experimental estimate (137°K).

Our calculations (with relativistic corrections) on CuAg shows a disorder to segregation transition temperature as 184°K. . This temperature in non relativistic case is slightly enhanced (201°K). Both the values are lower than experimental estimate (506°K).

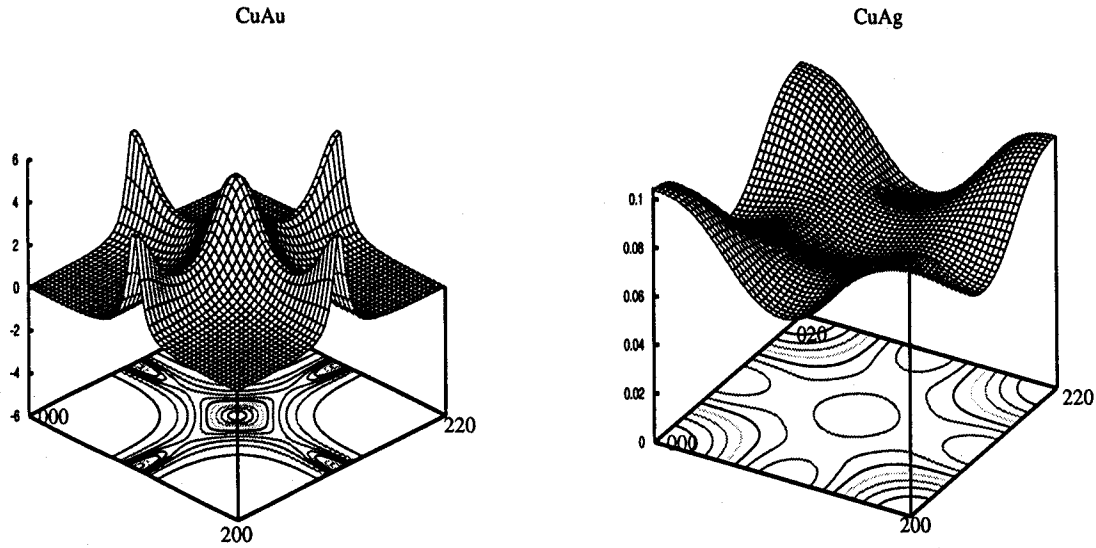


Figure 6.1: The short range order map $\alpha(\mathbf{k})$ for (left) CuAu and (right) CuAg.

6.1.3 Short-ranged order

The short-range order (SRO) patterns $\alpha(\mathbf{k})$ using the pair interaction energies for CuAg and CuAu are shown in Figure 6.1. These patterns are calculated above the ordering/segregation temperatures to examine the effect of the onset of SRO in the disordered phase. The SRO pattern for CuAu show peaks at $\langle 100 \rangle$ positions. This correspond to diffuse scattering peaks which clearly show the $L1_0$ short range ordering developing in this alloy. For CuAg the SRO pattern shows a peak at $\langle 000 \rangle$, confirming the onset of segregation in this alloy.

6.2 Summary

Our calculation for formation energies shows that CuAu alloys are stabilized by inclusion of relativistic effects. These effects ensures larger s - d hybridization by lowering s orbitals and raising d orbitals and lowers the strain and size mismatch in these alloys. Similar calculations show CuAg to be unstable and there is very little effect of relativity. The pair interaction calculations show CuAu has $L1_0$ as the stable ground state structure and CuAg to be a segregating system as predicted from experiments.

Chapter 7

Concluding remarks

Technically important and scientifically valuable alloy systems exhibit a variety of interesting thermodynamic and energetic properties including phase ordering and phase segregation. These properties can be understood in terms of electronic and magnetic structures and are useful for the actual determination of alloy phase stability. The development of a theory to study these properties has two aspects. First it can reproduce the experimental predictions which are already available and secondly it can potentially provide the predictive guidance for experiment and industry. The combination of first principles electronic structure and simple statistical models offer this great predictive potential.

The augmented space recursion combining with first principle tight binding linear muffin tin orbital (TB-LMTO) method has been established as an accurate method to study electronic and magnetic properties of alloys. The coupling of this method with orbital peeling technique is used to calculate effective pair interactions. Using these pair interactions as inputs in the statistical models like concentration wave method we calculate alloy phase stability. In this thesis we have taken into account the effects like scalar relativity, charge transfer, lattice relaxation and short range order which play important role in the determination of the correct tendency in electronic and magnetic properties as well as actual determination of ordering or segregation tendencies along with the determination of actual stable phase in the particular concentration of size mismatched alloy systems. We have generalized this methodology to study the effect of magnetism on chemical order.

The numerical details of calculations, convergence with the number of k-points in the Brillouin Zone integrations, choice of atomic sphere radii, proper convergences in the TBLMTO-ASR, the proper choice of the minimal basis set in the TB-LMTO, all of these affect the electronic, magnetic structure and phase stability properties.

In the application part we started from the study of effect of possible exchange correla-

tion functionals in Fe-Pt, Co-Pt and Ni-Pt alloy systems which indicates that the choice of exchange correlation potentials has considerable effect on the values of equilibrium lattice constants and magnetic moments in these alloys. The study of magnetic properties of disordered Fe-Pt, Co-Pt and Ni-Pt alloy systems shows that the single site coherent potential approximation (CPA) method works reasonably well for Fe-Pt and has close agreement with the results obtained using augmented space recursion method. The CPA starts deviating from ASR in Co-Pt and it fails in the case of Ni-Pt alloys showing increasing tendency of local magnetic moments of Ni with the increase of concentration of Pt which is opposite to the experimental and ASR trend. The inclusion of short range order effect in the calculation of magnetic moments of Ni-Pt alloys through generalized augmented space recursion method brings quantitative agreement with experimental results.

Our study on phase stability in Ni-Pt alloy system shows that, for the correct prediction of sign in formation energy, we need to include the scalar relativistic corrections in our electronic structure method. The inclusion of scalar relativistic corrections and the proper treatment of charge transfer are must to get the experimental trend of order disorder transition temperature in this alloy system.

The study on phase stability of Fe-Pt and Co-Pt indicates that the inclusion of magnetic contribution in the calculation of pair interaction energies in the cases where the magnetic transition temperature is higher than the chemical order disorder transition temperature as is the case of Co_3Pt system brings closer agreement with experimental pair interaction energies giving rise to the closer agreement with experimental chemical transition temperature. The systematic study in these systems indicates that there is short range order in the disordered phase of these alloys. The short range order maps compare well with the corresponding diffuse x-ray and neutron scattering experiments in Co_3Pt and CoPt_3 alloy systems.

In the study of ordering in $3d-5d$ (CuAu) and segregation in $3d-4d$ (CuAg) Systems, we show the differences in the stability of $3d-5d$ (CuAu) and $3d-4d$ (CuAg) alloys arise mainly due to relativistic corrections. We examine the effect of relativistic corrections to the pair energies and instability temperatures in these alloys. The short-ranged order or segregation patterns in CuAu/CuAg alloys is also studied using the Krivoglaz-Moss-Clapp model.

To summarize, we have systematically extended the augmented space recursion method with its generalization and carried out the charge self consistent calculations to take into account the short range ordering or clustering effects in the electronic structure of simple substitutional binary alloys or size mismatched alloys with properly taking care of relativistic corrections, charge transfer and lattice relaxation. We have generalized the

augmented space recursion coupled with orbital peeling technique to take into account of magnetism on chemical order of these alloy systems. The application part demonstrates that (i) the generalized augmented space recursion method is capable of estimating the effect of immediate environment (short range order or segregation) on electronic structure and magnetism, (ii) the augmented space recursion coupled with orbital peeling technique together with simple statistical mean field models can predict the experimental trends in chemical ordering or segregation including magnetism wherever it is necessary and then determine the stable phases in these alloy systems.

Bibliography

- Abrikosov I. A., Niklasson A. M. N., Simak S. I., Johansson B., Ruban A. V. and Skriver H. L., *Phys. Rev. Lett.* **76** 4203 (1996)
- Amador C., Lambrecht W. R. L., van Schilfgaarde M. and Segall B., *Phys. Rev.* **B47** 15276 (1993)
- Andersen O. K., *Phys. Rev.* **B12** 3060 (1975)
- Andersen O. K. and Jepsen O., *Phys. Rev. Lett.* **53** 2571 (1984)
- Andersen O. K., Jepsen O. and Šob M., *Electronic Band Structure and Its Applications* ed. M. Yussouff. Lecture Notes in Physics 283, Springer (1987,1992).
- Andersen O.K., Jepsen O. and Krier G., *Lectures on Methods of Electronic Structure Calculations* eds.: Kumar V., Andersen O. K., Mookerjee A., Singapore, World Scientific, (1994).
- Anderson D. G., *J. Assoc. Comput. Mach.* **12** 547 (1964)
- Bieber A., Gautier F., Treglia G. and Ducastelle F., *Solid State Commun.* **39** 149 (1981)
- Bieber A. and Gautier F. *Solid State Commun.* **38** 1219 (1981)
- Bieber A. and Gautier F., *J. Magn. Magn. Mater.* **54 -57** 967 (1986)
- Biswas P. P., Sanyal B., Fakhruddin M., Halder A., Mookerjee A. and Ahmed M., *J. Phys.: Condens. Matter* **7** 8569 (1995)
- Borici-Kuqo M., Monnier R. and Drchal V., *Phys. Rev.* **B58** 8355 (1998)
- Bose S. K., Kudrnovský J., Jepsen O. and Andersen O. K., *Phys. Rev.* **B45** 8272 (1992)
- Broyden C. G., *Math. Comput.* **19** 577 (1965)
- Burke N. R. , *Surf. Sci.* **58** 349 (1976)
- Buttler W. H., *Phys. Rev.* **B8** 4499 (1973)

- Cadeville M. C. and Morán-López J. L., *Physics Reports* **153** 331 (1987)
- Capitan M., Lefebvre S., Calvayrac Y., Bessière M., and Cénédèse P., *J. Appl. Crystallogr.* **32**, 1039 (1999)
- Caporaletti O. and Graham G. M., *J. Magn. Magn. Mater.* **22** 25 (1980)
- Ceperley D. M. and Alder B. J., *Phys. Rev. Lett.* **45** 566 (1980)
- Connolly J. W. D. and Williams A. R., *Phys. Rev.* **B27** 5169 (1983)
- Cowley J.M., 1950 *J. Appl. Phys.* **21** 24 (1950)
- Dahmani C. E., Cadeville, M. C., Sanchez J. M. and Moran-Lopez J. L., *Phys. Rev. Lett.* **55** 1208 (1985)
- Das G.P., *Electronic Structure of Alloys, Surfaces and Clusters*, Advances in Condensed Matter Science, Vol. 4, eds.: A. Mookerjee and D. D. Sharma, Taylor-Francis, (2003)
- Dasgupta I., Saha T., and Mookerjee A., *Phys. Rev.* **B51**, 3413 (1995)
- Dederichs P. H. and Zeller R., *Phys. Rev.* **B28**, 5462 (1983)
- Ebert H., Drittler B. and Akai H., *J. Magn. Magn. Mater.* **104-107** 733 (1992)
- de Fontaine D., in *Solid State Physics*, (eds.) Ehrenreich H., Seitz F. and Turnbull D., (Academic Press, New York, 1994), Vol. 47 p.33.
- Dreyssé H., Berera A., Wille L. T. and de Fontaine D., *Phys. Rev.* **B39** 2442 (1989) ;
Wolverton C., Ceder G., de Fontaine D. and Dreyssé H., *Phys. Rev.* **B48** 726 (1993)
- Ducastelle F., *Order and Phase Stability in Alloys* (Elsevier Science, New York, 1991).
- Ducastelle F. and Gautier F., *J. Phys. F: Met. Phys.* **F6** 2039 (1976)
- Ghosh S., Das N. and Mookerjee A., *Mod. Phys. Lett. B* **21** 723 (1999)
- Ghosh S., Chaudhuri C. B., Sanyal B. and Mookerjee A., *J. Magn. Magn. Mater.* **234** 100 (2001)
- Ghosh S., Das N. and Mookerjee A., *J. Phys.: Condens. Matter* **9** 10701(1997)
- Gonis A. and Garland J. W., *Phys. Rev.* **B16** 2424 (1977)
- Gonis A., Zhang X. G., Freeman A. J., Turchi P., Stocks G. M. and Nicholson D. M., *Phys. Rev.* **B36** 4630 (1987)

- Geerts W., Suzuki Y., Katayama K., Tanaka K., Ando K. and Yoshida S., *Phys. Rev.* **B50** 12581 (1994)
- Hamada N., *J. Phys. Soc. Jpn.* **46** 1759 (1979)
- Hamann D. R., *Phys. Rev. Lett.* **42** 662 (1979)
- Hasegawa H., *J. Phys. Soc. Jpn.* **46** 1504 (1979)
- Hasegawa H. and Kanamori J., *J. Phys. Soc. Jpn.* **31** 382 (1971)
- Haydock R., Heine V. and Kelly M. J., *J. Phys. C: Solid State Phys.* **C5** 2845 (1972) ;
Haydock R., *Solid State Physics* **35** (Academic Press, N. Y.) (1988)
- Hayn R. and Drchal V., *Phys. Rev.* **B58** 4341 (1998)
- Heine V., *Solid State Physics* **35** (Academic Press, N. Y.) (1988)
- Hennion M., *J. Phys. F: Met. Phys.* **13** 2351 (1983)
- Hicks T. J., *Phys. Lett.* **A32** 410 (1970)
- Hohenberg P. and Kohn W., *Phys. Rev.* **136**, B864 (1964).
- Ito Y., Sasaki T. and Mizoguchi T., *Solid State Commun.* **15** 807 (1974)
- Jo T., *J. Phys. Soc. Jpn.* **40** 715 (1976)
- Jo T. and Miwa H., *J. Phys. Soc. Jpn.* **40** 706 (1976)
- Johnson D. D., *Phys. Rev.* **B38** 12807 (1988)
- Johnson D. D., Staunton J. B. and Pinski F. J., *Phys. Rev.* **B50** 1473 (1994)
- Kakehashi Y., *J. Phys. Soc. Jpn.* **51** 94 (1982)
- Kanamori J. and Kakehasi Y., *J Physique Coloq.* **38** C7-274 (1977)
- Kashyap A., Garg K. B., Solanki A. K., Nautiyal T. and Auluck S., *Phys. Rev.* **B60** 2262 (1999)
- Kashyap A., Solanki A. K., Nautiyal T. and Auluck S., *Phys. Rev.* **B52** 13471 (1995)
- Kentzinger E., Parasote V., Pierron-Bohnes V., Lami J. F., Cadeville M. C., Sanchez J. M., Caudron R. and Beuneu B., *Phys. Rev.* **B61**, 14975 (2000)
- Khachaturyan A. G., *Prog. Mater. Sci.*, **22**, 1 (1978) ; *Theory of structural transformations in solids* , Willey, New York (1983).

- Koelling D. D. and Harmon B. N., *J. Phys. C: Solid State Phys.* **10** 3107 (1977)
- Koepernik K., Velický B., Hayn R. and Eschrig H., *Phys. Rev.* **B55** 5717 (1997)
- Kohn W. and Sham L. J., *Phys. Rev.* **140**, A1133 (1976).
- Kootte A., Haas C. and de Groot R. A., *J. Phys.: Condens. Matter* **3** 1133 (1991)
- Krivoglaz M. A. and Smirnov A. A., in *The theory of Order-Disorder in Alloys*, (McDonald, London, 1964).
- Kudrnovský J. and Drchal V., *Phys. Rev.* **B41** 7515 (1990)
- Kudrnovský J. and Drchal V., *Solid State Commun.* **70** 577 (1989)
- Kudrnovský J. and Maek J., *Phys. Rev.* **B31** 6424 (1985)
- Kulikov N. I., Kulatov E. T. and Yakhimovich S. I., *J. Phys. F: Met. Phys.* **15** 1127 (1985).
- Landau L. D. and Lifshitz E. M., in *Statistical Physics*, Second and Third Editions, Part 1, (Pergamon Press, Oxford, 1969 and 1980).
- Landau and Lifshitz, *Electromagnetism in material media*
- Lange R. J., Lee S. J., Lynch D. W., Canfield P. C., Harmon B. N. and Zollner S., *Phys. Rev.* **B58** 351 (1998)
- Langreth D. C. and Mehl M. J., *Phys. Rev. Lett.* **47** 446 (1981)
- Lide D.R., *Hand Book of Chemistry and Physics* 81st Ed. p12-119 (2000)
- Ling M. F., Staunton J. B. and Johnson D. D., *J. Phys.: Condens. Matter* **6** 5981 (1994)
- Ling M. F., Staunton J. B., Johnson D. D. and Pinski F. J., *Phys. Rev.* **B52** 3816 (1995)
- Lu Z. W., Wei S. H. Wei, and Zunger A., *Phys. Rev. Lett.* **66** 1753 (1991), **68** 1961 (1992)
- Lu Z. W., Laks D. B., Wei S. H. and Zunger A., *Phys. Rev.* **B50** 6642 (1994)
- Luchini M. U., Nex C. M. M., *J. Phys. C: Solid State Phys.* **20** 3125 (1987)
- Marshall W., *J. Phys. C: Solid State Phys.* **1** 88 (1968)
- Major Zs., Dugdale S., Jarlborg T., Bruno E., Ginatempo B., Staunton J. B. and Poulter J., *J. Phys.: Condens. Matter* **15** 3619 (2003)
- Mašek J. and Kudrnovský J., *Solid State Commun.* **58** 67 (1986)

- Mirebeau L., Cadeville M. C., Parette G. and Campbell I. A., *J. Phys. F: Met. Phys.* **12** 25 (1982)
- Mirebeau I., Hennion M. and Parette G., *Phys. Rev. Lett.* **53** 687 (1984)
- Mookerjee A., *J. Phys. C: Solid State Phys.* **C6** L205 (1973) ; *J. Phys. C: Solid State Phys.* **C6** 1340 (1973)
- Mookerjee A. and Prasad R., *Phys. Rev.* **B48** 17724 (1993)
- Müller-Hartmann, *Solid State Commun.* **12** 1269 (1973)
- Osterloh I., Oppeneer P. N., Sticht J. and Kubler J., *J. Phys.: Condens. Matter* **6** 285 (1994)
- Parra R. E. and Cable J. W., *Phys. Rev.* **B21** 5494 (1980)
- Pearson W. B., *A handbook of lattice spacings and structures of metals and alloys* Oxford, Pergamon Press (1958-1967)
- Perdew J. P. and Wang Y., *Phys. Rev.* **B33** 8800 (1986)
- Perdew J. P. and Zunger A., *Phys. Rev.* **B23** 5048 (1981)
- Pierron-Bohnes V., Cadeville M. C. and Parette G., *J. Phys. F: Met. Phys.* **15** 1441 (1985)
- Pierron-Bohnes V., Cadeville M. C. and Gautier F., *J. Phys. F: Met. Phys.* **13** 1689 (1983)
- Pinski F. J., Ginatempo B., Johnson D. D., Staunton J. B., Stocks G. M. and Györfy B. L., *Phys. Rev. Lett.* **66** 766 (1991); **68** 1962 (1992)
- Pisanty A., Amador C., Ruiz Y. and de la Vega M., *Z. Phys. B-Condensed Matter* **80** 237 (1990)
- Podgórný M., *Phys. Rev.* **B43** 11300 (1991); *Phys. Rev.* **B46** 6293 (1992)
- Pourovskii L. V., Ruban A. V., Abrikosov I. A., Vekilov Y. Kh. and Johansson B., *Phys. Rev.* **B64** 035421 (2001)
- Razee S. S. A., Staunton J. B., Ginatempo B., Bruno E., and Pinski F. J., *Phys. Rev.* **B64**, 014411 (2001)
- Ruban A. V., Abrikosov I. A., and Skriver H. L., *Phys. Rev.* **B51** 12958 (1995)
- Ruban A. V., Simak S. I., Korzhavyi P. A and Skriver H. L., *Phys. Rev.* **B66** 024202 (2002)

- Saha K. K., Saha-Dasgupta T., Mookerjee A. and Dasgupta I., *J. Phys.: Condens. Matter* **16** 1409 (2004)
- Saha T., *Ph.D. Thesis*, Calcutta University, (1995)
- Saha T., Dasgupta I. and Mookerjee A., *Phys. Rev.* **B50** 13267 (1994)
- Saha T., Dasgupta I. and Mookerjee A., *J. Phys.: Condens. Matter* **6** L245 (1994)
- Saha T. and Mookerjee A., *J. Phys.: Condens. Matter* **8** 2915 (1996)
- Sanchez J. M., Moran-Lopez J. L., Leroux C. and Cadeville M. C., 1988 *J. Phys. C: Solid State Phys.* **21** L1091 (1988)
- Sanyal B., Biswas P. P., Mookerjee A., Das G. P., Salunke H. and Bhattacharya A. K., *J. Phys.: Condens. Matter* **10** 5767 (1998)
- Sato H., Arrott A. and Kikuchi R., *J. Phys. Chem. Solids* **10** 19 (1959)
- Shick A. B., Drchal V., Kudrnovský J. and Weinberger P., *Phys. Rev.* **B54** 1610 (1996)
- Singh P. P., *J. Magn. Magn. Mater.* **261** 347 (2003)
- Singh P. P., *Pramana - J. Phys.* **47** 99 (1996)
- Singh P. P., and Gonis A., *Phys. Rev.* **B49** 1642 (1994)
- Singh P. P., Gonis A. and Turchi P. E. A., *Phys. Rev. Lett.* **71** 1605 (1993)
- Soven P., *Phys. Rev.* **156** 809 (1967)
- Stahl B., Ellrich J., Theissmann R., Ghafari M., Bhattacharya S., Hahn H., Gajbhiye N. S., Kramer D., Viswanath R. N., Weissmüller J. and Gleiter H., *Phys. Rev.* **B67**, 014422 (2003)
- Staunton J. B., Ling M. F. and Johnson D. D., *J. Phys.: Condens. Matter* **9** 1281 (1997)
- Staunton J. B., Johnson D. D. and Pinski F. J., *Phys. Rev.* **B50** 1450 (1994)
- Swalin R. A., *Thermodynamics of solids*, Wiley, New York, (1962)
- Tohyama T., Ohta Y. and Shimizu M., *J. Phys.: Condens. Matter* **1** 1789 (1989)
- Treglia G. and Ducastelle F., *J. Phys. F: Met. Phys.* **17** 1935 (1987)
- Turchi P. E. A., Stocks G. M., Butler W. H., Nicholson D. M., and Gonis A., *Phys. Rev.* **B37** 5982 (1988)
- Uba S., Yaresko A. N., Uba L., and Perlov A. Ya, *Phys. Rev.* **B57** 1534 (1998)

- Uba L., Uba S., Antonov V. N., Yaresko A. N., and Gontarz R., *Phys. Rev.* **B64** 125105 (2001)
- Uhl M., Sandratskii L.M., and Kubler J., *Phys. Rev.* **B50** 291 (1994)
- von Barth U. and Hedin L., *J. Phys. C: Solid State Phys.* **5** 1629 (1972)
- Vonsovskii S. V., *Magnetism* (Wiley, New York, 1974)
- Vosko S. H., Wilk L. and Nusair M., *Can. J. Phys.* **58** 1200 (1980)
- Wang L. G. and Zunger A., *Phys. Rev.* **B67**, 092103 (2003)
- Weller D., Harp G. R., Farrow R. F. C., Cebollada A. and Sticht J., *Phys. Rev. Lett.* **72** 2097 (1994)
- Wijn H. P. J., Landolt-Bornstein (Eds.), *Magnetic Properties of Metals, 3d, 4d and 5d Elements, Alloys and Compounds*, New Series, Group III, Vol. 19 Part a, Springer-Verlag, Berlin, (1986)
- Wolverton C., Ozolins V. and Zunger A., *Phys. Rev.* **B57** 4332 (1998)
- Wright H., Weightman P., Andrews P. T., Folkerts W., Flipse C. F. J., Sawatsky G. A., Norman D. and Padmore H., *Phys. Rev.* **B35** 519 (1987)